Spring 2015

Feasibility for spinal muscles creating pure axial compressive load or follower load in the lumbar spine in 3-D postures

Tianjiao Wang
University of Iowa

FEASIBILITY FOR SPINAL MUSCLES CREATING PURE AXIAL COMPRESSIVE LOAD OR FOLLOWER LOAD IN THE LUMBAR SPINE IN 3-D POSTURES

by

Tianjiao Wang

A thesis submitted in partial fulfillment
of the requirements for the Doctor of
Philosophy degree in Biomedical Engineering
in the Graduate College of
The University of Iowa

May 2015

Thesis Supervisor: Professor Tae-Hong Lim

Graduate College
The University of Iowa
Iowa City, Iowa

CERTIFICATE OF APPROVAL

_____

PH.D. THESIS

_____

This is to certify that the Ph.D. thesis of

Tianjiao Wang

has been approved by the Examining Committee for
the thesis requirement for the Doctor of Philosophy degree
in Biomedical Engineering at the May 2015 graduation.

Thesis Committee: _____
Tae-Hong Lim, Thesis Supervisor

_____
Kyung K. Choi

_____
Nicole M. Grosland

_____
David G. Wilder

_____
Laura A. Frey Law

To my parents

ACKNOWLEDGMENTS

I would like to express my deepest appreciation and thanks to my advisor Prof. Tae-Hong Lim, he has been an incredible mentor for me. He is always available when I need his help. He always inspires me to think more deeply about the research and my future. His passion for this research always motivates me. He cares about my future career and helps me to find a position after graduation. I am very grateful and blessed to have him as my research advisor.

I would also like to thank the previous Ph.D student, Byeong Sam Kim, for all his teaching and help. He taught me how to use the finite element software when I just started my Ph.D program. He prepared me for my research topic. Even though he has left this lab, he always patiently answers my questions about the software and research through email. I am very thankful for everything he has done for me.

I also want to thank my parents and my fiancée for their love, sacrifice, support and encouragement. I would not be at the place I am now without their support. I would like to thank my roommate, Alice Hwan, for taking care of me during the busy seasons. I would like to thank my church family for all their prayers. I would like to thank my lab mates Ino Song and Daniel Vite for all their support and help.

Finally, I would sincerely thank ESI Korea, Co., LTD for their permission to use the finite element software, LS-Dyna. I would like to thank all of my committee members for your comments and suggestions for my research. I would like to thank the Department of Biomedical Engineering for giving me this opportunity to pursue this study.

ABSTRACT

Previous *in-vivo* studies showed that compressive force acting on the spine may exceed 2600 N. However, the ligamentous lumbar spine becomes unstable when subjected to compressive loads less than 100 N. It is generally accepted that the ligamentous spine itself is unstable but can be stabilized by muscle forces (MFs) *in vivo.* Nevertheless, normal spinal muscle contraction patterns remain unknown.

In recent *in vitro* studies, when the direction of the applied load was controlled along the spinal curvature so that the internal spinal load became perfect compressive follower loads (CFLs) at all lumbar levels, the ligamentous lumbar spine was found to withstand large compressive load (up to 1200 N) without buckling while maintaining its flexibility in neutral or flexed postures. The results of *in-vivo* animal studies also have shown that shear stress has a more detrimental effect on the rate of disc degeneration compared to compressive stress. These results suggest CFLs in the lumbar spine would be a normal spinal load whereas the transverse (or shear) load abnormal. An initial test of this postulation would be to investigate whether the spinal muscles can create perfect internal CFLs in the lumbar spine in all 3-D postures. In addition, small intrinsic muscles (SIMs) are crucial for better control of the direction of the internal spinal load along the spinal axis was also proposed.

A finite element (FE) model together with an optimization model were used for this study. Both models consist of the trunk, sacrolumbar spine and 244 spinal muscles. Different from other studies, 54 SIMs were also included in the models. The FE model was validated by comparing the ROM of the spine with the literature data. Minimization of the summation of the spinal loads and moments was used as the cost function for the optimization model. The geometrical data obtained from the FE

model was used as the input for the optimization model; it was then used to calculate the MFs required for creating the CFLs at all lumbar spine levels. The MFs determined in the optimization model were then imported back to the FE model as input loads to check the stability of the spine under this loading condition. Five different postures were studied: neutral, flexion 40°, extension 5°, lateral bending 30° and axial rotation 10°.

Many optimization solutions for spinal muscle force combinations creating pure CFLs in the lumbar spine were found available in each posture. However, FE analyses showed that only muscle forces and patterns solved at FLPs along the curve in the vicinity of the baseline curve stabilized the lumbar spine. Stability was determined by small displacement of the trunk (≤5 mm) due to small deformation of the lumbar spine. The magnitudes of joint reaction forces (JRFs) predicted from the optimization model were comparable to those reported in the literature. When the SIMs were removed, optimization solutions were still feasible in all five postures, but JRFs and trunk displacement were increased. This suggests the need of SIM inclusion in future spine biomechanics studies and clinically, damages to the SIMs may have a high risk of future spinal problems, such as spinal instability, early disc degeneration, deformity and/or early failure of spinal fixation devices.

The results from this study supported the hypothesis that the perfect CFLs at all lumbar levels could be the normal physiological load under which the lumbar spinal column could support large load without buckling while allowing flexibility. SIMs played an important role in creating CFLs as by including SIMs in the models, the JRFs at all lumbar spine levels were lowered and the stability of the spine was increased.

PUBLIC ABSTRACT

About 80% of adults suffer low back pain (LBP) during their lifetime and this affects the socioeconomic system as billions of dollars are spent on healthcare each year because of it. Although LBP causes such socioeconomic burden to the society, the mechanics of the spine remain unknown. It is unclear what the normal spinal muscle contraction patterns and the normal spinal loads are during daily activities. It is also unclear what mechanics are used for the spine to stay stable and flexible. Without answering these, treatment and prevention of LBP remain challenging.

This research investigated the normal spinal load and normal muscle contraction patterns. It is proposed that the compressive axial forces - forces that are perpendicular to the cross-sectional area of each lumbar spinae, are normal; while shear forces, forces that are parallel to the cross-sectional area of the spinae, are abnormal. Since joint spinal loads are mainly caused by the spinal muscles, mathematical and computational methods were used in this study to check whether it is feasible for the spinal muscles to create only axial forces on the lumbar spine joint during various postures.

It was found that it is feasible for spinal muscles to create only axial force on the lumbar spine, thus it can be concluded that pure axial compressive load can be the normal spinal load. If this is true, the spinal muscle contraction patterns can be predicted and the prevention and treatment of LBP can be significantly improved.

TABLE OF CONTENTS

LIST OF TABLES

LIST OF FIGURES

LIST OF ABBREVIATIONS

ALL - Anterior Longitudinal Ligament
CFLs - Compressive Follower Loads
CG - Center of Gravity
EMG - Electromyography
EO - External Oblique
ES - Erector Spinae
FE - Finite Element
FLP - Follower load path
FSU - Functional Spinal Unit
GC - Geometrical Center
IO - Internal Oblique
JRFs - Joint Reaction Forces
LBP - Low Back Pain
LD - Latissimus Dorsi
PLL - Posterior Longitudinal Ligament
PM - Psoas Major
QL - Quadratus Lumborum
RA - Rectus Abdominis
ROM - Range of Motion
SIMs - Short Intrinsic Muscles
SPI - Serratus Posterior Inferior

CHAPTER 1

INTRODUCTION

In the United States, low back pain (LBP) is the second most common neurological disease other than headache. About 60-80% of American adults population have LBP and at least $50 billion dollars are spent on it every year [1]. It is also the most common cause for job-related disability, a leading contributor to work absence. Every year, about 13 million Americans go to doctor because of chronic LBP. Among these, about 2.4 million chronically are disabled and another 2.4 million are temporarily disabled [1]. LBP also occurs in similar proportions around the world [2]. Nearly everyone will have LBP that affect their daily routine and work performance at some point of life [3]. Even though some of these LBPs are caused by defined organic diseases, in most cases the cause remains unknown. The overall judgment for a LBP patient may involve both acute and long terms of neurological deficit and pain, but the root of the problem is most likely due to the mechanical insufficiency of the spinal column [4, 5].

The lumbar spine is a long and slender column supporting the upper body. By treating the spine as an Euler column, Crisco et al. found that ligamentous lumbar spine, spine without muscles, buckles under a compressive load of 88N [6]. However, Nachemson et al., by measuring the intervertebral disk pressure *in vivo*, showed that the compressive force acting on the spine may exceed 2600N. Biomechanical assessment of occupational low back disorders suggests that the spinal compression load below 3400N can be considered safe for the majority of the working age population [7]. Thus, 88N is significantly below the load capacity of the spine *in vivo*.

More recently, Patwardhan et al. demonstrated through *in vitro* experiment that under follower load mechanism, the ligamentous lumbar spine could withstand up to 1200N compressive load without buckling and maintaining its flexibility in both neutral posture and forward flexed posture [8]. Follower load is defined as the directions of the joint reaction forces (JRFs) are parallel to the curvature of the spine, thus follower load could also be considered as pure axial compressive load or compressive follower load (CFL). Additionally, the results of *in-vivo* animal studies have shown that by applying different types of load on the disk of a rat, the disk degenerated under a compressive stress greater than 0.8MPa but only 0.33MPa shear stress [9, 10]. Thus, shear stress on the intervertebral disk has a detrimental effect on the rate of disk degeneration compared to compressive stress. The results from these studies suggest that CFL in the lumbar spine would be the normal spinal load whereas transverse (or shear) load would be abnormal.

The purpose of this study was to investigate whether the spinal muscles can create CFL in 3-D postures under physiological load while stabilizing the spine. Computational analyses were conducted in this study using finite element (FE) and optimization models. Since short intrinsic muscles (SIMs) are known to be important for spinal stability by increasing the stiffness of the spine [11], the role of the SIMs in stabilization of the spine via follower load mechanism was also studied. It is proposed that spinal muscles can create CFLs in 3-D postures while keeping spine stable and SIMs play an important role in stabilization of the spine. Five postures were studied: neutral standing, flexion 40°, extension 5°, lateral bending 30°, and axial rotation 10°.

In this dissertation, Chapter 2 provides some background and literature review that are related to this study. The computational model development methods

for the 3-D optimization model and the FE model are introduced in Chapter 3. Chapter 4 shows the results obtained from the optimization model and the FE model when CFLs are forced to pass through the geometrical center (GC) of each lumbar vertebra. The study of the roles of SIMs in spinal stabilization is also described in Chapter 4. Chapter 5 talks about other feasible solutions that are also create CFL and stabilize the spine in all the postures of this study. Parametric studies on body weight variation and disc property variation are described in Chapter 6. Chapter 7 discusses the results obtained from the whole study, the limitations of this study and future work. It also includes the validation of the results with literature data. Finally, Chapter 8 concludes the whole study and specifies the important findings from this research.

CHAPTER 2

BACKGOUND AND LITERATURE REVIEW

LBP is a serious problem because it affects many people's daily routine and work performance. It has been found that most incidences can be prevented by keeping strong back muscles and practicing good body mechanics in daily activities [1]. However, without a good understanding on how the muscles work together to maintain a stable and flexible spine, our knowledge and methods on diagnosis, prevention and treatment of LBP are limited. Thus, a comprehensive understanding of normal spinal muscle contraction patterns is crucial for prevention and treatment of low back disorders.

The interest in studying the cause and prevention of LBP has increased since 1960s; however, the studies have faced many limitations and challenges. First, measurement of spinal loads *in vivo* is very invasive. It was done by inserting a pressure transducer in the form of a needle into the interested level of intervertebral disks. Hence, the investigator is limited in introducing this technique for studies due to concerns on damaging the spinal disks [12, 13] and to control the many variables involved. Because of these concerns, it is also challenging to recruit subjects for the study. There have not been many studies on the *in vivo* measurement of the spinal loads, and sample sizes were small in the studies that have been published.

Second, measurement of the muscle activities using electromyography (EMG) is also limited in many aspects. It is almost impossible to measure every individual back muscle forces experimentally, especially the SIMs, which are also the stabilizers. Although EMG is a powerful tool that can be used to obtain muscle

activity information, it has many limitations. EMG functions by measuring the electrical signals (action potentials) generated during muscle contractions. However, because there are many things going on in the body and surroundings at the same time, such as heart rate, other muscle activities, electrical sources, etc, noises are added to the true EMG signal. Some of the noises can be removed through post processing of the data, but others cannot. If the electrodes are placed too close to each other, cross-talk between the signals can occur. Therefore, there are many artifacts and limitations of EMG that hinder the accurate measurement of the muscle forces. Another important limitation of EMG is that it does not provide a quantitative measure of the muscle force [14]. It does not provide an exact muscle force, but the muscle activity is normalized by using the maximum voluntary contraction.

Animal models have also been used to study human lumbar spine. However, no other species have a vertebral column that is structurally similar to that of humans and used in a comparable manner. These animals are either not bipedal or do not habitually use their vertebral column in an upright posture [15]. For these reasons, *in vitro* human spine models, mathematical models and computer models were developed by the investigators to investigate the biomechanics of the lumbar spine. In this study, a mathematic model (optimization model) and a computer model (FE model) were primarily used. The purposes of using these models are analyzing the nature, distribution, and magnitude of forces exerted on the lumbar spine and back muscles, and predicting the changes in stresses that might occur in various postures and activities [15]. However, computer modeling also has many limitations. It is unrealistic for the model to perfectly match the real human spine; many assumptions and simplicities need to be made in the model. Thus, the model has to be validated by

comparing its results with the results from the literature data or experiments data in order to confirm their accuracy.

2.1 Anatomy of the lumbar spine and its function

The human spine is a long and slender column that functions to support body weight and external weight. It provides stability and flexibility to the body that allows the body to perform movement smoothly. It also provides a base for both the upper and lower extremities and protects the spinal cord. The human spine is composed of many components: spinal muscles, bony and cartilaginous elements, intervertebral disks, ligaments, tendons and fasciae. All these components work together to maintain the stability and flexibility of the spine.

The spine contains an abundant number of spinal muscles and they are organized in three layers: superficial, intermediate and deep as shown in Figures 2-1 to 2-4. The superficial layer contains latissimus dorsi (LD), external oblique (EO), internal oblique (IO) and rectus abdominis (RA). The intermediate layer contains erector spinae (ES) and serratus posterior inferior (SPI). The deep layer contains rotatores, intertransversarii, interspinales, quadratus lumborum (QL), psoas major (PM) and multifidi. Rotatores, intertransversarii and interspinales together are all called SIMs. Different back muscles have different orientations that determine their functions. Based on the location and orientation of a muscle, it can operate best as a flexor, an extensor, or a rotator. For example, the orientations of ES indicate they are back extensors. The function of these spinal muscles is to provide stability to the trunk in a given posture, to generate movement during physiologic activity and to protect the spine during trauma in which there is time for voluntary control.

In Bergmark's paper "stability of the lumbar spine", he divided the spinal muscles into local and global systems. The local system controls the curvature of the spine and provides sagittal and lateral stiffness to the lumbar spine to keep the spine

stable. This local system includes all the muscles in the deep layer with the exception of QL and PM [11]. These muscles are also called intrinsic muscular stabilizers and have their origin at the vertebrae. Their relative high density of the muscle spindles and short lumbar segments span enhance their fine-tuning ability [13]. The global system transfers the load between the thoracic cage and the pelvis [11]. It includes the rest of the muscles and these muscles are also called extrinsic muscular stabilizers. These muscles are relatively long and cross a broad region of the trunk, thus they are likely to provide relative coarse control over spinal stability. However, they are important torque generators that cause the spine to flex, extend and rotate [13].

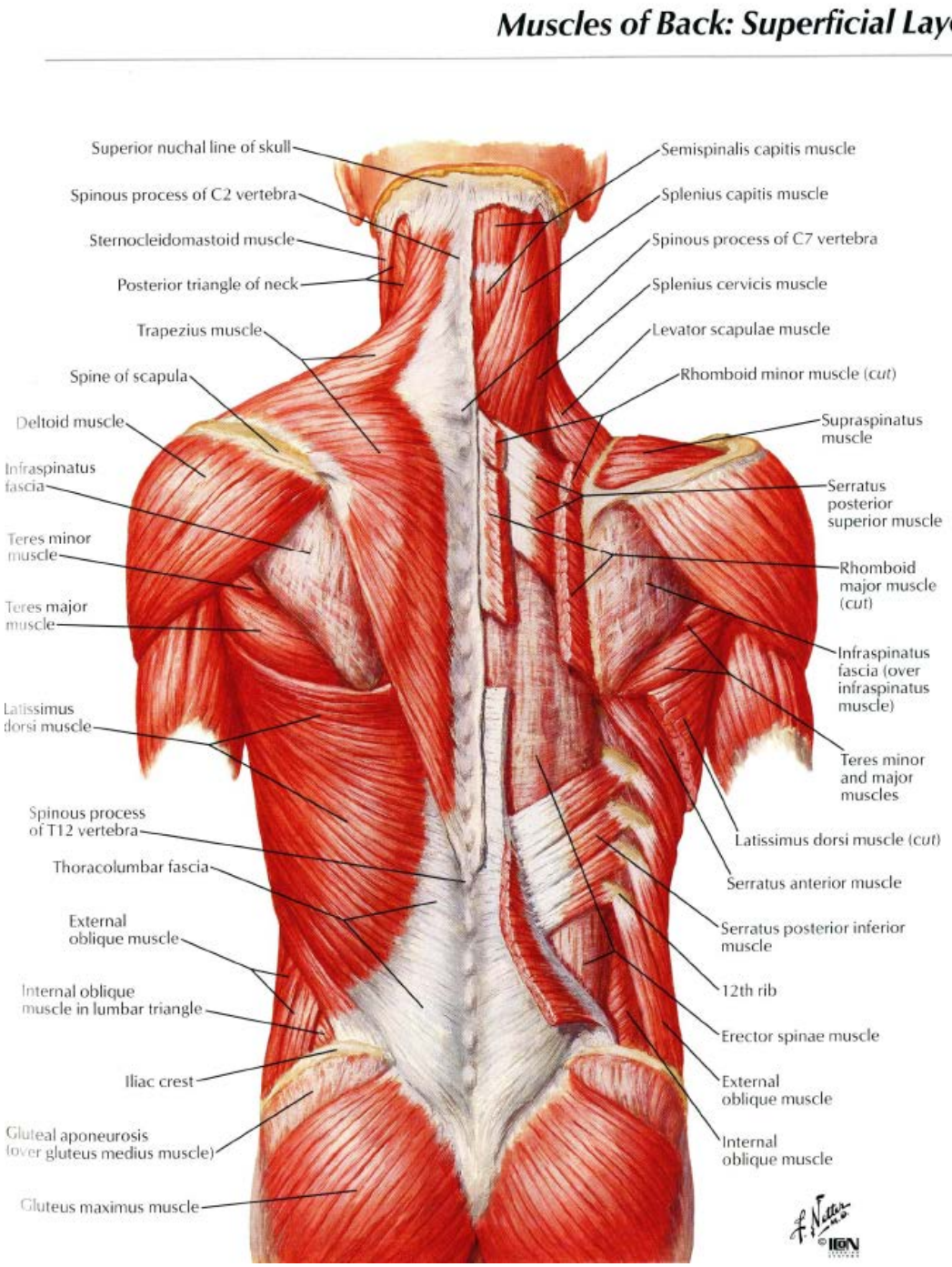

Figure 2-1 Anatomy of the superficial layer of the back muscles [16]

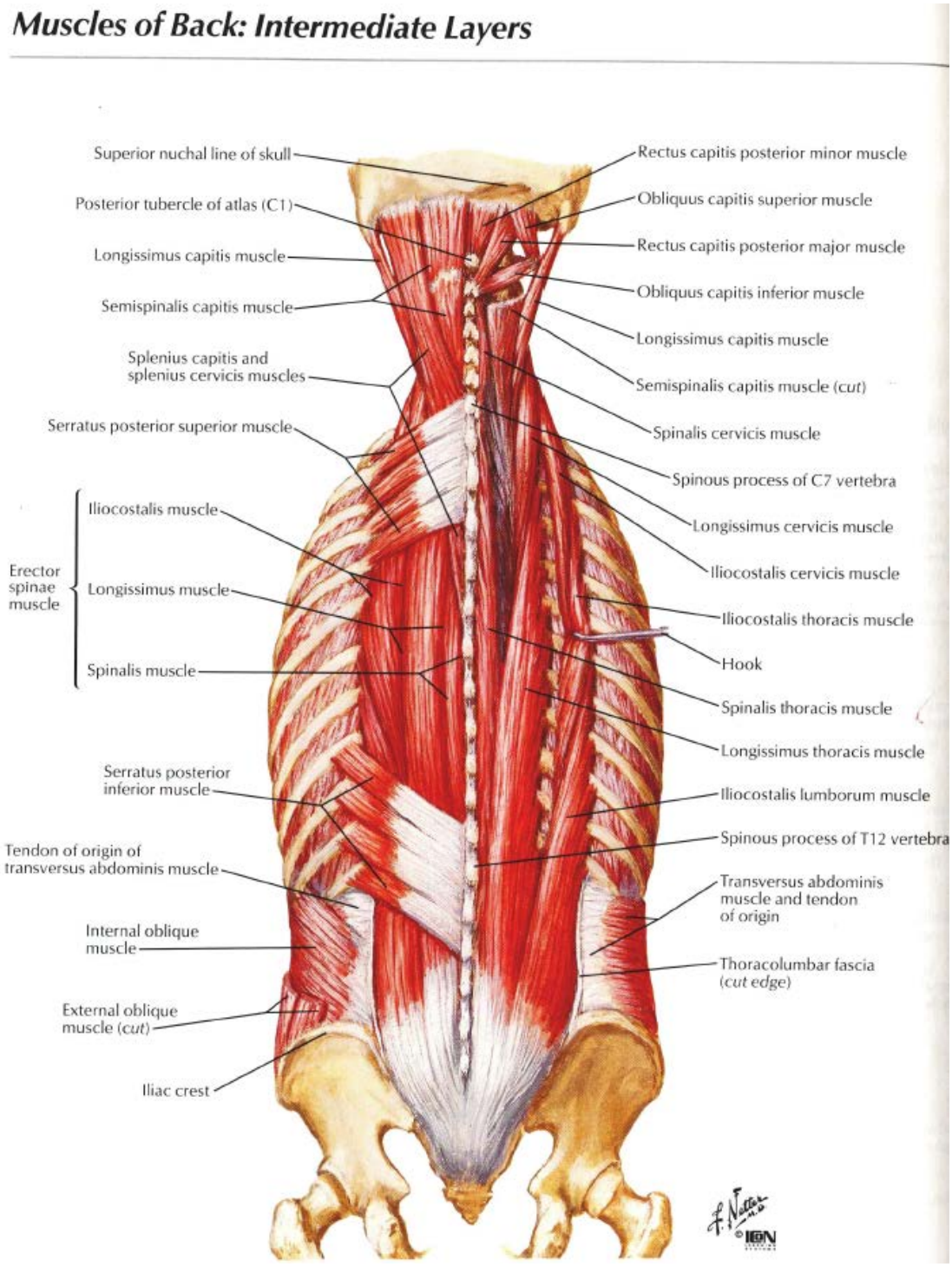

Figure 2-2 Anatomy of the intermediate layer of the back muscles [16]

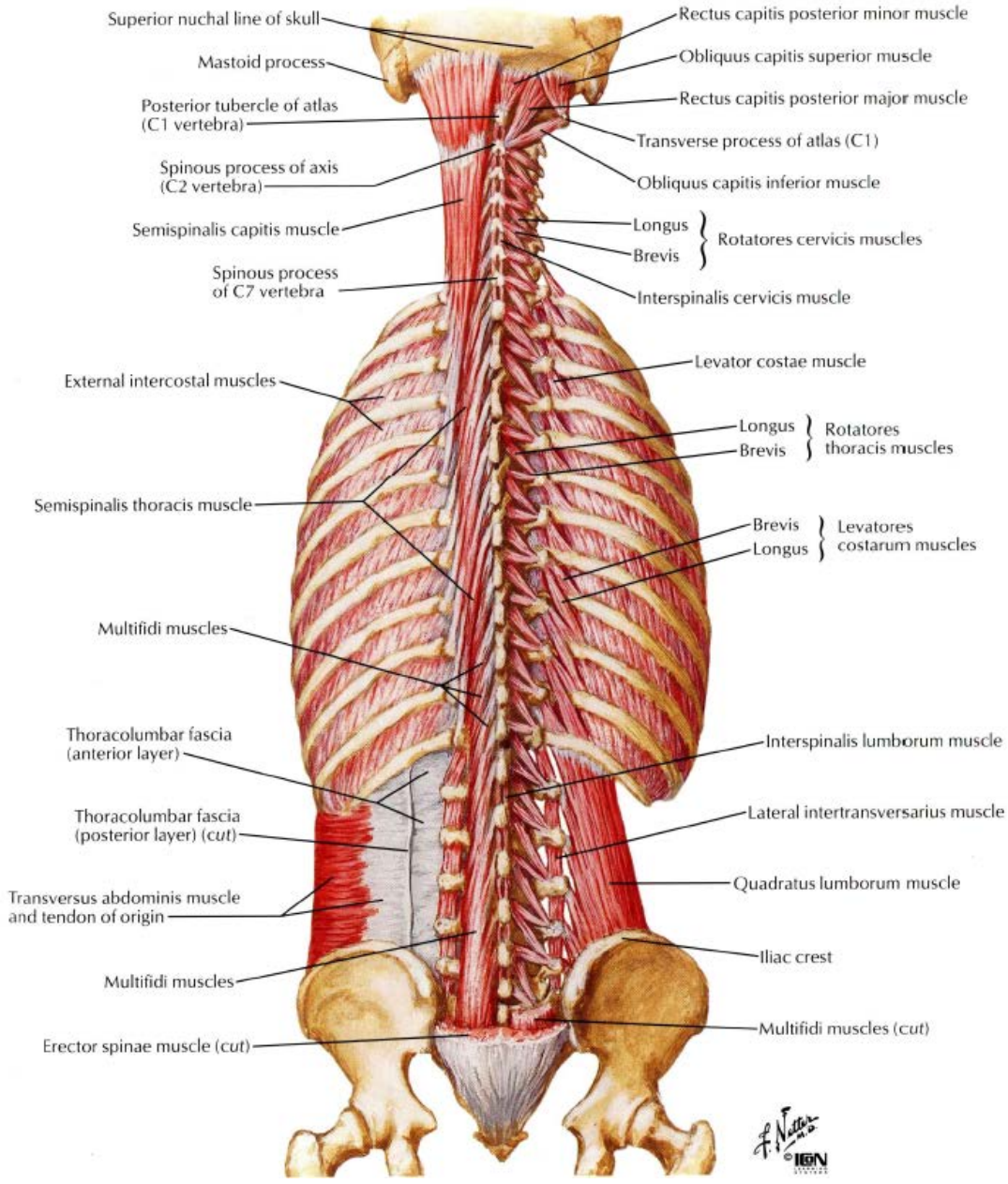

Figure 2-3 Anatomy of the deep layer of the back muscles [16]

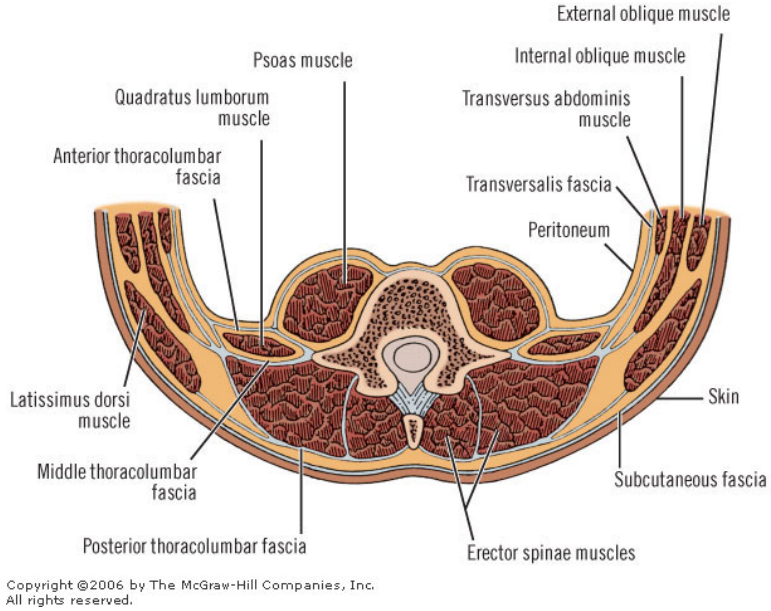

Figure 2-4 A superior view of a horizontal cross section of the lumbar spinal muscles [17]

Muscle contracts and relaxes through the activities of active proteins of the muscle, actin and myosin, and the force generated is called the active (or contraction) force. Other than generating active force, muscles also generate passive forces through the passive components: series elastic components and parallel elastic components shown in Figure 2-5. Series elastic components include tissues that lie in series with the active proteins of the muscle (actin and myosin), such as tendon and titin. Parallel elastic components include tissues that lie in parallel with the active protein of the muscle, such as the structural proteins. These passive components of the muscle come into play when the muscle is stretched or lengthened from its resting length shown in Figure 2-6. When the muscle is over stretched, these passive components eventually generate a larger tensile force than the active components of the muscle. The spinal muscles are called the active elements of the spinal stabilization system. This is because the muscle force is not dependent on the muscle length within the physiological range of motion (ROM). There is no unique relation

between the geometrical configuration of the muscle and its force [11].

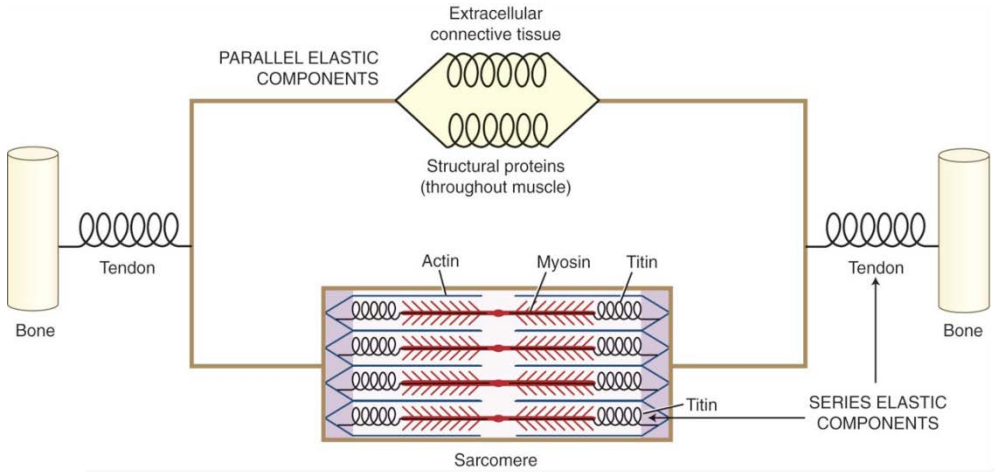

Figure 2-5 A highly diagrammatic model of a whole muscle attaching between two bones [13]

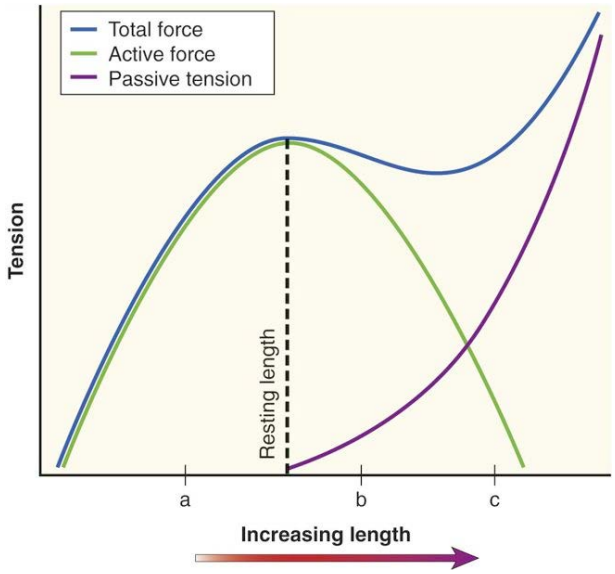

Figure 2-6 Length-tension curve for a typical muscle. At shortened lengths *(a)*, all force is generated actively. As the muscle fiber is stretched beyond its resting length *(b)*, passive tension begins to contribute to the total force. In *(c)* the muscle is further stretched, and passive tension accounts for most of the total force [13]

Other than the active element, the spinal stabilization system also contains the passive elements. These include bony and cartilaginous elements, ligaments, tendons

and fasciae shown in Figure 2-7. The deformation of these passive elements is only dependent on the force applied on the spine. The facet joint contains the articular facets and the capsular ligament. It stabilizes the intervertebral junctions, provides kinematic constraints to the movement of the motion segment and transfers forces. During flexion, it transfers tensile forces via capsular ligaments between the articular facets of two adjacent vertebrae. During extension, it transfers compressive forces via mechanical contact between the tips of the articular facets and the arc of the vertebra below [11]. The ligaments stabilize the spinal motion segment by providing resistance during excess moment, such as hyper-flexion or hyper-extension, of the vertebra [13].

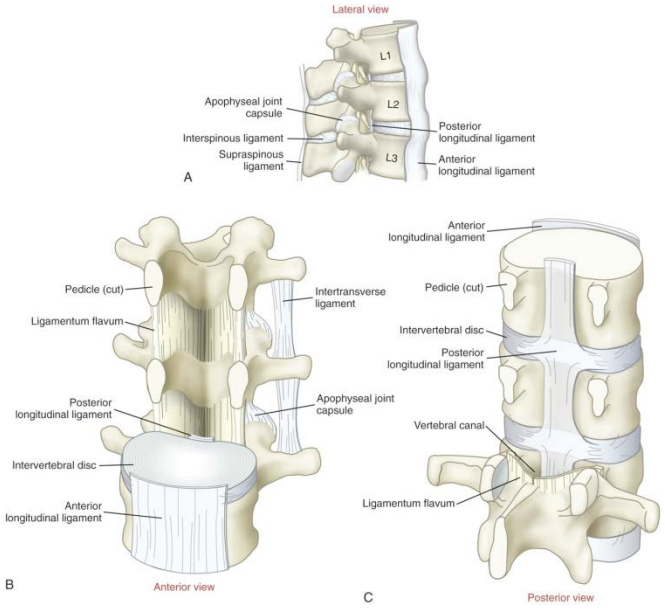

Figure 2-7 Anatomy of some of the passive elements of the spinal stabilization system [13]

The intervertebral disk is composed of nucleus pulposus, annulus fibrosis and cartilage end-plate as shown in Figure 2-8(a). The nucleus pulposus is a gelatinous matrix which contains 80%-90% of water and 15%-50% of collagen fibrils and it is well suited for withstanding compressive forces [18]. The annulus fibrosis is composed of 50%-60% collagen fibrils and they are organized in about 15 to 25 interlacing concentric layers that surround the nucleus pulposus [18]. These concentric layers are orientated about 45° to 65° from the vertical direction and the adjacent layers have their fibers running in the opposite directions as shown in Figure 2-8(b) [13]. Such construction of the annulus fibrosis helps the disk to resist against intervertebral distraction (vertical separation), shear (sliding) and torsion (twisting) effectively [13]. Thus, it is an important stabilizer for the spine. Other than its stabilizing function, the intervertebral disk also supports weight. For example, when a person is in a standing posture, approximately 80% of the load is supported by the lumbar vertebral bodies which are jointed with the intervertebral disk and the remaining 20% is supported by the posterior elements, such as apophyseal joints and laminae [13]. The intervertebral disk supports the load through hydrostatic pressure as shown in Figure 2-9. As a compressive load is applied to the disk, the nucleus pulposus will be compressed, since it cannot go anywhere due to the surrounding annulus fibrosis and it is incompressible, hydrostatic pressure will build up in it to support the load and provide shock absorption for the spine. On the other hand, this increased pressure elevates the tension in the annulus fibrosis and exert upward and downward forces to the cartilage end-plate [13].

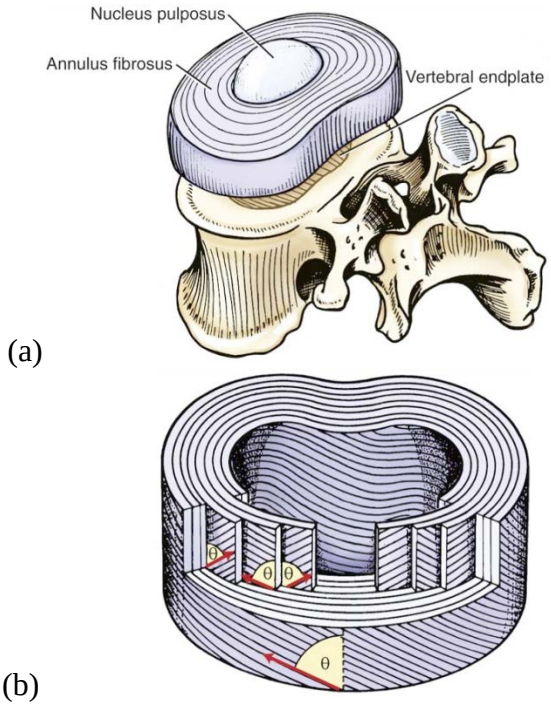

(a)

(b)

Figure 2-8 (a) Illustration of the intervertebral disk. (b) The detailed organization of the annulus fibrosis where θ refers to the orientation of each collagen fiber which is about 45° to 65° from the vertical [13]

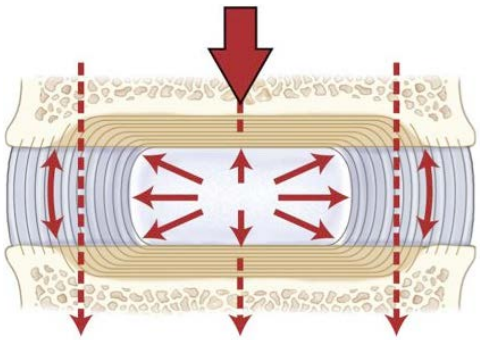

Figure 2-9 Mechanics of the intervertebral disk on force transmission. The pressure is evenly distributed to the surrounding tissues [13]

2.2 Spinal stability and load

In mechanics, stability is defined as the ability of a loaded structure to maintain static equilibrium even at small fluctuations around the equilibrium position [11]. It is not a continuous variable as the system is either stable or unstable. However, for physicians, stability is associated with clinical stability. According to White and Panjabi, clinical stability is defined as “the ability of the spine under physiological loads to limit patterns of displacement so as not to damage or irritate the spinal cord or nerve roots, in addition to prevent incapacitating deformity or pain due to structural changes” [5]. Since clinical stability is associated with the magnitude of the deformation when the spine is loaded, it is considered to be a continuous variable. The main difference between the two is that mechanical stability is only concerned about the ability of the spine to carry spinal loads while clinical stability also takes the clinical consequences of neurological deficit or pain of the spine into consideration [14].

To explain the whole spine stability system, Panjabi proposed that the spinal stabilization system is consisted of three subsystems (Figure 2-10): the spinal column which acts as a transducer that provides information about the mechanical status of the spine, the spinal muscles which acts as actuators and the neural control unit which evaluates and determines the stability of the spine and gives the corresponding commands to both the spinal column and the spinal muscle to perform actions to keep the spine stable [14]. It is widely accepted that the abnormal patterns of the spinal muscles or the mechanical insufficiency of the spinal column causes the neurological deficit or pain. However, the mechanics of the spine, how it stabilizes the spine while maintaining its flexibility, is still poorly understood.

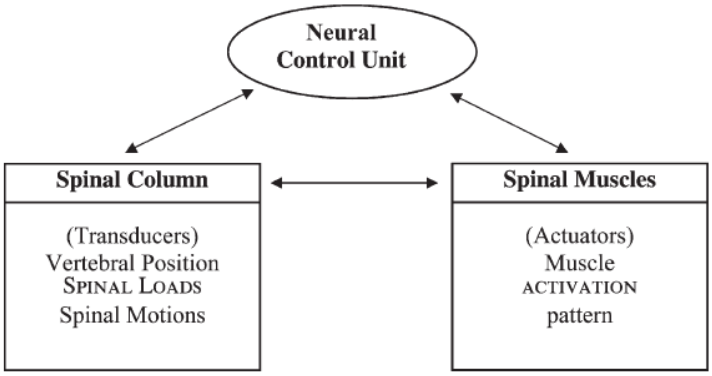

Figure 2-10 The spinal stabilizing system with the three subsystems [14]

In order to quantify the stability of the spine, researchers developed the "stability index" by assuming the spine to be a conservative system. The stability index is determined by minimizing the potential energy of the degrees of freedom for each intervertebral joint. This was done by taking the second derivative of the potential energy with respect to the generalized coordinates, thus a Hessian matrix is obtained. The spine is said to be stable if the determinant and the principal minors of the Hessian matrix is positive, which means the Hessian matrix is positive definite. The physical meaning of the stability index is the "root average" of the spine stiffness slope in all directions [19]. However, the problem with this method is that since the subjects went through these studies did not experience buckling of the spine *in vivo*, the stability index would always be positive definite in all these studies. Additionally, this method does not provide any information on the muscle control mechanism on the spine. Finally, it is questionable to consider the spine to be a conservative system.

2.3 Euler's Load vs. Follower Load

In 1744, Swiss mathematician Leonhard Euler developed mathematical theories to compute the maximum axial compressive load that a slender column can support before it buckles under different end constraints, an example is shown in Figure 2-11. This maximum axial compressive load is called the critical load [14]. When a load that is larger than critical load is applied to the slender column, the column will deflect which is called buckling. According to Euler's theory, the critical load is directly proportional to the stiffness of the column. Thus, a stiffer slender column will have a greater critical load. Based on this theory, Crisco et al. performed an *in vitro* experiment on human cadavers by applying a compressive vertical load and they found that the average critical load for the whole ligamentous lumbar spine was 88N [6]. However, based on Nachemson's *in vivo* measurement of the disk pressure, the load on the spine can be as high as 2100N. Since spinal muscles are activated during *in vivo* situation, researchers think that these muscles must act as guy wires to stiffen the spine and increase the critical load and stability of the spine.

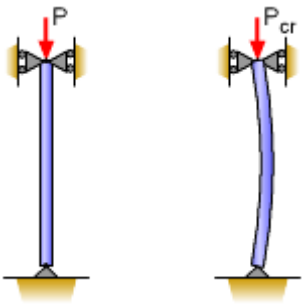

Figure 2-11 Euler's column and critical load [20]

The follower load concept was first introduced by Timoshenko, Gere and Bazant [21, 22]. It is defined that the direction of the applied compressive load is

tangential to the deflection curve of the beam as shown in Figure 2-12 [22]. In terms of buckling, Timoshenko showed that the critical load for a beam under follower load is significantly higher than the critical load for the Euler's column [21, 23]. Since the critical load of ligamentous lumbar spine under Euler's theory is significantly lower than the *in vivo* spinal load, follower load theory would be the mechanism the spine uses to obtain the high critical load *in vivo*.

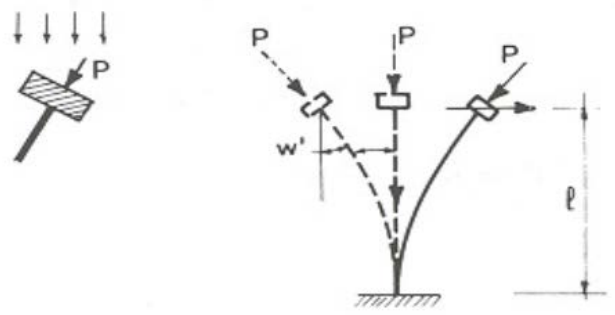

Figure 2-12 Beam loaded by a constant follower force [22]

In general, the internal forces in the lumbar spine or JRFs of the lumbar spine can be decomposed into axial direction and transverse (shear) direction as shown in Figure 2-13 (a). The forces along the axial direction are called axial compressive force and the forces along the transverse direction are called shear force. These internal forces are mostly caused by the activation of the muscle forces. If the muscle forces can minimize shear forces to zero at all lumbar spine levels, only axial compressive forces will be left as JRFs with their directions following the spinal curvature. Such axial compressive forces are called CFLs in this study also shown in Figure 2-13 (a). These CFLs vectors can pass through the GC of each vertebra, however, they do not always have to pass through the GC of each vertebra; they can be shifted around the

areas within the vertebra bodies as long as their directions follow the curvature of the spine as shown in Figure 2-13 (b). The distance between the GCs of the vertebrae to the CFLs is called follower load path (FLP).

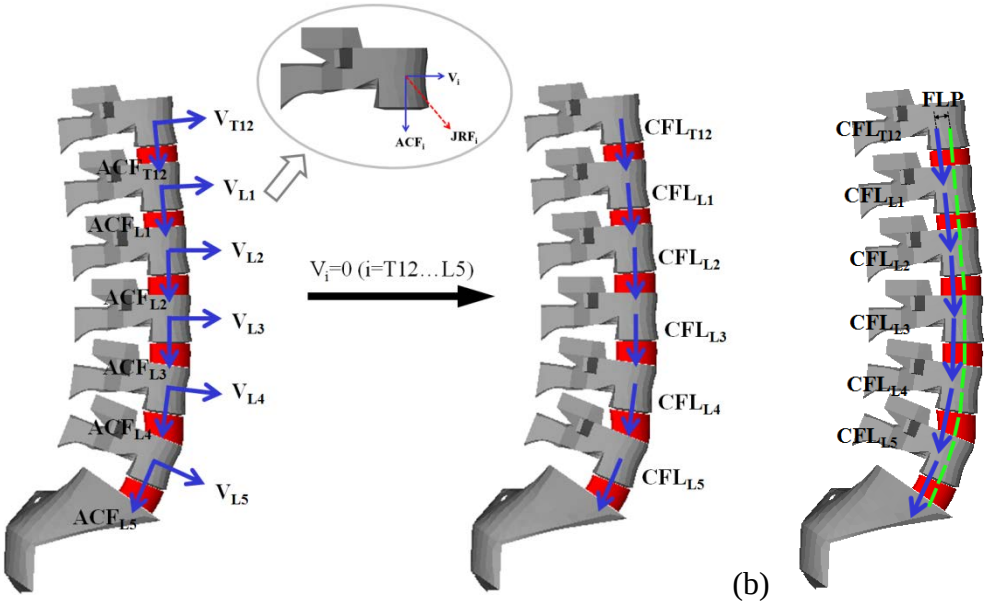

Figure 2-13 Schematic of the JRFs on the spine. When shear forces go to zero, the joint reaction forces (JRFs) become the compressive follower loads (CFLs). (ACF=axial compressive force; V=shear force; FLP=follower load path)

Patwardhan et al. adopted the follower load concept and conducted an *in vitro* study by applying the follower load using cables and dead weights bilaterally on the lumbar spine as shown in Figure 2-14 [8]. By applying the follower load, the resultant internal compressive load at each intervertebral joint is tangential to the curvature of the lumbar spine. The internal shear forces and bending moments at all lumbar levels are also minimized at the same time [8]. They found that the ligamentous lumbar spine supported a load up to 1200N without damage or instability while maintaining its flexibility under follower load [8]. Due to the limitation of the cable placement and

orientation, they only conducted their experiments in sagittal plane. However, since 1200N is much closer to the *in vivo* spinal load compared to 88N and the flexibility of the spine was maintained, their study suggested the feasibility of follower load mechanism to be the potential physiological mechanism operated by the spine.

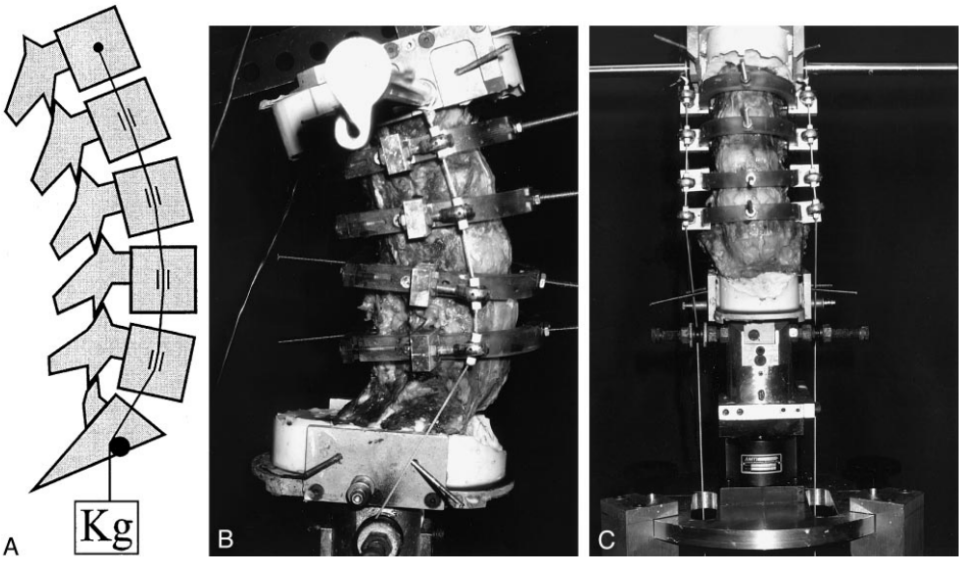

Figure 2-14 A human cadaveric lumbar spine subjected to a compressive follower load [8]

One significant limitation of their study is that their experiment did not include any spinal muscles, thus they did not show the feasibility of spinal muscles generating the internal CFL. Later on, they performed another study using a 2-D beam-column model of the lumbar spine in the frontal plane to study the role of the muscles. However, their model was very simplified; it only contained five spinal muscles and a single column to represent the spine. The SIMs was absent in their model and they did not impose any physiological bounds on the muscle forces as they did not formulate the model as an optimization problem [24].

Kim and Kim's group further investigated the follower load mechanism on the spine by developing a 3-D FE lumbar spine model and solved the problem as an optimization problem. Their model included 117 pairs of trunk muscles and among the 117 pairs, 59 pairs were deep muscles. The sacrum-pelvis was fixed and an upper body weight of 300N plus 3Nm of flexion moment were applied to T12; additionally a vertebral weight of 10N was added to each lumbar vertebra from L1 to L5. The squared sum of all the resultant joint forces (follower forces and shear forces) and joint moments were minimized. However, they could not find perfect follower load from their results as shear forces were always present in their solutions. Thus, they called their results as modified follower load since they contain shear forces [25, 26].

Han et al.'s group also further investigated the follower load as the potential mechanism the spine uses to stability itself. They developed a 3-D static model of the lumbar spine and used an optimization technique to solve the muscle forces and the CFLs. Their model contains 116 pairs of spinal muscles, and out of the 116 pairs, 27 pairs were SIMs. The sacrum-pelvis was fixed in the sagittal plane and an upper body weight of 350N was applied at the center of gravity (CG) of the trunk. The summation of the follower load and joint moment at all lumbar levels were minimized. Their results showed that it is feasible for the spinal muscles to create pure CFLs in neutral posture. This means the shears forces were zero at all lumbar levels. However, they only performed their study in neutral posture and also they did not show the stability and flexibility of the lumbar spine under pure CFLs [27, 28].

Following Han et al.'s study, Kim et al. developed a 3-D FE model of the lumbar spine incorporating the same 116 pairs of spinal muscles and the same boundary and loading conditions. By applying the muscle forces obtained from the

optimization analysis, the FE model was able to check the deformation of the spine under the CFLs created by the spinal muscles. The deformation of the spine caused the displacement of the trunk and they defined spinal stability as the displacement of the trunk that is smaller than 10mm. They found that the spine could be stabilized under CFLs in neutral posture. In addition, they also performed studies on flexion and extension postures. They found that it is feasible for the spinal muscles create CFLs and stabilize the spine in flexed postures. However, they could not find spinal muscles create CFLs that stabilize the spine in extended postures.

In this study, the feasibility of the spinal muscles create internal CFLs and stabilize the spine in neutral standing, flexion, extension, lateral bending and axial rotation are studied. Only by proofing the spinal muscles are able to create CFLs and stabilize the spine in all 3-D postures while maintain its flexibility, follower load can be concluded as the potential normal physiological load on the spine.

CHAPTER 3

METHODS

A FE model together with a 3-D optimization model was used for this study. Both models consisted the trunk, the sacrolumbar spine, the spinal ligaments and 244 (122 pairs) spinal muscle fascicles (4 SPI, 14 LD, 12 EO, 12 IO, 48 longissimus, 24 iliocostalis, 12 PM, 10 QL, 8 RA, 6 spinalis thoracis, 40 multifidi, 12 interspinales, 20 intertransversarii and 22 rotatores). The FE model provided the geometrical data of the spinal muscles, which was used to obtain the force vectors of spinal muscles, to the optimization model. The optimization model calculated all the muscles forces and JRFs and moments through force balances, moment balances and follower load constraints. These muscle forces were then imported back into the FE model to check if the spine could be stabilized under these muscle forces by using explicit computational analysis. The whole process is presented in Figure 3-1. An upper body weight of 350N was applied on both models as a concentrated force at 10mm in front of the GC of the T12 vertebra. Sacrum-pelvis was fixed in both models as the boundary condition. Five different postures were studied: neutral standing, flexion 40°, extension 5°, lateral bending 30° and axial rotation 10° shown in Figures 3-2 and 3-3.

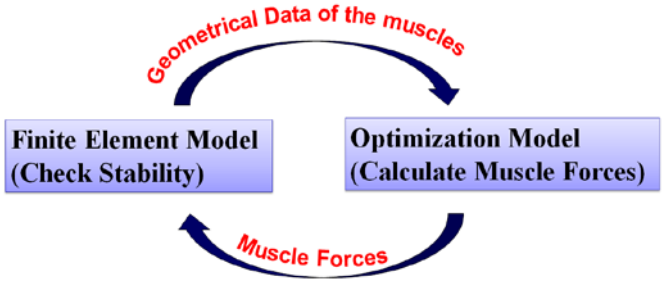

Figure 3-1 Schematic diagram of the correlation between the FE model and the optimization model. The geometrical data obtained from FE was used as the input for the optimization model to calculate muscle forces, and the muscle forces were then imported back to the FE model to check the stability of the spine

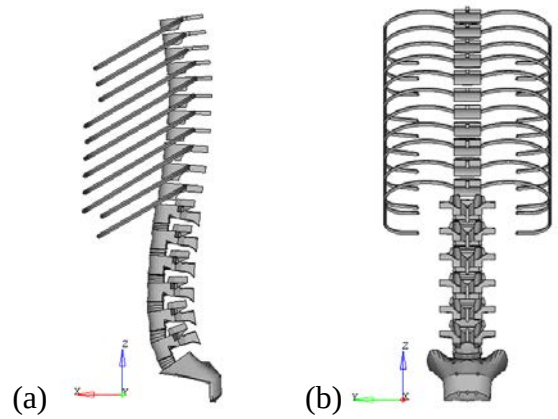

(a) (b)

Figure 3-2 Schematic diagrams of neutral posture (a) side view (b) back view, with the corresponding global coordinate system

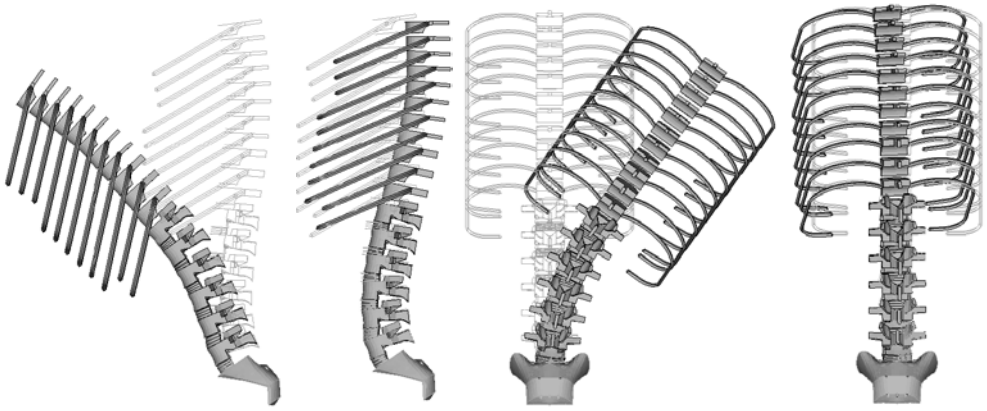

(a) (b) (c) (d)

Figure 3-3 Schematic diagrams of different postures performed in this study (a) flexion 40°, (b) extension 5°, (c) lateral bending 30°, (d) axial rotation 10°

3.1 The 3-D FE Spinal Model

Finite element software, LS-DYNA version 971, was used to build the FE spine model. This model was originally developed by Kim et al., but it is edified for this study [29]. The FE model is consisted of eight rigid bodies (trunk, six vertebrae (T12-L5) and sacrum-pelvis) connected by six intervertebral joints as shown in Figure 3-4(a). Each intervertebral joint contains one intervertebral disc and two facet joints. The intervertebral disc was modeled using nonlinear elastic 8-node element, whereas facet joints were modeled using non-linear compression-tension spring elements shown as blue lines in Figure 3-4(b). These spring elements allowed both compression and tension in order to mimic the mechanical properties of apophyseal joint (bony contact and capsular ligament). The trunk was connected to the L1 vertebra through T12-L1 intervertebral joint. The trunk and the vertebrae were modeled as rigid bodies and the intervertebral discs were modeled as deformable bodies which allowed segmental motion due to deformation

All spinal ligaments, except anterior longitudinal ligament (ALL), posterior longitudinal ligament (PLL), and capsular ligament, were modeled using a single tension spring element on each functional spinal unit (FSU) shown as red lines in Figure 3-4(b). Only tensile forces were generated by these spring elements since spinal ligaments were considered to be the passive elements of the spinal stability system. They could not generate compressive force, but only tensile force during elongation. The effects of ALL and PLL were incorporated in the disc material properties [23].

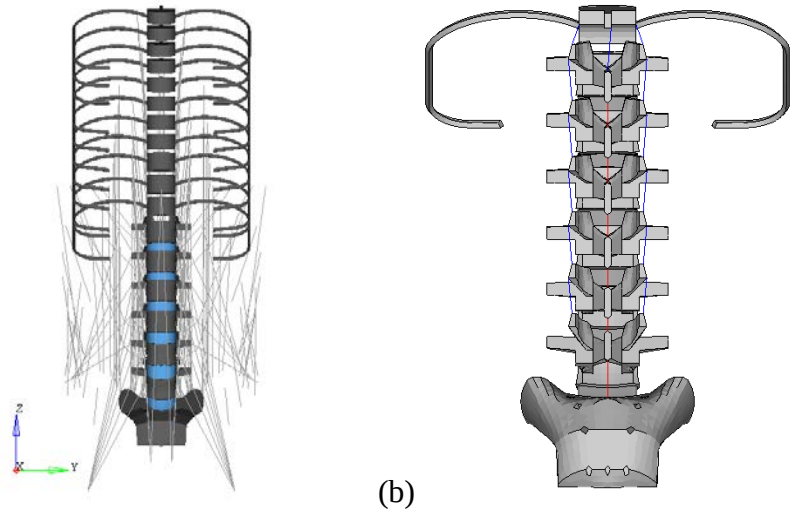

(b)

Figure 3-4 (a) Schematic diagram of the FE model. (b) Blues lines are the modeled facet joints which resist both compression and tension. Red lines are the modeled spinal ligaments which only resist tension

All the muscles were modeled using tension spring elements. The muscle forces calculated in this study indicate that such force vectors are required to create follower load in the spine and need to be made by spinal musculature (contraction and passive forces). Figure 3-5 illustrates all the spinal muscles that were incorporated in the FE model. All three layers of spinal muscles were included in this study. Different from many other studies, 54 deep SIMs (intertransversarii, interspinales and rotatores) were also incorporated in our models. These are deep muscles that span one or two FSU shown in Figure 3-5. For the long muscles that span three or more motion segments, wrapping points were created that these muscles were forced to pass through several nodes rigidly attached to various vertebrae. These wrapping points are necessary to represent more accurate muscle lines of action during various spinal motions.

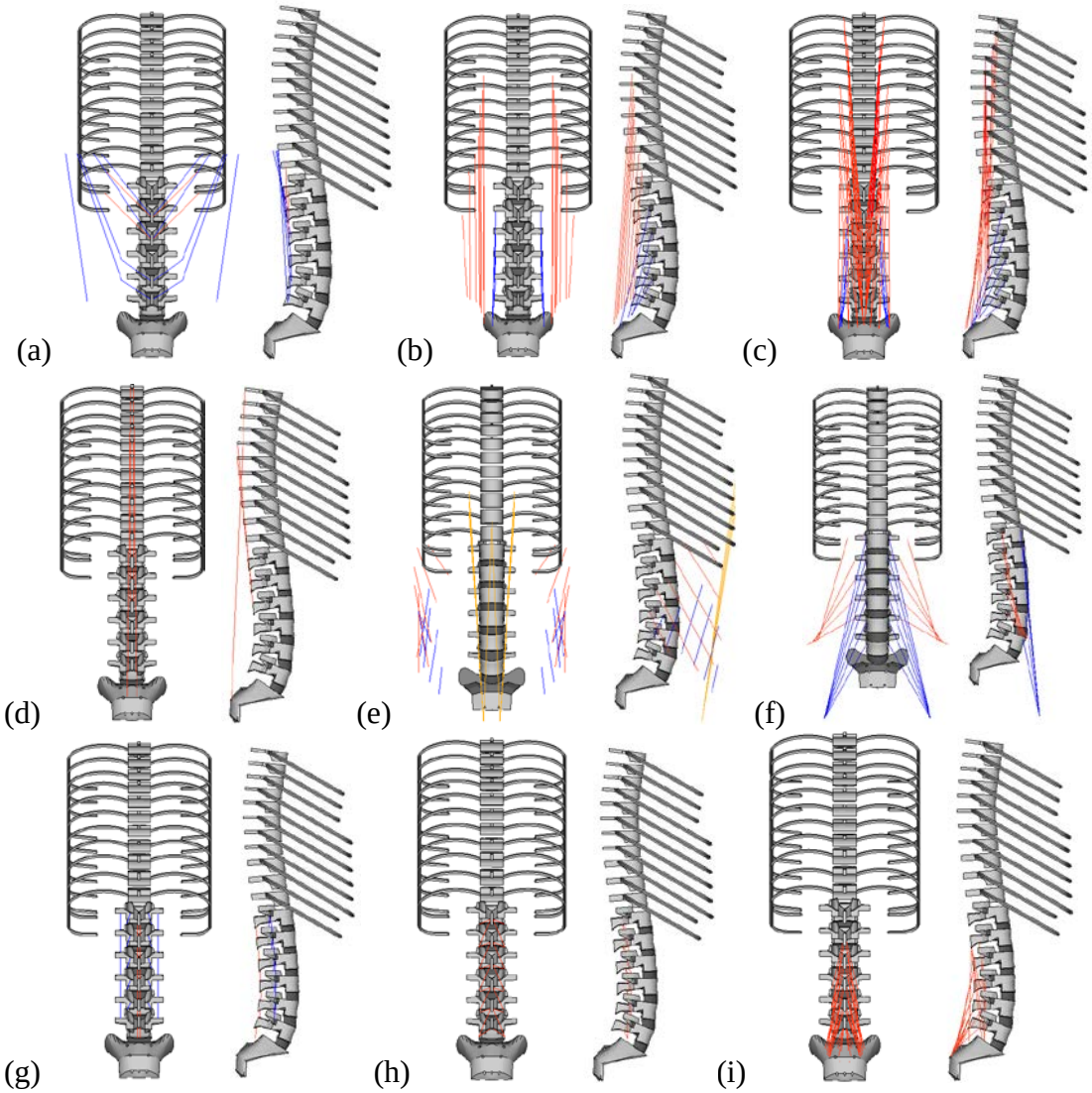

Figure 3-5 Schematic diagrams of the FE model with each muscle group. (a) Blue: LD (14 muscle fascicles); Red: SPI (4 muscle fascicles); (b) Blue: iliocostalis pars lumborum (8 muscle fascicles); Red: iliocostalis pars thoracis (16 muscle fascicles); (c) Blue: longissimus pars lumborum (10 muscle fascicles); Red: longissimus pars thoracis (38 muscle fascicles); (d) Red: spinalis thoracis (6 muscle fascicles); (e) Blue: EO (12 muscle fascicles); Red: IO (12 muscle fascicles); Yellow: RA (8 muscle fascicles); (f) Blue: PM (12 muscle fascicles); Red: QL (10 muscle fascicles; (g) Blue: intertransversarii(20 muscle fascicles); Red: interspinales (12 muscle fascicles); (h) Red: rotatores (22 muscle fascicles); (i) Red: multifidi (40 muscle fascicles)

The lordosis of the FE model of the lumbar spine in neutral posture was 50 degrees using Cobb's angle, measured between the superior end plates of L1 and S1

shown in Figure 3-6. The changes in lordosis for different postures in sagittal plane were compared to the lordosis for neutral posture shown in Figure 3-6. Each line was created by connecting the GC of each vertebra in that posture. It was a challenge to define the lordosis in neutral posture since people have different lordosis in neutral posture and lordosis can change within the same person depending on the age, weight, health, and etc. Adults without LBP have lumbosacral lordosis, measured by using Cobb's angle, approximately 56.6±9.1 degrees [30, 31]. Since there is a wide range of the degrees in lordosis between people, the lordosis of neutral posture for one person could be the lordosis of flexion or extension for another person. Hence, depending on how the lordosis in neutral posture was defined, the lordosis of extension 5° in this model can be actually extension 10° for a person.

Figure 3-6 The Cobb's angle (L1-S1) is shown as 50° in neutral posture. The lordosis for flexion 40° (blue line), extension 5° and extension 10° (red lines) were compared to the lordosis for neutral standing (black line).

The FE model of the ligamentous lumbar spine was validated by comparing the ROM of the spine in sagittal plane at each FSU with those measured in *in-vivo* and *in-vitro* studies [23, 29]. Also, in order to check the accuracy of the FE model, the results obtained from the optimization model have to match the results obtained from the FE model. Thus, the ROM of each FSU from the optimization model was

calculated and compared to the output data (ROM) from the FE model for each posture. The JRFs from both models for each posture were also compared. It was found that the results of the ROMs and JRFs from both models agreed with each other for all the postures.

Different postures were created in the FE model by applying pure moments on the neutral posture in different axes. All the different postures analyzed in this study are shown in Figure 3-2 and 3-3. The exact 3-D orientations for all the postures are shown in Table 3-1. Figure 3-2 shows that x-z plane forms the sagittal plane, y-z plane forms the coronal plane and x-y plane forms the transverse plane. X-axis directs front and back with front as positive, y-axis directs left and right with left as positive and z-axis directs up and down with up as positive. Rotation around x-axis produces lateral bending, rotation around y-axis produces flexion and extension and rotation around z-axis produces axial rotation. For the rotations, right hand rule was used to determine a positive or a negative rotation. Thus, positive lateral bending corresponds to right lateral bending and negative lateral bending corresponds to left lateral bending. Positive axial rotation refers to left axial rotation and negative axial rotation refers to right axial rotation. Flexion is positive and extension is negative. One reason that these postures are not perfectly one-dimensional rotation, e.g. flexion 40° has slightly lateral bending and axial rotation instead just flexion, was because the FE spine model was not perfectly symmetric sagittally. The surface of the FE spine model was obtained from the CT-scan of a skeleton model. This skeleton model was not perfectly symmetric sagittally, however this should not be a problem since in reality human beings are not perfectly symmetric sagittally and as a result the rotation in one plane is always couple with rotations in other planes.

Table 3-1 The 3-D orientation for each posture in this study

	Flex 40° (deg)	Ext 5° (deg)	Ext 10° (deg)	LB 30° (deg)	AR 10° (deg)
x-rotation (LB)	0.35	0.00	-0.02	30.02	-2.55
y-rotation (FLEX-EXT)	39.72	-5.58	-10.26	-2.99	-0.89
z-rotation (AR)	-0.02	0.02	0.05	-1.52	10.02

The FE analyses were performed to investigate how much the trunk sways (i.e., translation of the CG of the upper body) with respect to the fixed sacrum after applying the muscle forces that were predicted in the optimization model for all five postures. A trunk sway of less or equal to 5mm in all directions, which is about 1.5 degrees in both trunk roll and trunk pitch angle, was considered to be stable for all postures. *In vivo*, trunk sway can be very different depending on the person's physical condition, age, posture, and etc. 5mm is reasonable choice since other studies have shown that with standing on two legs, eyes open and under normal support; the trunk pitch angle for a healthy middle-aged person is about 1.5 degrees [32]. Bended postures may have higher trunk sway than normal standing posture.

3.2 Development of the 3-D Optimization Spinal Model

Musculoskeletal system is an indeterminate problem since the number of unknowns is greater than the number of the equations. An optimization model was developed to solve for all the unknowns. T12 to S1 of the lumbar spine were considered in the model. There were 244 unknown muscle forces, 6 unknown compressive spinal loads (T12-L1 lumbar level to L5-S1 lumbar level), 18 unknown joint reaction moments (moments around x, y, and z axis at each level) and 21 unknown compressive FLP locations (x, y, z coordinates of the FLP at each T12 to S1 vertebra) shown as ρ in Figure 3-7. With all these unknowns, there were 36 equality constraints of force and moment balances: 18 force balances and 18 moment balances at T12 to L5 shown in equations 3.2 and 3.3. This optimization problem was solved by using What's Best! 11.0. 1.0, Lindo Systems, INC.

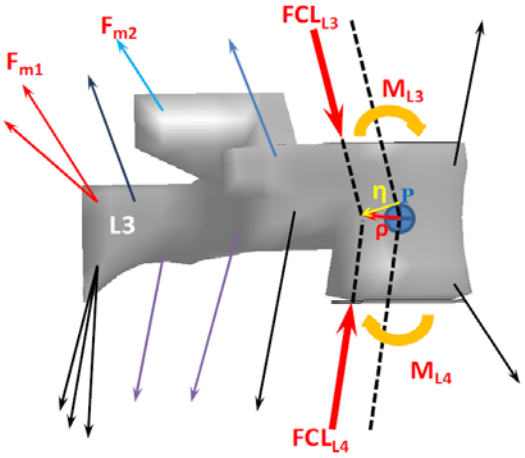

(a)

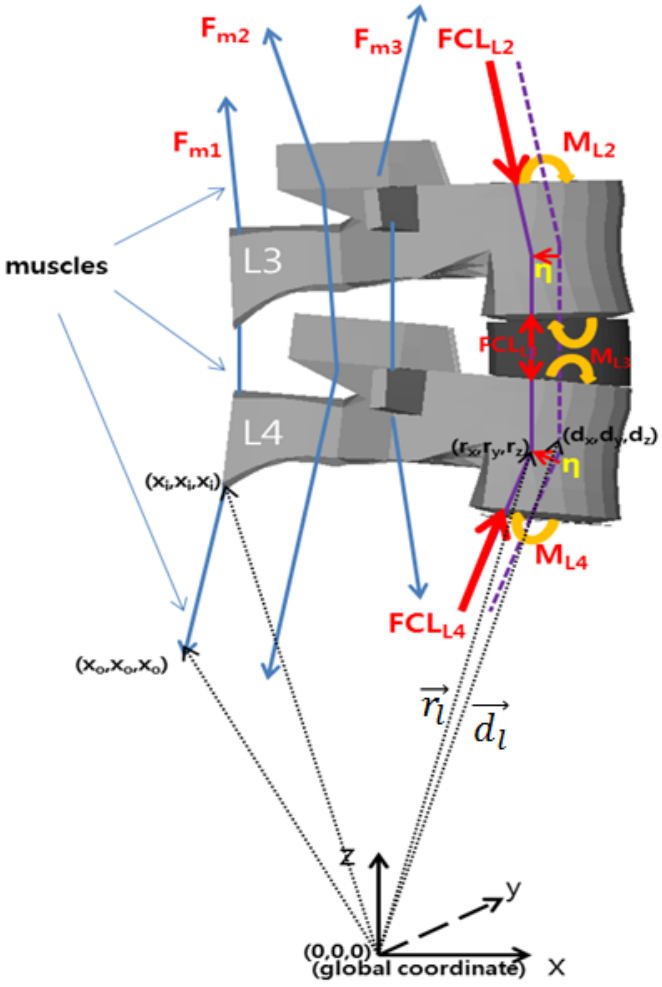

(b)

Figure 3-7 Schematic diagrams of the free body diagram used in the optimization model where the force balances and the moment balances were formulated. The directions of the JRFs are parallel to the lines connecting the center of the vertebrae body to create the follower load constraint.

3.2.1 Cost Function

Many cost functions have been developed in previous researches to calculate the muscle forces, such as minimization of the sum of muscle forces, minimization of the sum of muscle stresses, minimization of the sum of squared muscle stresses, minimization of modulus of the joint reaction force, and etc [33]. However, it remains unclear which cost function is the most physiologically acceptable. Parnianpour et al. compared six cost functions and they found that each cost function may highlight one particular aspect of this redundant biomechanical system of human spine. For example, sum of the muscle forces tends to recruit muscles with the largest moment arms; sum of muscle stresses encourages more synergistic muscle recruitment, and etc [33]. In this model, minimization of the summation of the CFLs and joint reaction moments was used as shown in equation 3.1. This cost function enhances the margin of safety of the passive system since the endplate is the first anatomical structure to fail at neutral posture [33]. Also, protection of the lumbar spine system was chosen to be the first importance in this study compared to the minimization of the total amount of muscle forces. This is because muscles can generally be trained or strengthened to generate more forces, but the intervertebral disc or the endplates cannot be trained to support more forces.

$$min(f) = \sum_{l=1}^{7} \| F_l^{jt} \| + \sum_{l=1}^{7} \| M_l^{jt} \| \tag{3.1}$$

where F_l^{jt} and M_l^{jt} are the intervertebral JRFs and moments on the *l-th* vertebra. The JRFs refer to pure CFLs in this study. Again, CFL is defined as the directions of the JRFs are parallel to the lines connect the GCs of the two adjacent intervertebral bodies

as shown in Figure 3-7. It can also be defined as the JRFs are tangential to the curvature of the lumbar spine shown in Figure 2-13.

3.2.2 Equality Constraints

The equality constraints contain 18 force balance and 18 moment balance equations shown in equations 3.2 and 3.3.

- Force balance (18 equations):

$$\sum_{k=1}^{6} \vec{F}_{k,l}^{m} + \sum_{k=1}^{6} \vec{F}_{k,l}^{ext} + \vec{F}_{l}^{jt} + \vec{F}_{l+1}^{jt} = 0 \quad (l = 1, \dots, 6) \tag{3.2}$$

- Moment balance (18 equations):

$$\sum_{k=1}^{6} \vec{r}_{k,l}^{m} \times \vec{F}_{k,l}^{m} + \sum_{k=1}^{6} \vec{r}_{k,l}^{ext} \times \vec{F}_{k,l}^{ext} + \vec{\rho}_{k,l}^{jt} \times \vec{F}_{l}^{jt} + \vec{\rho}_{k,l+1}^{jt} \times \vec{F}_{l+1}^{jt} + \sum_{k=1}^{6} \vec{M}_{k}^{jt} = 0 \quad (l = 1, \dots, 6) \tag{3.3}$$

where $\vec{F}_{k,l}^{m}$ and $\vec{F}_{k,l}^{ext}$ are the muscle forces and external forces on the *l-th* vertebra. $\vec{r}_{k,l}^{m}$ and $\vec{r}_{k,l}^{ext}$ are the moment arms of the muscles and the external forces, which are the vectors from the center of the *l-th* vertebra body to the muscle attachment points for $\vec{r}_{k,l}^{m}$ and to the point where external force is applied for $\vec{r}_{k,l}^{ext}$. $\vec{\rho}_{k,l}^{jt}$ are the moment arms of the intervertebral joint forces, which are the vectors from the center of the *l-th* vertebra body to the point where two joint forces from *l+1-th* vertebra and *l-1-th* vertebra intersect (see Figure 3-7(a)). $\vec{\rho}_{l}$ is also referred as FLP in this paper and calculated as:

$$\vec{\rho}_l = \vec{r}_l - \vec{d}_l$$

(3.4)

where $\vec{r}_l$ is the position vector from the origin of the global coordination system to the point where two joint forces from (*l+1)-th* vertebra and (*l-1)-th* vertebra intersect shown in Figure 3-7(b). $\vec{d}_l$ is the position vector from the origin of the global coordination system to the center of the *l-th* vertebra body shown in Figure 3-7(b).

3.2.3 Follower Load Constraints:

Six follower load constraints were formulated to indicate the direction of the compressive spinal load at each level has to be parallel to the line joining the GC of the two adjacent vertebral bodies to create the pure CFLs shown in equation 3.5 and Figures 3-7 and 2-13.

$$(\vec{r}_{l+1} - \vec{r}_l) \,//\, (\vec{d}_{l+1} - \vec{d}_l) \qquad (l = 1, \dots, 6)$$

(3.5)

To write this constraint mathematically, parallel equation was used. If $\vec{u}_{(l+1)-l}$ is the unit vector of $(\vec{d}_{l+1} - \vec{d}_l)$, $\vec{r}_{l+1}$ can be calculated by multiplying this unit vector with a certain magnitude and then add $\vec{r}_l$ shown in equation 3.6. An initial value of $\vec{r}_{T12}$ needed to be chosen as the starting point for the optimization.

$$\vec{r}_{l+1} = \vec{r}_l + s_l \vec{u}_{(l+1)-l}$$

(3.6)

where $\vec{u}_{(l+1)-l}$ is the unit vector of $(\vec{d}_{l+1} - \vec{d}_l)$. *s* is the length of $(\vec{r}_{l+1} - \vec{r}_l)$. The shortest distance between the two parallel lines is the line that perpendicular to both

lines and this distance has to be the same everywhere between the parallel lines. If the shortest distance vector is directed from CFLs intersection point to vector ($\vec{d}_{l+1} - \vec{d}_l$) and named as $\vec{\eta}_l$ (see Figure 3.7), then the length of $\vec{\eta}_l$ has to be the same at all lumbar levels show in equation 3.7. Because the shortest distance is the distance perpendicular to both parallel lines, equation 3.8 has to hold true.

$$\| \vec{\eta}_l \| = \| \vec{\eta}_{l+1} \| = \| \vec{\eta} \| \qquad (l = 1, \dots, 6) \tag{3.7}$$

$$\vec{\eta}_l \cdot \left(\vec{d}_{l+1} - \vec{d}_l\right) = 0 \tag{3.8}$$

3.2.4 Inequality Constraints

Many inequality constraints were formulated to restraint the muscle forces and FLP ranges. The absolute muscle force has to be between zero and the maximum force the muscle can generate, shown in equation 3.9. The maximum force capacity was chosen to be 45N/cm^2 for all the back muscles [34-36]. For detailed calculation on the maximum forces of the muscles, please see Han et al. [27]. The absolute values of the muscle forces were used in this model; they included both the active and the passive forces of the muscles. The FLP has to be between zero (the vertebrae center) and the most outer part of the vertebrae body (approximately 15mm) shown in equation 3.10. The range of s was set to be between 20mm and 50mm corresponding to the vertebra height shown in equation 3.11.

MFC: $0 \leq \left\|\vec{F}_j^m\right\| \leq F_{max}^m \quad (j = 1, \ldots, 244)$

(3.9)

Range of FLP: $0 \leq \| \vec{\rho} \| \leq 15$

(3.10)

Magnitude of each interval: $20 \leq s_l \leq 50 \quad (l = 1, \ldots, 6)$

(3.11)

3.3 Analyses Procedures

Both FE and optimization models were used to find CFL creating muscle forces that stabilize the spine. As explained at the beginning of this Chapter, geometrical data of the FE lumbar spine models in the five different static postures (described in Section 3.1), and their corresponding muscles and ligaments attachment points, were provided to the corresponding optimization model as input data. The optimization model then used these data to predict the muscle forces and patterns required to generate CFLs at all lumbar spine levels. Following that, the muscle forces predicted from the optimization analysis were imported to the corresponding FE model as muscle force input data. FE analysis was then performed to investigate the amount of trunk sway (translation of the CG of the trunk resulted from the applied muscle forces). The lumbar spine was considered to be in stable condition if the resultant trunk sway is less or equal to 5 mm in any direction.

It was proposed that there was more than one muscle pattern available to create CFLs at all lumbar spine levels in a given posture. In order to find these different CFLs creating muscle patterns at a given posture, the FLP values in the optimization model was set to different values. As the FLP was set at a different value, the CFLs creating muscle forces and patterns would be different. For example, the muscle forces and patterns solved at FLP equal to zero would be different from the results solved at FLP equal to 2mm. Due to this reason, numerous optimum solutions of CFLs creating muscle forces could be found for all postures. However, not all the optimum solutions could stabilize the spine, the optimum solutions obtained close to the base FLP , where $\rho = 0$mm, were found to be able to stabilize the spine in all postures.

Another important issue studied was about the roles of SIMs in lumbar spine stabilization system since SIMs were rarely incorporated in previous studies of the spinal muscles. For this purpose, SIM components were removed from both the optimization models and the FE models for all postures. The same analysis procedure was then repeated to investigate if there were still muscle forces and patterns feasible to create CFLs at all lumbar spine levels and stabilize the spine in all simulated postures. To simplify the process, the SIM study was only done at the base FLP, which was at $\rho = 0$mm. The predictions of the FE and the optimization models with no SIMs were then compared with those obtained from FE and optimization models with SIMs.

A heuristic approach was made when finding other possible muscle recruiting patterns that can stabilize the spine while keeping the follower load constraint. First, few random FLPs that were close to the GC of the vertebra were picked to check the feasibility of other solutions. After it was found that there were other feasible muscle recruiting patterns available, a more strategic plan was made to find the trend of these feasible solutions. First, a random FLP point along the positive x-axis was chosen as the start point shown as D in Figure 3-8. Then, trial and error was performed to solve for the muscle forces until these muscle forces produced a trunk sway about 5mm in the FE model. For example, in Figure 3-8, if the muscle forces obtained from the optimization model at point D produce a trunk sway less than 5mm in the FM model, a FLP point further along the positive x-axis would be chosen; e.g. point C in this example. If the muscle forces solved at point C cause a trunk sway greater than 5mm in the FE model, a FLP point closer to point D would be chosen for the next trial, e.g point B in this example. This process would be repeated until a FLP point was found

that the muscle forces creating CFLs along this FLP cause a trunk sway approximately equal to 5mm in the FE model.

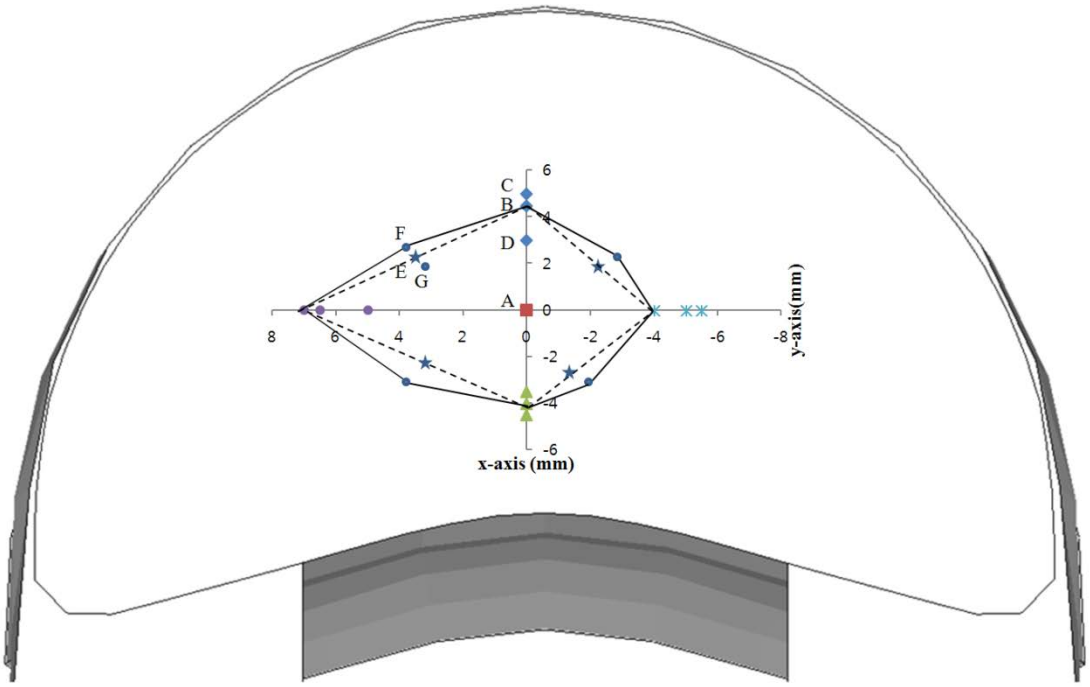

Figure 3-8 An illustration of the trial and error method used to find the limiting FLP points in x and y axes. This picture is a transverse section of the vertebral body with the posterior side cut off and it is not drawn in scale. The FLP points in this picture are not the FLP points that were used in the study, but they were only for illustration purpose.

Second, a random FLP point along the negative x-axis was chosen and the same trial and error process was performed until a FLP point was found that the muscle forces generating this FLP could stabilize the spine shown in Figure 3-8. After finding the two limiting FLP points along the x-axis, the same process was done for the y-axis to find another two limiting FLP points (Figure 3-8). After finding the four limiting points in x and y axes, these points were joined together with straight lines in Excel, shown as dash lines in Figure 3-8. Random FLP points on the four straight lines (stars on Figure 3-8) were then picked to check if there would be muscle

recruiting patterns feasible to stabilize the spine at these points. The same trial and error protocol used to find the limiting FLP points was then used to find the limiting FLP points along the line, shown as E, F, and G on Figure 3-8. In this figure, F was shown to be the limiting FLP point along the line. From this procedure, an additional four limiting FLP points would be found. All the eight points were then joined together by straight lines forming a boundary shown in Figure 3-8. The area within the boundary for each posture is called stable FLP range in this paper. It was assumed that any FLP within the boundary would have muscle recruiting patterns feasible to stabilize the spine. On the other hand, there would not be any feasible solutions available outside the boundary. To test this hypothesis, random FLP points were picked both inside and outside this boundary to test the feasibility of the solutions.

3.4 Parametric Studies

Variations in the *in-vivo* spinal system affecting the *in-vivo* stability of the lumbar spine can be found in numerous aspects. For example, there are numerous muscle contraction patterns available to keep the same posture. Cholewicki et al. found that one individual used his muscles in a quite different way from other subjects during the experiment [37] . The maximum muscle forces can also vary significantly from individual to individual. Other possible individual variations can be found in the external weight (body weight and handling weight) and the stiffness of the spinal segment. The impact of such variations on the lumbar spine stability achieved through the follower load mechanism should also be investigated in order to claim that the CFLs are physiological load in the lumbar spine *in-vivo*. In this study, the following parametric studies were conducted to investigate the effect of variations in the body weight and the segmental stiffness on the feasibility of CFL construction by the spinal muscle forces.

3.4.1 Body Weight Variation

The first part of the parametric study is to find how the results, such as muscle recruiting patterns, muscles forces, JRFs, and joint reaction moment, would change with the variation in the body weight. Four different body weights were studied: 50kg, 70kg, 80kg and 90kg. If the percentage of the trunk is chosen to be 50% of the body weight, the upper body weight of these different weights would be 25kg, 35kg, 40kg and 45kg. To perform this study, the upper weight of the body was simply changed to each interested weight in both the FE model and the optimization model. The maximum trunk weight where CFLs could be created was also studied for all the

postures. This was done by continually increasing the body weight in both models until no solution could be found in the optimization model or the spine buckled in the FE model.

3.4.1 Disk Property Variation

The second part of the parametric study is to understand how the changes in the segmental stiffness can affect the biomechanics of the spine under follower condition. Since the disc stiffness change is known to vary the segmental stiffness and L4-L5 and L5-S1 levels are the most common places for disk degeneration, studies on these two levels were performed. As the disk degenerates, the nucleus pulposus becomes dehydrated and thus exerts less hydrostatic pressure when compressed [13]. To simulate this condition, the non-linear elastic young's modulus of the disks was reduced by 25% and 50% respectively. Four cases were tested: 25% and 50% reduction in disk modulus at L4-L5 level and 25% and 50% reduction in disk modulus at L5-S1 level. Since the optimization model does not contain any information about disk property, these changes were incorporated in the FE model.

CHAPTER 4

MODEL PREDICTIONS AT FLP=0 MM AND SIM STUDY

In all five postures, it was feasible to obtain optimum solutions of muscle forces creating reaction forces along numerous curves parallel to the spinal curvature (or satisfying the constraint (equation 3.5)). However, a large movement of trunk, indicating the buckling-like or unstable behavior of the lumbar spine, was predicted from FE analyses in response to the application of the optimum muscle forces creating JRFs with minimum magnitudes. On the other hand, the optimum solutions of muscle forces obtained by constraining the location of the JRFs along a curve located in the vicinity of the line connecting the GC of the vertebral bodies (ρ (in Figure 3-7) < 3 mm) were predicted to cause stable deformation in the lumbar spine in all five postures.

When constraining the direction and location of JRFs along the lines joining the GC of the vertebral bodies (ρ=0 mm), optimization solutions for CFLs were feasible from the models with all spinal muscles including the deep SIMs for all five postures. The muscle forces required to create CFLs with ρ=0 mm in neutral, 40° flexed, 5° extended, 30° right laterally bent and 10° left axially rotated spines in Figure 4-1 and Table 4-1. The predicted forces of the other muscles not listed in these Tables were zero. Under the action of these muscle forces and upper body weight, FE model predictions in all five postures showed that the spine was able to be stabilized. This was determined by small displacement of the trunk (0.5 – 1 mm) due to small deformation of the lumbar spine. Table 4-1 also shows the total force for each back muscle layer of each posture. Although the addition of the force magnitudes without

considering the force directions is not appropriate for vector addition, these total forces can be used to approximately compare the relative contribution of muscle forces in different layers since the directions of spinal muscle forces are not drastically different among each other. It was found that the total force of SIM forces was generally larger than the total force of all the other muscle forces in all the other muscle layers. For example, in neutral posture, the total forces of all muscles in the superficial, intermediate, deep, and deep short intrinsic layers were 157 N, 179 N, 0 N, and 371 N, respectively. 371N was larger than all the other muscle layer total forces and a similar trend was observed for most other postures. Thus, the comparison of these total forces clearly demonstrate the significant contribution of deep SIM forces for the stabilization of the lumbar spine in all five postures by creating the JRFs along the spinal curvature.

When the SIMs were removed, optimization solutions were also feasible in all five postures as shown in Figure 4-1 and Table 4-2. However, compared to the cases with SIMs, it was predicted that the JRFs increased substantially (48 – 78%) in all postures as shown in Figure 4-2. The increase in JRFs was significantly larger in extension 5° and axial rotation 10° compared to neutral posture and flexed postures. Such increases in JRFs resulted from the forces in more ES and multifidus required to create internal axial compressive JRFs in the lumbar spine. Table 4-2 also showed that when the deep SIMs were removed, the total forces were increased in all the other muscle layers for all five postures. For example, in neutral posture, the total forces in the superficial, intermediate and deep layers were 157 N, 179 N, and 0 N, respectively with SIMs, but increased to 266N, 510N and 140N respectively when the SIMs were removed. This increase in total force of each muscle layer increased the total JRFs for

each posture. Furthermore, FE model predictions under these muscle forces demonstrated an increase in the displacement of the trunk in all postures from those under muscle forces predicted from the optimum models with SIMs. For example, the trunk displacements with and without SIM contributions were 0.5 mm and 1.1 mm in neutral, 0.7mm and 1.6mm in flexion, 0.8mm and 2.1mm in LB, and 0.7mm and 7.3mm in AR, respectively. In case of extension 5°, the trunk displacement increased to 18.7mm from 1mm while the increase in JRFs was largest in all lumbar levels. These results indicate that it would be very challenging to maintain the lumbar spine in extended posture particularly without SIM force contribution.

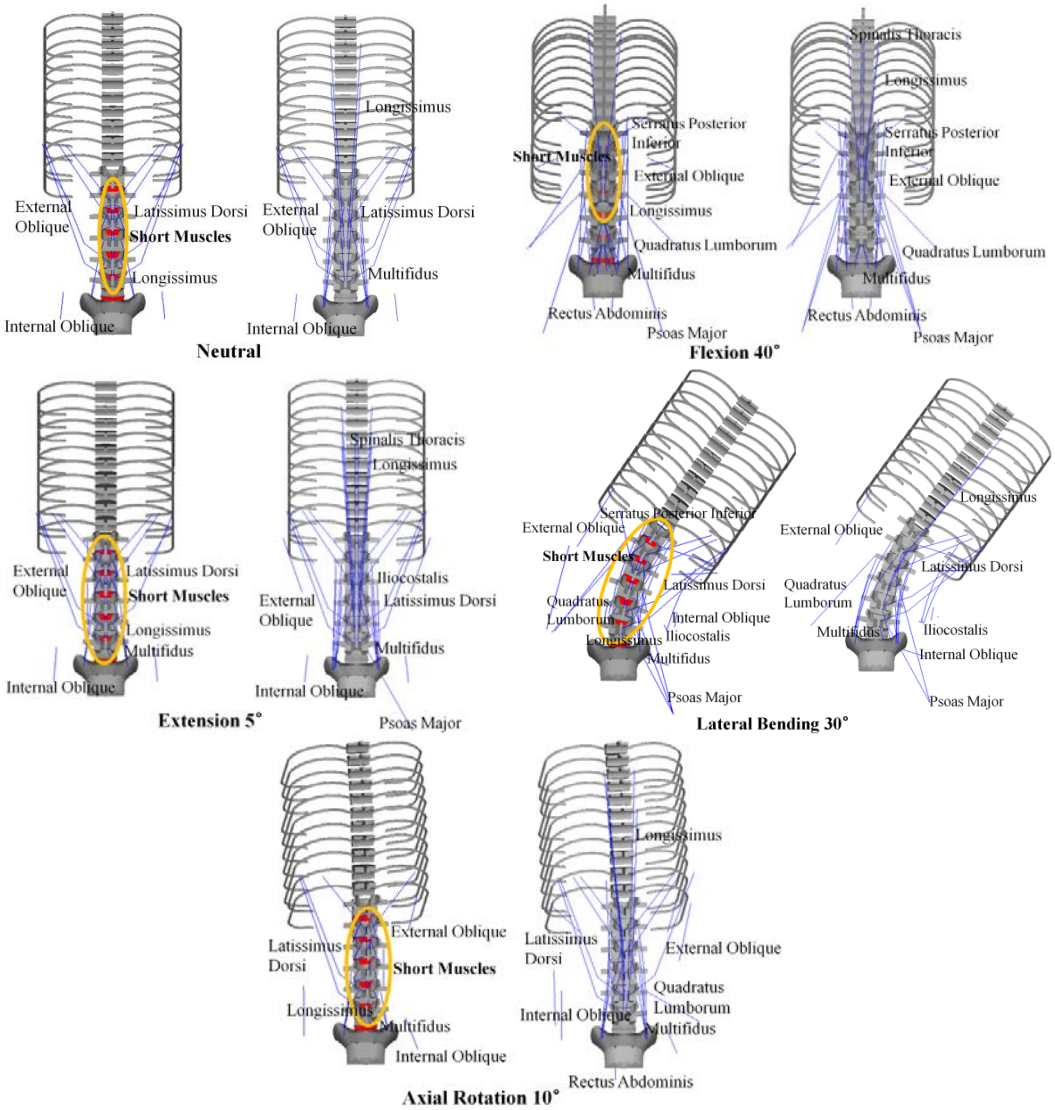

Figure 4-1 Activated spinal muscles creating CFLs in various postures, with SIMs and without SIMs. The ellipse circles the SIMs

Table 4-1 Recruited muscles for all the postures with SIM; all the muscle fibers that are not included here are having zero force. All these muscle forces are in Newtown (N). Each of the muscles is represented by its origin and insertion points. For example, LD L1_Humerus means the LD fascicle with origin on L1 and insertion on humerus. L is left, R is right, Me is mediales, La is lateales and F is fascicles. ∑MF refers to total muscle force in each layer for all postures.

Layer	Recruited Muscles	Neutral	Flex. 40°	Ext. 5°	LB 30°	AR 10°
Superficial	**LD**					
	L1_Humerus_L	69	0	85	0	78
	L1_Humerus_R	69	0	85	59	85
	L2_Humerus_L	31	0	17	0	0
	L2_Humerus_R	31	0	17	20	0
	L3_Humerus_L	11	0	37	0	31
	L3_Humerus_R	11	0	37	43	0
	L4_Humerus_L	5	0	0	0	25
	L4_Humerus_R	5	0	0	25	0
	Abdominal Muscles					
	Rectus Abdominis_L	0	18	0	0	0
	Rectus Abdominis_R	0	13	0	0	0
	External Oblique_L	12	88	49	31	1
	External Oblique_R	12	88	49	192	47
	Internal Oblique_L	29	0	28	0	4
	Internal Oblique_R	29	0	28	207	43
	∑MF	314	207	432	577	314
Intermediate	**Longissimus pars Thoracis**					
	Sacrum_Rib11_R	0	46	0	0	0
	Sacrum_Rib12_R	0	11	0	0	0
	L3_T3_L	0	35	0	0	0
	L3_T3_R	0	24	0	0	0
	Sacrum_T12_L	0	58	0	0	0
	Longissimus pars Lumborum					
	Sacrum_L3_L	0	0	27	0	3
	Sacrum_L3_R	0	0	27	88	0
	Sacrum_L4_L	98	31	129	0	108
	Sacrum_L4_R	98	33	128	178	88
	Sacrum_L5_L	81	0	107	0	57
	Sacrum_L5_R	81	0	107	72	35

Table 4-1 Continued

Layer	Recruited Muscles	Neutral	Flex. 40°	Ext. 5°	LB 30°	AR 10°
Intermediate	**Iliocostalis pars Thoracis**					
	Sacrum_Rib12_R	0	0	0	20	0
	Serratus Posterior Inferior					
	L1_Rib11_L	0	82	0	0	0
	L1_Rib11_R	0	75	0	0	0
	L2_Rib12_L	0	0	0	20	0
	∑MF	360	395	523	378	291
Deep	**Multifidus**					
	Sacrum_L4_F1	0	3	0	0	0
	Sacrum_L4_F1_L	0	30	0	0	0
	Sacrum_L4_F1_R	0	30	0	0	0
	Sacrum_L5_F1_R	0	27	0	0	0
	Sacrum_L5_F2_L	0	45	0	0	0
	Sacrum_L5_F3_L	0	17	0	0	0
	Sacrum_L5_F3_R	0	59	0	0	0
	Sacrum_L5_F4_R	0	0	0	144	76
	Psoas Major					
	Femur_L2_L	0	22	0	0	0
	Femur_L2_R	0	37	0	0	0
	Femur_L3_R	0	0	0	30	0
	Femur_L4_R	0	0	0	2	0
	Femur_L5_R	0	0	0	71	0
	Quadratus Lumborum					
	Pelvic_L1_L	0	0	0	7	0
	Pelvic_L2_L	0	1	0	72	0
	Pelvic_L3_L	0	16	0	0	0
	Pelvic_L3_R	0	15	0	0	0
	∑MF	0	302	0	326	76
Deep SIM	**Intertransversarii**					
	L1_T12_La_R	0	4	0	45	0
	L1_T12_Me_L	0	45	0	0	0
	L1_T12_Me_R	0	45	0	0	0

Table 4-1 Continued

Layer	Recruited Muscles	Neutral	Flex. 40°	Ext. 5°	LB 30°	AR 10°
Deep SIM	L2_L1_La_R	0	0	0	45	0
	L2_L1_Me_L	0	22	0	45	5
	L2_L1_Me_R	0	32	0	0	0
	L3_L2_La_L	0	0	12	0	0
	L3_L2_La_R	0	0	12	45	22
	L3_L2_Me_L	0	0	44	0	35
	L3_L2_Me_R	0	0	45	45	0
	L4_L3_La_L	0	0	45	0	8
	L4_L3_La_R	0	0	45	7	8
	L4_L3_Me_L	45	0	45	0	45
	L4_L3_Me_R	45	0	45	45	27
	L5_L4_La_L	0	0	0	45	31
	L5_L4_Me_L	45	0	45	21	32
	L5_L4_Me_R	45	0	45	45	45
	Rotatores					
	L1_T12_L	45	0	45	45	45
	L1_T12_R	45	0	45	8	45
	L2_T12_L	0	0	45	45	26
	L2_T12_R	0	0	45	0	45
	L2_L1_L	45	0	36	45	45
	L2_L1_R	45	1	36	19	42
	L3_L1_L	34	0	14	0	39
	L3_L1_R	34	0	14	28	45
	L3_L2_L	19	0	45	9	27
	L3_L2_R	19	0	45	0	39
	L4_L3_L	0	43	0	0	5
	L4_L3_R	0	45	0	40	0
	L5_L4_R	0	0	0	45	0
	Sacrum_L5_L	0	5	0	0	0
	Interspinales					
	L2_L1_L	17	45	45	11	11
	L2_L1_R	17	20	43	45	28
	L3_L2_L	45	0	45	45	0
	L3_L2_R	45	0	45	45	45
	L4_L3_L	45	0	45	40	45
	L4_L3_R	45	0	45	45	45

Table 4-1 Continued

Layer	Recruited Muscles	Neutral	Flex. 40°	Ext. 5°	LB 30°	AR 10°
Deep SIM	L5_L4_L	14	0	35	0	0
	L5_L4_R	14	0	35	0	27
	∑MF	709	307	1091	903	862

Table 4-2 Recruited muscle fascicles for all the postures without SIM; Muscle fibers that are not included here are having zero force. All these muscle forces are in Newtown (N). Each of the muscles is represented by its origin and insertion points. For example, LD L1_Humerus_L means the left LD fiber with origin at L1 and insertion on the humerus. L is left, R is right, Me is mediales, La is lateales and F is fascicles. ∑MF refers to total muscle force in each layer for all postures.

Layer	Recruited Muscles	Neutral	Flex. 40°	Ext. 5°	LB 30°	AR 10°
Superficial	**LD**					
	L1_Humerus_L	76	0	85	0	62
	L1_Humerus_R	76	0	85	51	85
	L2_Humerus_L	26	0	60	0	48
	L2_Humerus_R	26	0	60	57	58
	L3_Humerus_L	43	0	43	0	43
	L3_Humerus_R	43	0	43	43	18
	L4_Humerus_L	5	0	25	0	25
	L4_Humerus_R	5	0	25	18	0
	Abdominal Muscles					
	Rectus Abdominis_L	0	33	0	0	4
	Rectus Abdominis_R	0	28	0	0	0
	External Oblique_L	71	88	192	88	85
	External Oblique_R	71	88	192	192	192
	Internal Oblique_L	45	0	72	0	129
	Internal Oblique_R	45	0	72	188	28
	∑MF	532	237	954	637	777
Intermediate	***Spinalis***					
	L2_T5_L	0	19	23	0	0
	L2_T5_R	0	78	27	0	0
	Longissimus pars Thoracis					
	Sacrum_Rib11_L	0	26	0	0	0
	Sacrum_Rib11_R	0	58	0	0	0

Table 4-2 Continued

Layer	Recruited Muscles	Neutral	Flex. 40°	Ext. 5°	LB 30°	AR 10°
Intermediate	L3_T3_L	26	13	68	0	2
	L3_T3_R	26	23	65	89	76
	L4_T4_L	0	0	0	0	54
	L4_T5_L	0	0	65	0	88
	L4_T5_R	0	3	68	19	0
	L5_T6_L	58	0	70	0	70
	L5_T6_R	58	0	70	0	70
	Sacrum_T11_L	0	58	0	0	0
	Sacrum_T11_R	0	49	0	0	0
	Sacrum_T12_L	0	25	0	0	0
	Longissimus pars Lumborum					
	Sacrum_L1_L	2	0	32	11	11
	Sacrum_L1_R	2	0	35	21	13
	Sacrum_L2_L	46	0	88	0	59
	Sacrum_L2_R	46	0	88	61	67
	Sacrum_L3_L	89	0	182	0	143
	Sacrum_L3_R	89	0	181	88	129
	Sacrum_L4_L	140	71	269	0	268
	Sacrum_L4_R	140	76	269	179	196
	Sacrum_L5_L	123	0	216	0	201
	Sacrum_L5_R	123	0	216	220	184
	Iliocostalis pars Thoracis					
	Sacrum_Rib11_R	0	0	0	1	0
	Sacrum_Rib12_R	0	0	0	58	0
	Iliocostalis pars Lumborum Sacrum_L1_L	0	0	2	0	0
	Sacrum_L2_L	0	0	6	1	0
	Sacrum_L2_R	0	0	6	0	0
	Sacrum_L3_L	0	0	0	122	0
	Sacrum_L4_L	0	1	0	22	0
	Serratus Posterior Inferior					
	L1_Rib11_L	0	57	0	0	0
	L1_Rib11_R	0	54	0	0	0
	L2_Rib12_L	0	3	0	0	0
	∑MF	968	615	2046	892	1631

Table 4-2 Continued

Layer	Recruited Muscles	Neutral	Flex. 40°	Ext. 5°	LB 30°	AR 10°
Deep	**Multifidus**					
	L4L1_F4_L	70	0	58	61	66
	L4L1_F4_R	70	3	57	70	57
	L5_L2_L	0	0	41	0	2
	L5_L2_R	0	0	41	0	0
	Sacrum_L4_F4_R	0	0	0	17	0
	Sacrum_L5_F3_L	0	53	0	0	0
	Sacrum_L5_F3_R	0	62	0	0	0
	Sacrum_L5_F4_L	0	35	0	0	0
	Sacrum_L5_F4_R	0	30	0	54	0
	Psoas Major					
	Femur_L1_L	0	26	0	0	0
	Femur_L1_R	0	38	0	0	0
	Femur_L2_L	0	29	0	0	0
	Femur_L2_R	0	36	0	0	0
	Femur_L3_R	0	4	0	123	0
	Femur_L5_R	0	0	1	58	0
	Quadratus Lumborum					
	Pelvic_L1_L	0	7	0	0	0
	Pelvic_L2_L	0	0	0	5	0
	Pelvic_L3_L	0	34	0	0	0
	Pelvic_L3_R	0	33	0	0	0
	Pelvic_L4_R	0	0	0	0	56
	∑MF	140	390	198	388	181

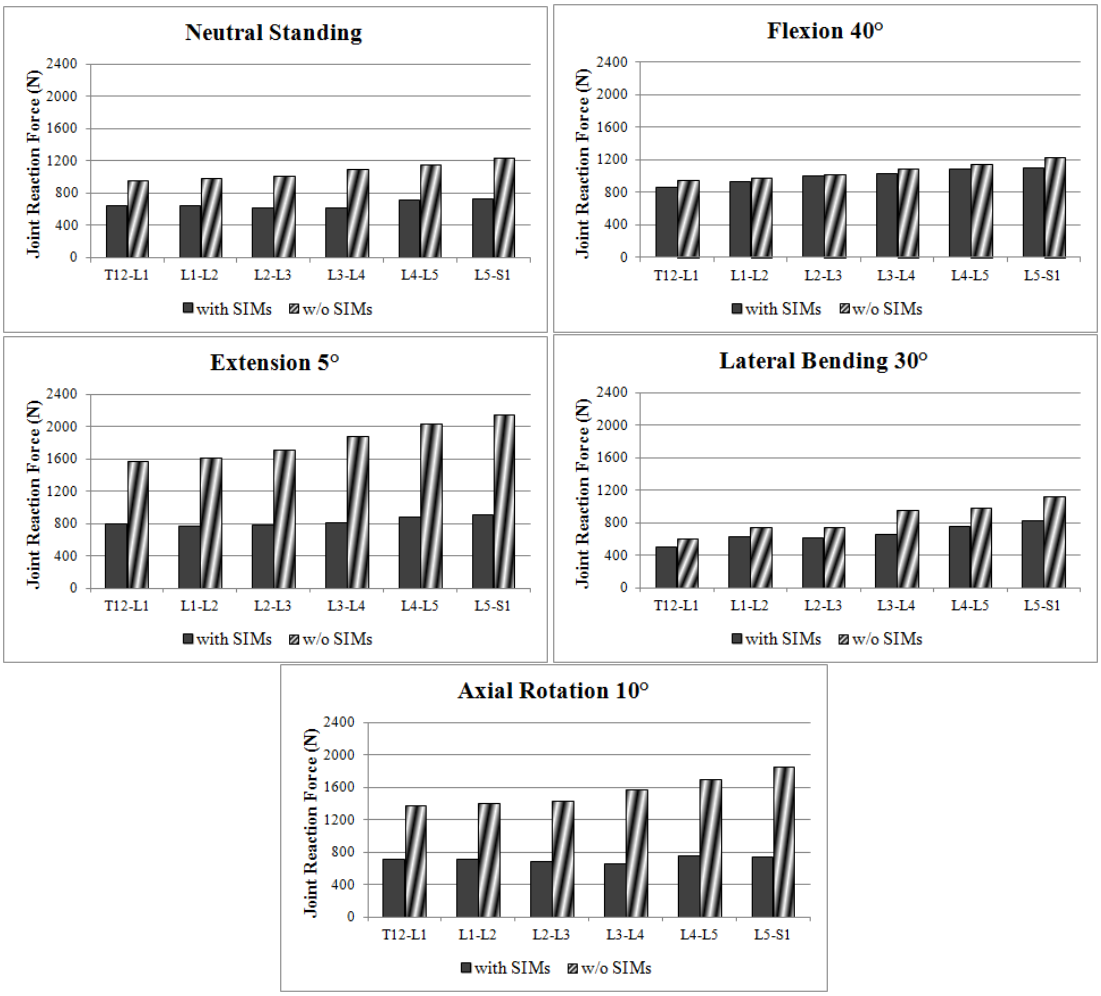

Figure 4-2 JRFs (or CFLs) at each level for all five postures both with and without SIMs

The JRFs at each level were the lowest during neutral posture and highest during extension 5°. The JRFs for lateral bending and axial rotation are lower than flexion and extension. Another observation is that the trends of the JRFs are not increasing steadily from the trunk level to L5 level. For neutral posture and axial rotation 10°, the result showed that the lowest JRF occurred at L3 disc, however for flexion 40°, the JRF at L3 disc was the largest. For both extension and lateral bending postures, the JRFs seemed to increase steadily from the trunk to L5. At L3 disc, the disc load was found to be about 620N for neutral posture and 840N for flexion 40°. These findings are close to Nachemson's study as shown in Figure 4-3. He found that

the disc load at L3 disc was 500N for neutral posture and 1000N for flexion 40° [12]. Since the cost function minimizes both JRFs and joint reaction moments, the joint reaction moments were minimized to zero in all postures other then lateral bending 30°.

Approximate axial load on the L3 disc in a person weighting 70 Kg (from Nachemson, Spine 6:93-96, 1981)

Loading and Posture	Disc Load (N)
Supine, awake	250
Spine, tilt table 50 deg	400
Supine, arm exercise	500
Upright sitting, without support	700
Sitting with lumbar support, back rest inclination 110 deg	400
Standing at ease	500
Coughing	600
Forward bend 20 deg	600
Forward bend 40 deg	1000
Forward bend 20 deg with 20 Kg	1200
Forward bend 20 deg and rotated 20 deg with 20 Kg	2100
Sit up exercise	1200
Lifting 10 Kg, back straight, knee bent	1700
Lifting 10 Kg, back bent	1900
Holding 5 Kg, arms extended	1900

Figure 4-3 Nachemson's results on JRFs at L3 disc [12]

CHAPTER 5

MODEL PREDICTIONS AT ALL FEASIBLE FLP

Multiple optimum solutions for spinal muscle forces creating CFLs at all lumbar spine levels for each posture was obtained from the optimization model. However, not all these solutions were able to stabilize the spine in the FE model. FE analyses showed that only solutions creating CFLs close to the GC of the vertebra produced spinal stability as shown in Figure 5-1. There is an area (the area where all the circles overlap) on the vertebra where the CFLs could be created and spinal stability be maintained for all the postures. Any FLP points outside these areas/ranges for all the postures produced buckling of the spine under CFLs. Extension posture had the smallest FLP range that stabilizes the spine, while flexion and lateral bending had larger FLP range. Spinal stability was defined as small movement of the trunk due to small deformation of the lumbar spine and it was measured by the amount of trunk sway. A trunk sway of $\leq$ 5mm in all directions was considered to be stable.

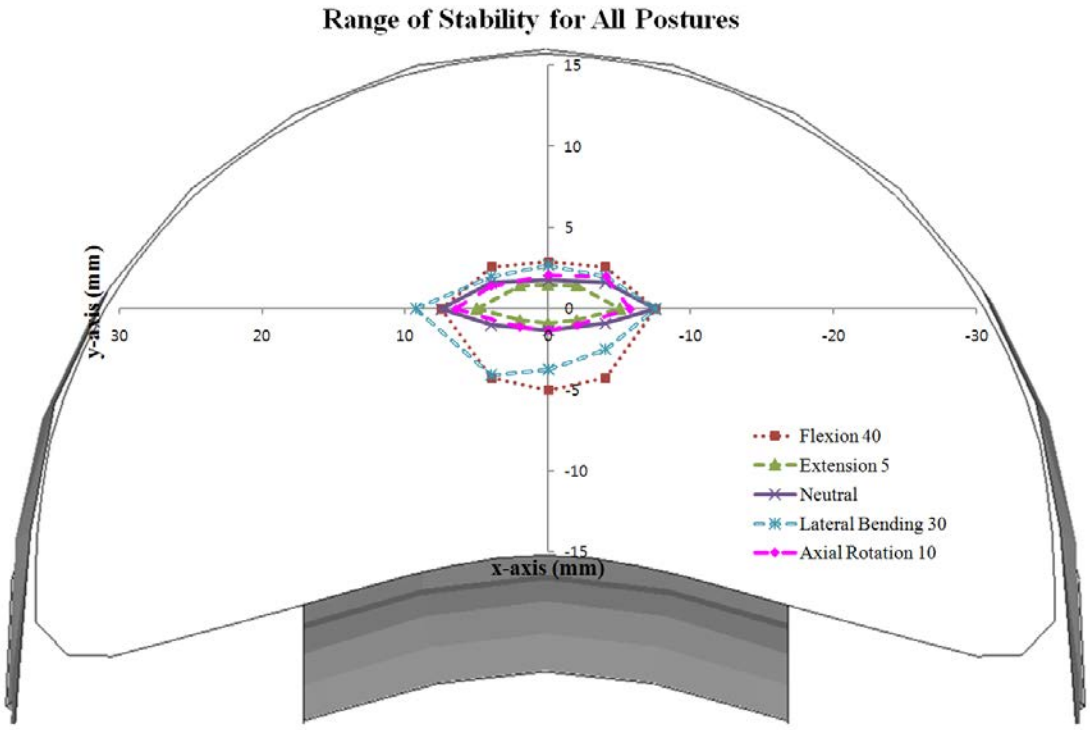

Figure 5-1 Each circle refers to the upper limit range where pure axial compressive loads or CFLs can be created to produce stability in the lumbar spine at each posture. Any points within the circle were able to stabilize the spine.

5.1 Neutral Posture (MFC=45 N/cm^2)

The stable FLP range for neutral posture was found to be between FLP equal to -1.3mm and 1.8mm along x-axis or sagittal plane and between FLP equal to -7.5mm and 7.5mm along y-axis or coronal plane shown in Figure 5-1. The JRFs calculated from the optimization model at these FLP ranges along each axis are compared and shown in Figures 5-2 and 5-3. Along x-axis, the JRFs increased as FLP moved from the posterior part of the vertebra body to the anterior part. The highest JRFs occurred at FLP equal to 1.8mm and the lowest JRFs occurred at FLP equal to -1.3mm. This is because the muscle forces were increased as FLP moved toward the anterior part from the GC of the vertebrae body. Also, the number of recruited muscle fascicles was increased from 36 to 40 shown in Figure 5-4 and Table 5-1 (this table is at the end of this Chapter). The muscle forces in LD, IO, SIMs, and longissimus were increased.

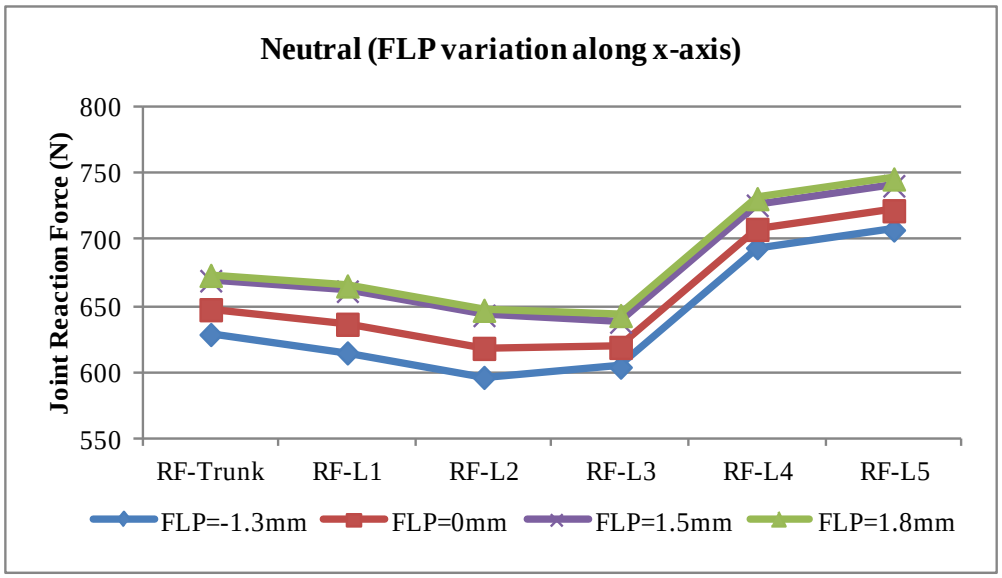

Figure 5-2 Comparison of JRFs (or CFLs) with FLP variation along x-axis (front and back) for neutral posture (y=0mm)

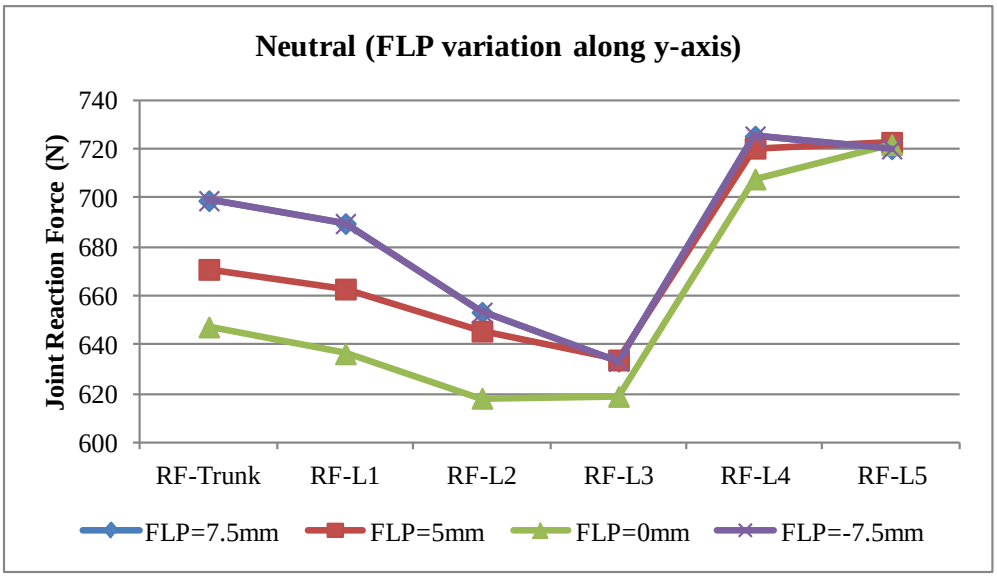

Figure 5-3 Comparison of JRFs (or CFLs) with FLP variation long y-axis (left and right) for neutral posture (x=0mm)

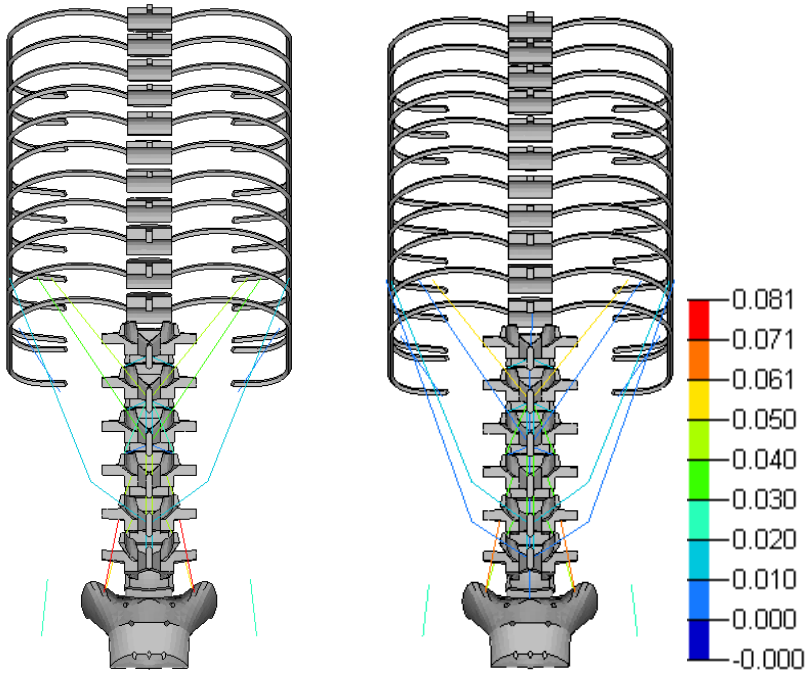

(a) FLP= -1.3mm (36 muscles) (b) FLP= 1.8mm (40 muscles)

Figure 5-4 Muscles recruited when (a) FLP= -1.3mm and (b) FLP= 1.8mm along x-axis (all muscle forces are in kN)

Along y-axis, because of the symmetry of both the body and the posture, the

JRFs at FLP equal to -7.5mm were exactly the same as the JRFs at FLP equal to 7.5mm shown in Figure 5-3. The lowest JRFs occurred at FLP equal to zero and the JRFs increased as FLP moved always from the GC of the vertebrae body. This is because as FLP moved either to the right or left, the moment arm of the JRFs would increase. In order to counterbalance the moments generated by the JRFs, more spinal muscles would be recruited on either right or left side of the body as shown in Figure 5-5. Since the JRFs were the lowest at y equal to 0mm and negative x (posterior part of the GC of the vertebra body), muscle recruiting patterns solved at FLP equal to -1.3mm resulted the lowest JRFs and stabilized the spine at the same time.

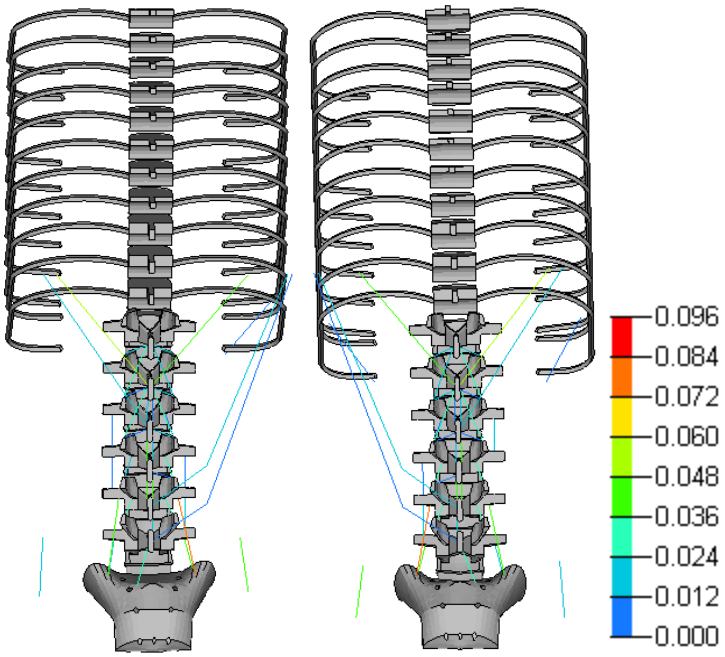

(a) FLP=-7.5mm (b) FLP=7mm

Figure 5-5 Muscles recruited when (a) FLP=-7.5mm and (b) FLP=7mm along y-axis (all muscle forces are in kN)

The absolute trunk sways at different FLPs within the stable FLP range along x-axis are shown in Figure 5-6. The absolute values of the trunk sway were used for the plot since the trunk can sway both in front and behind of the GC of the trunk. The

trunk oscillated behind the GC of the trunk when FLP was more towards the posterior part of the vertebrae body. The trunk oscillated in front of the GC of the trunk when FLP was more toward the anterior part of the body. Only the magnitude of the sway was considered to check the stability of the spine. It was found that there was a parabolic relationship between the trunk sway and the stable FLP range along x-axis shown in Figure 5-6. The minimum trunk sway occurred at about FLP equal to 0.3mm. The CFLs creating muscle recruiting patterns calculated at FLPs outside of the stable FLP range caused a dramatic increase in the trunk sway as shown in Figure 5-7, indicating spinal buckling. Since the lowest JRFs were obtained at FLP equal to -1.3mm as explained earlier, the lowest JRFs did not result the most stable spine. If the trunk sway was to be minimized, FLP equal to 0.3mm along x-axis would result the least amount of trunk sway in neutral posture.

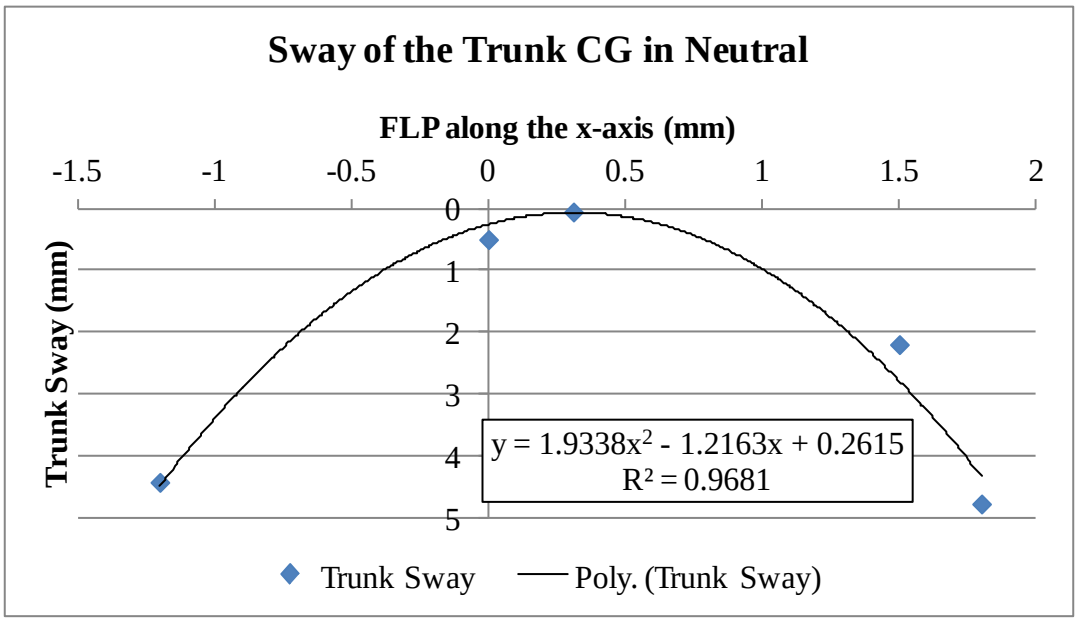

Figure 5-6 Trunk sway at different FLPs within the stable FLP range along x-axis (y=0mm)

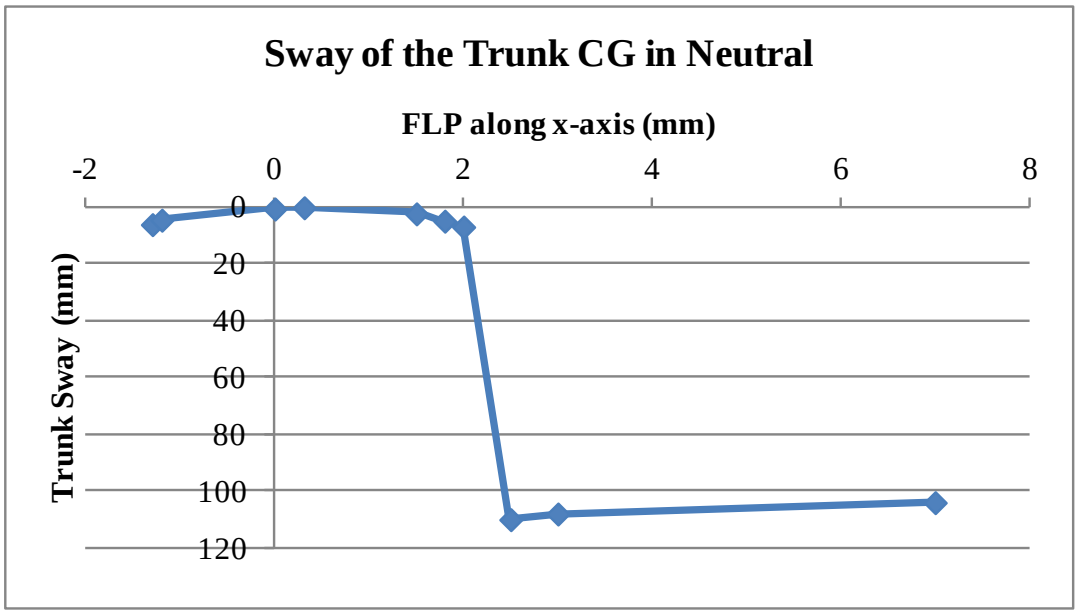

Figure 5-7 Trunk sway at different FLPs along x-axis (y=0mm)

5.2 Flexion 40° (MFC=45 N/cm^2)

In flexion 40°, the muscle recruitment patterns that stabilized the spine was found to be between FLP equal to 3mm and -5mm along x-axis and between 7.5mm and -7.5mm along y-axis shown in Figure 5-1. The JRFs calculated from the optimization model at different FLPs were compared and shown in Figures 5-8 and 5-9. When the FLP was varied along x-axis, the JRFs increased at all lumbar levels as the FLP moved from the posterior part of the vertebra body to the anterior. The highest JRFs occurred at FLP equal to 3mm and the lowest JRFs occurred at FLP equal to -5mm. As FLP moved from -5mm to 3mm, the muscle pattern was slightly changed shown in Figure 5-10, but the total number of the recruited muscles stayed the same (56 muscles). Thus, the increase in JRFs was caused by the increase in the resultant muscle forces. Table 5-1 shows the detailed muscle recruitment patterns; there was a significant increase in the muscle forces of RA and multifidus.

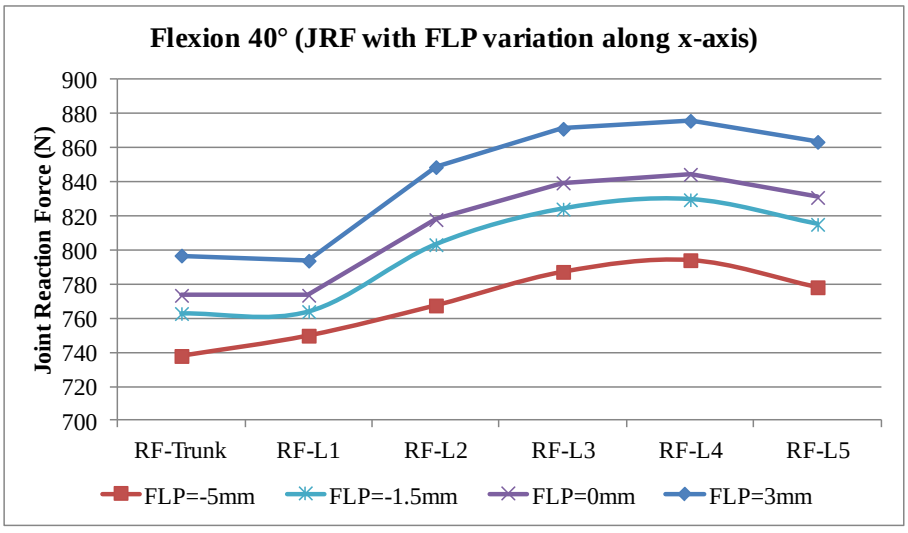

Figure 5-8 Comparison of JRFs (or CFLs) with FLP variation along x-axis for flexion 40° (y=0mm)

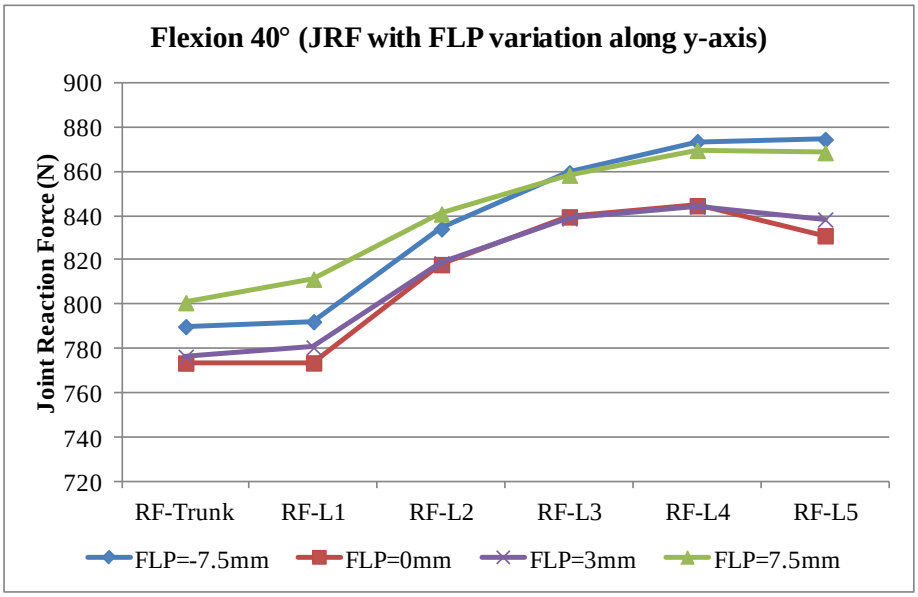

Figure 5-9 Comparison of JRFs (or CFLs) with FLP variation along y-axis for flexion 40° (x=0mm)

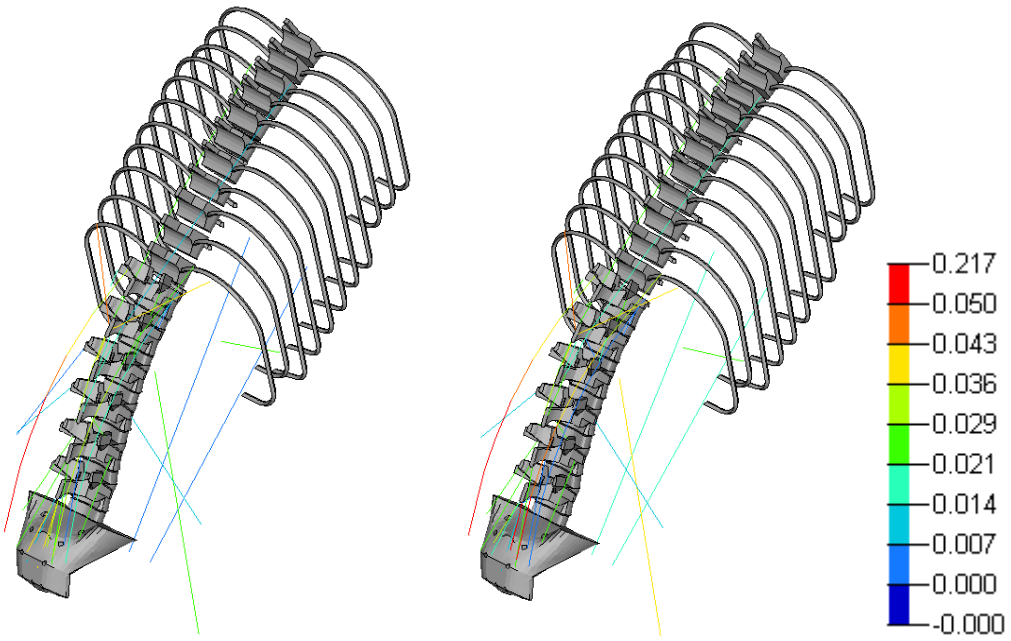

(a) FLP= -5mm (56 muscles) **(b) FLP= 3mm (56 muscles)**

Figure 5-10 Muscles recruited when (a) FLP= -5mm and (b) FLP=3mm along x-axis (all muscle forces are in kN)

Along the y-axis, the JRFs at FLP equal to -7.5mm are slightly different with the JRFs at FLP equal to 7.5mm shown in Figure 5-9. This was because the flexion 40°

posture was not perfectly symmetric as indicated in Table 3-1; the posture was slightly laterally bended to the right and axially rotated which caused the differences in the JRFs. The lowest JRFs still occurred approximately at FLP equal to zero along y-axis. As the FLP moved away from the GC of the vertebrae body, the JRFs increased. This result is the same as the result obtained from neutral posture and the same reason applies. As the FLP moved either to the right or left from the GC of the vertebrae body, the moment arm of the CFLs increased. In order to counterbalance these moments, more muscles were recruited either on the right or left side of the body shown in Figure 5-11. Combing the effect of both x and y axis, FLP equal to -5mm along x-axis would give the least JRFs for flexion 40° while maintain the stability of the spine.

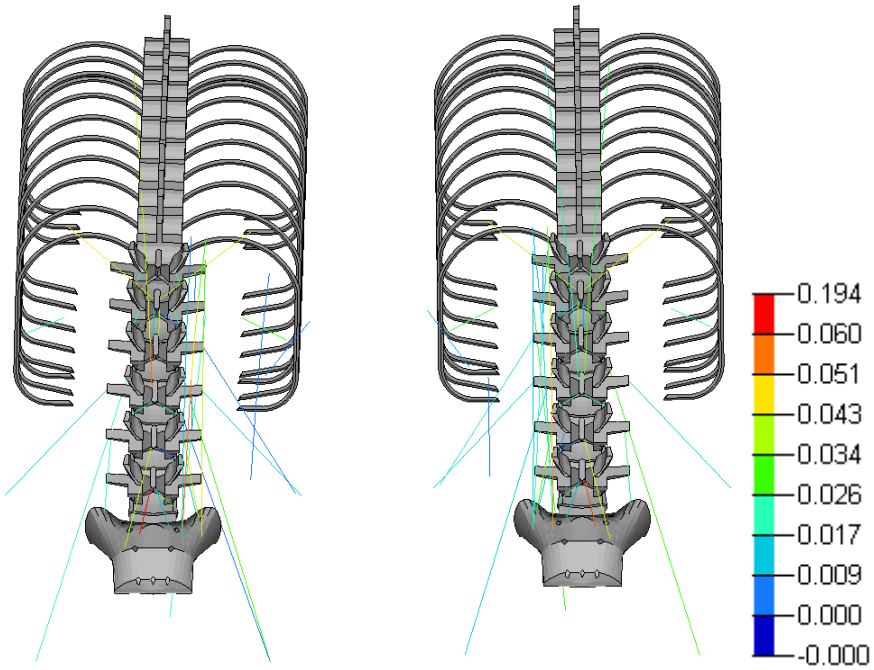

(a) FLP= -7.5mm **(b) FLP= 7.5mm**

Figure 5-11 Muscles recruited when (a) FLP= -7.5mm and (b) FLP=7.5mm along y-axis (all muscle forces are in kN)

The absolute trunk sway at different FLPs within the stable FLP range in sagittal plane for flexion 40° is shown in Figure 5-12. A parabolic relationship was

also observed between the trunk sway and FLPs along x-axis. The minimum sway of the trunk occurred at about FLP equal to -1mm. Since the lowest JRFs occurred at FLP equal to -5mm, the muscle patterns obtained at the lowest JRFs did not result the least trunk sway. It the trunk sway is optimized, FLP= -1mm would be the optimized solution. When the FLP moved outside the stable range, the calculated muscle patterns caused large trunk sway shown in Figure 5-13, thus unstable spine.

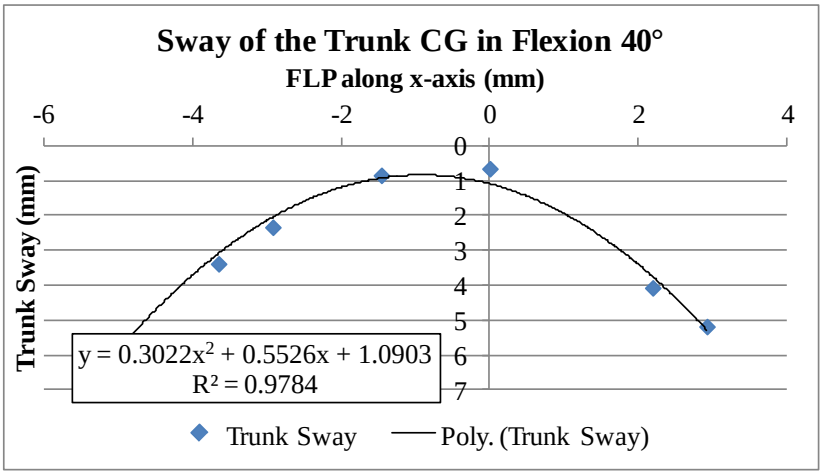

Figure 5-12 Trunk sway at different FLPs within the stable FLP range along x-axis (y=0mm) for flexion 40°

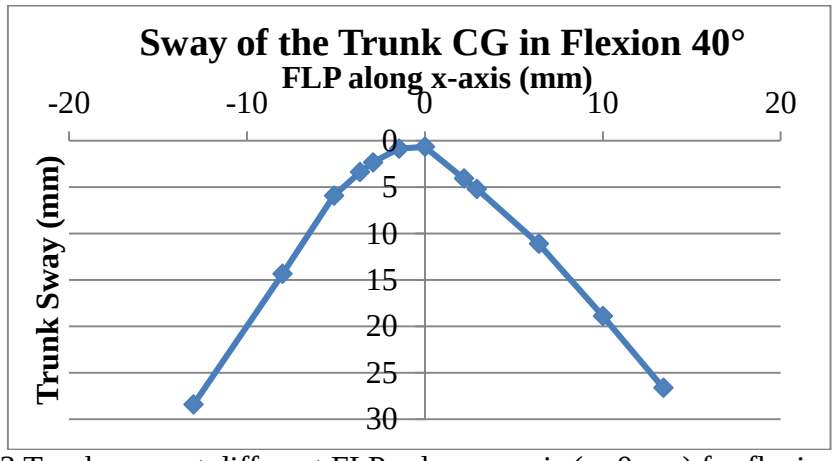

Figure 5-13 Trunk sway at different FLPs along x-axis (y=0mm) for flexion 40°

5.3 Extension 5° (MFC=45 N/cm^2)

The FLP range for extension 5° that result spinal muscle patterns to stabilize the spine was found to be between 1.5mm and -1mm along x-axis and between 5mm and -5mm along y-axis shown in Figure 5-1. The JRFs calculated from the optimization model at different FLPs are compared and shown in Figures 5-14 and 5-15. The JRFs increased as FLP moved to the anterior part from the GC of the vertebra body along x-axis. This result was the same as other postures in the sagittal plane for the same reason. JRFs was the highest at FLP=1.5mm and the lowest at FLP= -1mm. This is explained by the increase in muscle forces and number of recruited muscles as the FLP was moved from -1mm to 1.5mm shown in Figure 5-16. 54 muscles were recruited at FLP= -1mm and 66 muscles were recruited at FLP=1.5mm. There were more longissimus and SIMs muscles recruited, and the muscles forces of LD and oblique muscles were increased as shown in Table 5-1.

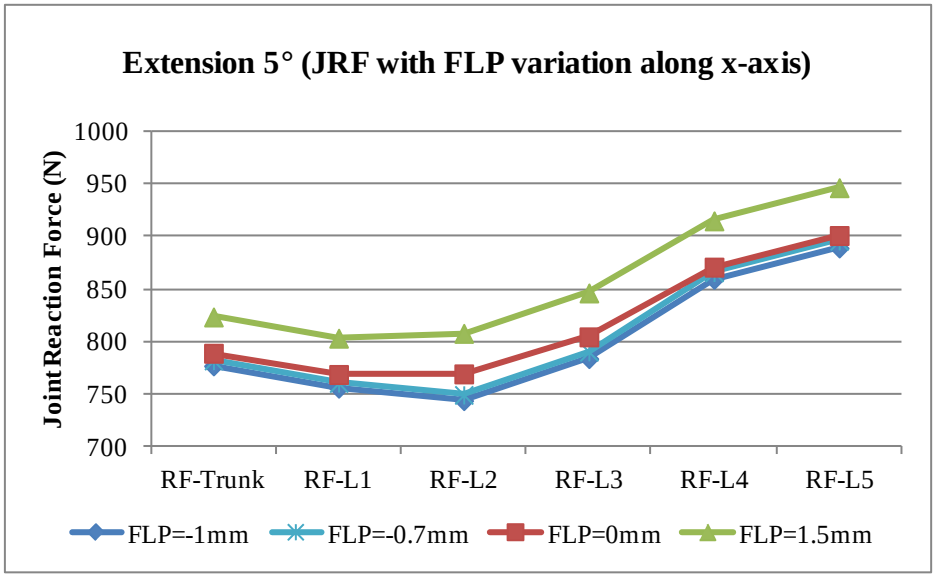

Figure 5-14 Comparison of JRFs (or CFLs) with FLP variation along x-axis for extension 5° (y=0mm)

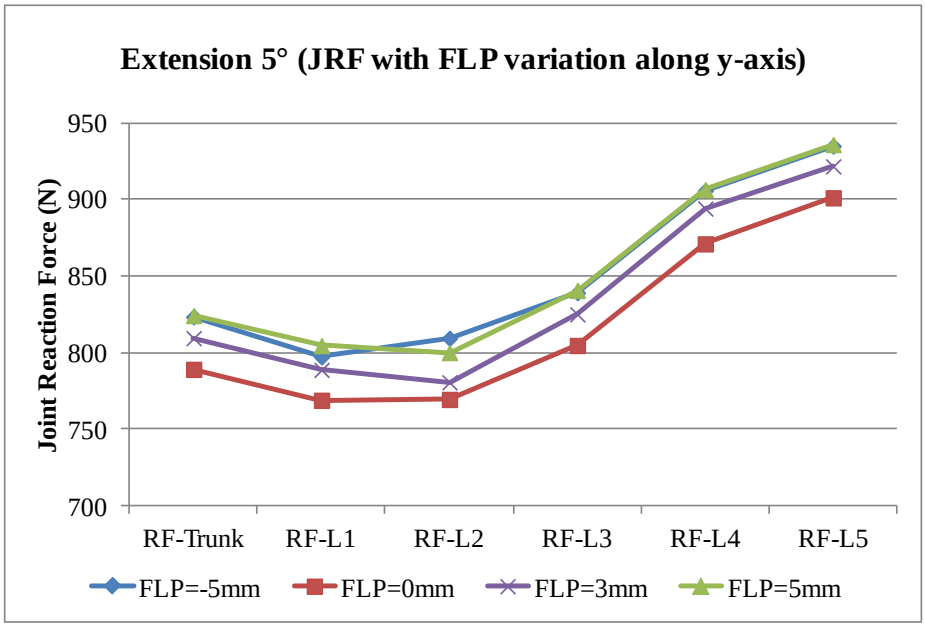

Figure 5-15 Comparison of JRFs (or CFLs) with FLP variation along y-axis for extension 5° (x=0mm)

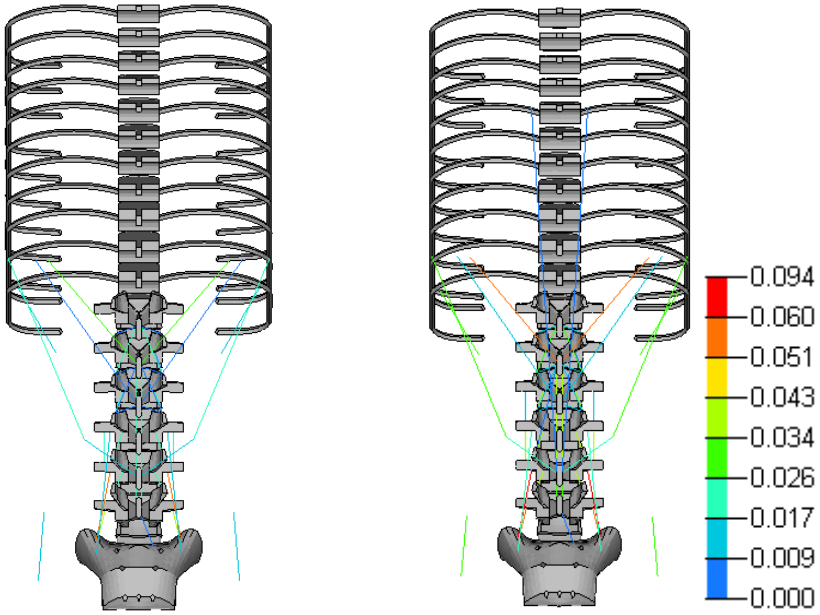

(a) FLP= -1mm (54 muscles) (b) FLP=1.5mm (66 muscles)

Figure 5-16 Muscles recruited when (a) FLP= -1mm and (b) FLP=1.5mm along x-axis (all muscle forces are in kN)

In coronal plane, the JRFs at FLP= -5mm were approximately the same as the JRFs at FLP= 5mm shown in Figure 5-15. Again, this was due to the approximately

symmetry of the body and the posture from left and right. The slight differences at L1 and L2 level may be caused by the slight axial rotation of the posture shown in Table 3-1. The lowest JRFs again occurred at FLP equal to zero. As the FLP moved away from the central line of the vertebrae body, the JRFs increased. Even though it is not as obvious as in neutral and flexion 40°, Figure 5-17 shows that more muscles were recruited on either right or left side of the spine in order to counterbalance the moments produced by the CFLs when FLP moved either to the right or left of the GC of the vertebra body. The lowest JRFs occurred at FLP= -1mm along x-axis for extension 5° when the spine was kept stable.

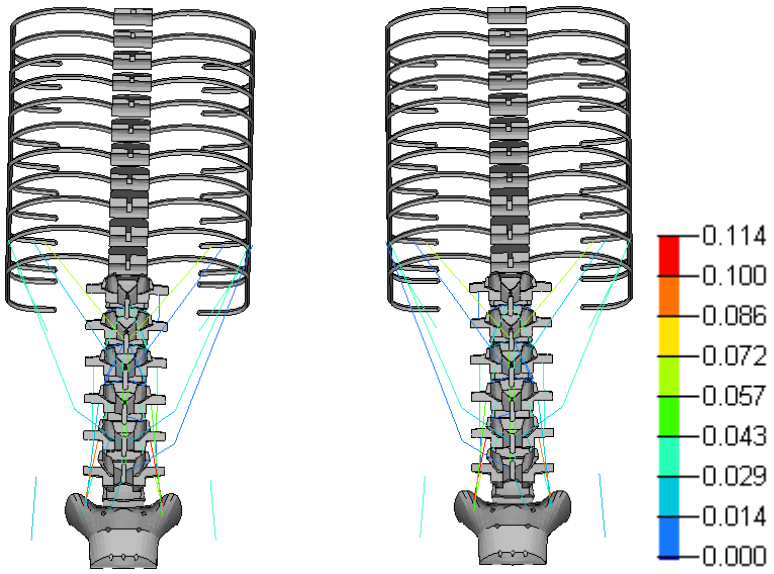

(a) FLP= -5mm (b) FLP=5mm

Figure 5-17 Muscles recruited when (a) FLP= -5mm and (b) FLP=5mm along y-axis (all muscle forces are in kN)

The absolute trunk sway at different FLPs along x-axis that kept the spine stable for extension 5° is shown in Figure 5-18. The minimum trunk sway occurred at about FLP=0.4mm. The muscle patterns produced the lowest JRFs (at FLP=-1mm) again did not result the least trunk sway. If the trunk sway is to be optimized, FLP=

0.4mm would be the optimized solution. There was a sudden buckling of the spine as the FLP moved away from the stable range shown in Figure 5-19.

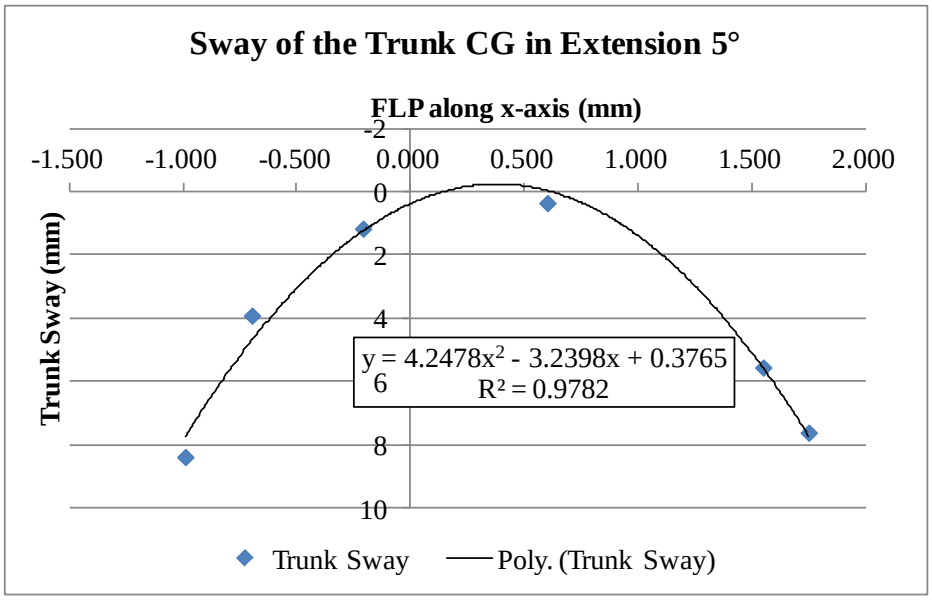

Figure 5-18 Trunk sway at different FLPs within the stable FLP range along x-axis (y=0mm) for extension 5°

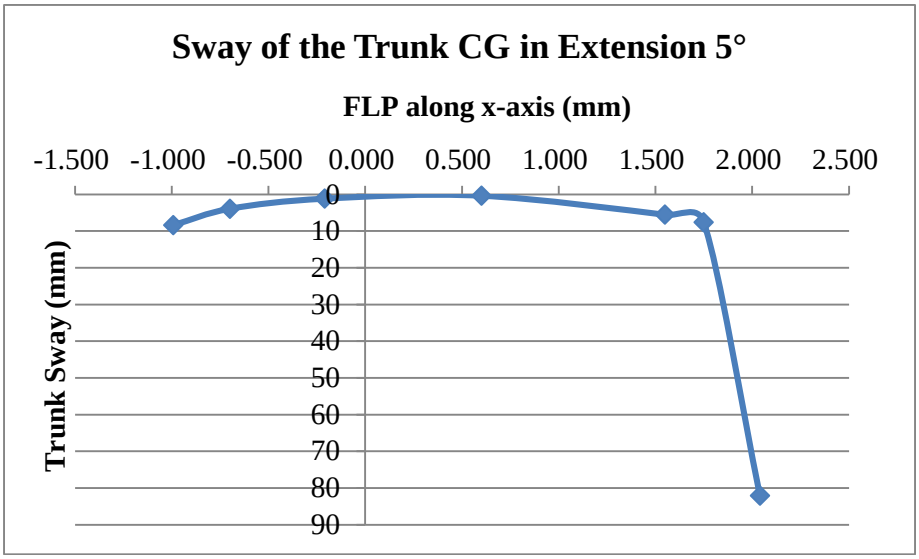

Figure 5-19 Trunk sway at different FLPs along x-axis (y=0mm) for extension 5°. The spine buckled and no solution was obtained after FLP=-1mm.

5.4 Right Lateral Bending 30° (MFC=45 N/cm^2)

The stable FLP range for right lateral bending 30° was found to be between 2.7mm and -3.8mm from GC of the vertebra body along x-axis and between 9.3mm and -7.5mm along y-axis shown in Figure 5-1. The JRFs calculated from the optimization model at different FLPs are compared and shown in Figures 5-20 and 5-23. Unlike all the other postures, the JRFs decreased as the FLP moved to the anterior part of the vertebrae body along the x-axis. Also, the joint reaction moments were no longer zero at all lumbar spine levels shown in Figure 5-21. They were needed to balance the moments caused by the muscle forces and JRFs. The moment around y-axis at T12 level was the highest; this may resulting from the posture contained 3° of extension. The joint reaction moments were required to balance the moments generated around y-axis as a result of extension. Also, Van Dieen and Kingma found that the lateral shear forces increased with asymmetry [38]. This may also correspond to the joint reaction moments calculated for lateral bending since the lateral shear forces were forced to be zero under follower load condition.

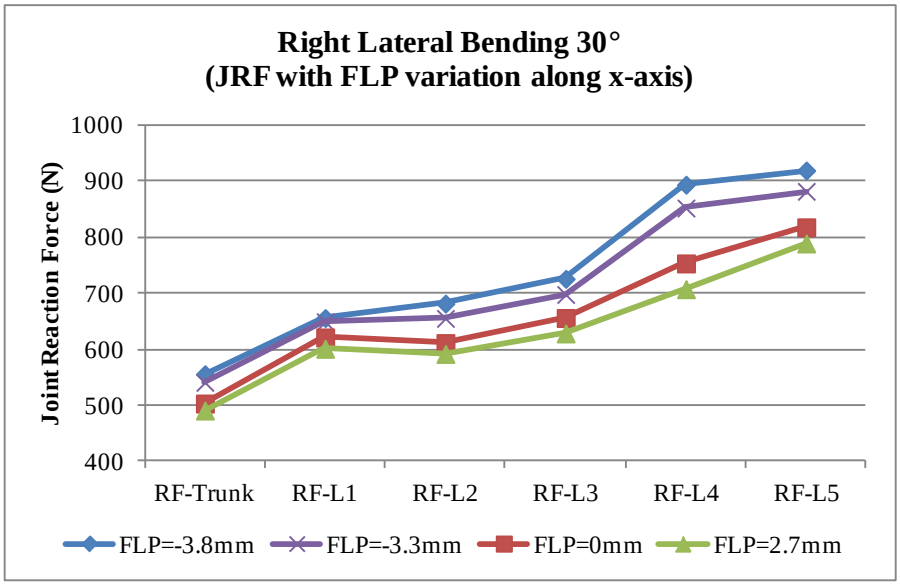

Figure 5-20 Comparison of JRFs (or CFLs) with FLP variation along x-axis for right lateral bending 30° (y=0mm)

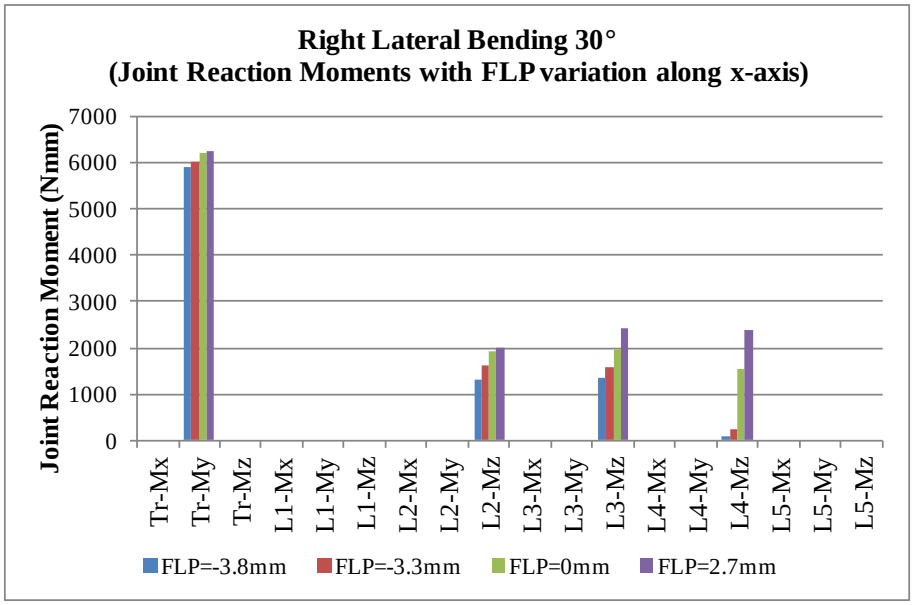

Figure 5-21 Comparison of joint reaction moments with FLP variation along x-axis for right lateral bending 30° (y=0mm)

The joint reaction moments at each level increased as the FLP moved to the anterior part of the vertebrae body. Since both JRFs and joint reaction moments were minimized in the cost function, Figure 5-22 indicated that the cost function increased linearly as the FLP moved toward the anterior part of the vertebrae body. Figure 5-26 showed that the number of recruited muscles decreased from 66 to 56 as FLP moved from -3.8mm to 2.7mm along x-axis, which explains why the JRFs decreased. There was also a change in muscle pattern with the change in FLP. At FLP=2.7mm, more EO and SPI forces were required as shown in Table 5-1, however the forces of LD , SIMs, multifidus and PM were decreased.

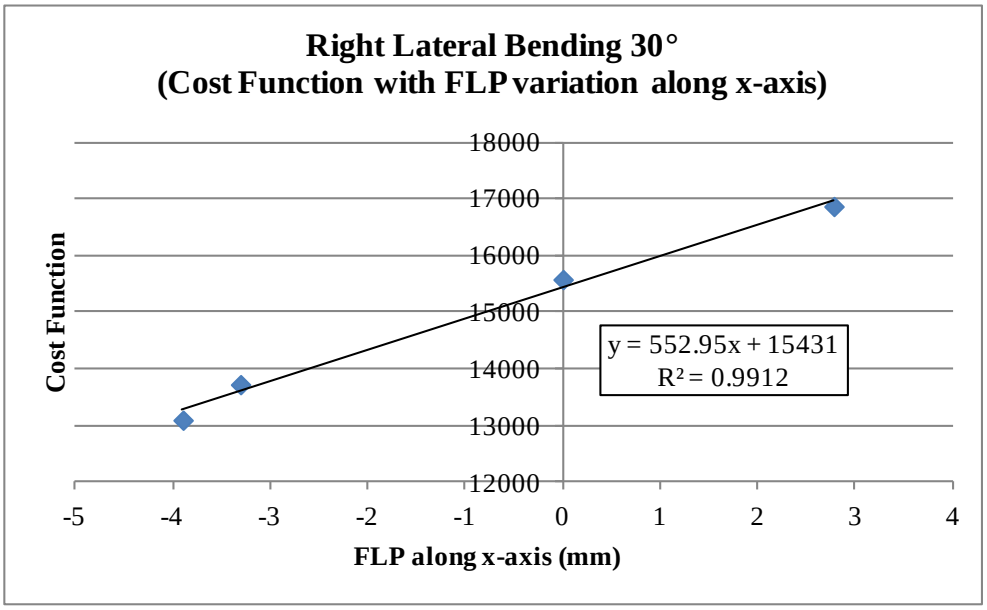

Figure 5-22 Comparison of cost functions with FLP variation along x-axis for right lateral bending 30°

Unlike all the postures in the sagittal plane, lateral bending is asymmetric in coronal plane. Figure 5-23 shows that the JRFs at each level are very different as FLP moved from right to left side of the body. At trunk, L1 and L2 level, the JRFs were higher when FLPs were on the positive y-axis. The JRFs at L3, L4 and L5 level are the opposite; they were higher when FLPs were on the negative y-axis. This is caused by the difference in muscle recruiting pattern as FLP moved along y-axis shown in Figure 5-27. The total number of muscles recruited at FLP= -7.5mm and 9.3mm were about the same. However, at FLP=9.3mm, more muscles were recruited at the upper levels of the lumbar spine and at FLP= -7.5mm, more muscles were recruited at the lower levels of the lumbar spine. This result exactly corresponded to the trend in the JRFs. The lowest JRFs still approximately occurred at FLP equal to zero. Since joint reaction moments were generated in lateral bending 30°, Figure 5-24 shows that the total joint reaction moment was higher as FLP moved to the positive y-axis. There was also a linear relationship between cost function and FLP along y-axis shown in

Figure 5-25. The cost function increased as FLP moved from the negative y-axis to the positive. Overall, the lowest JRFs were calculated at FLP=2.7mm along x-axis and the lowest cost function was calculated at FLP= -3.8mm along x-axis.

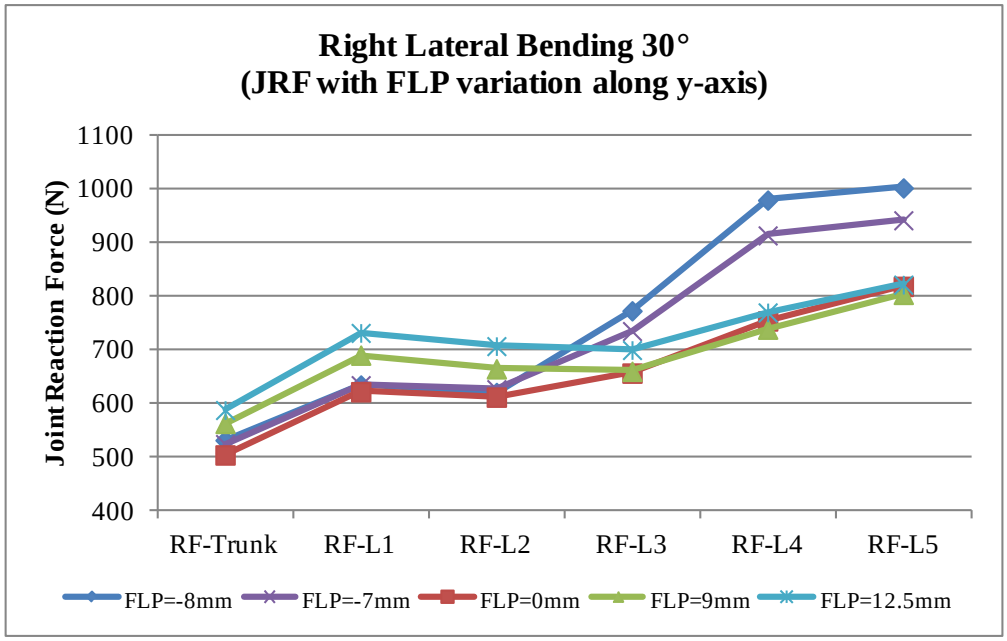

Figure 5-23 Comparison of JRFs (or CFLs) with FLP variation along y-axis for right lateral bending 30° (x=0mm)

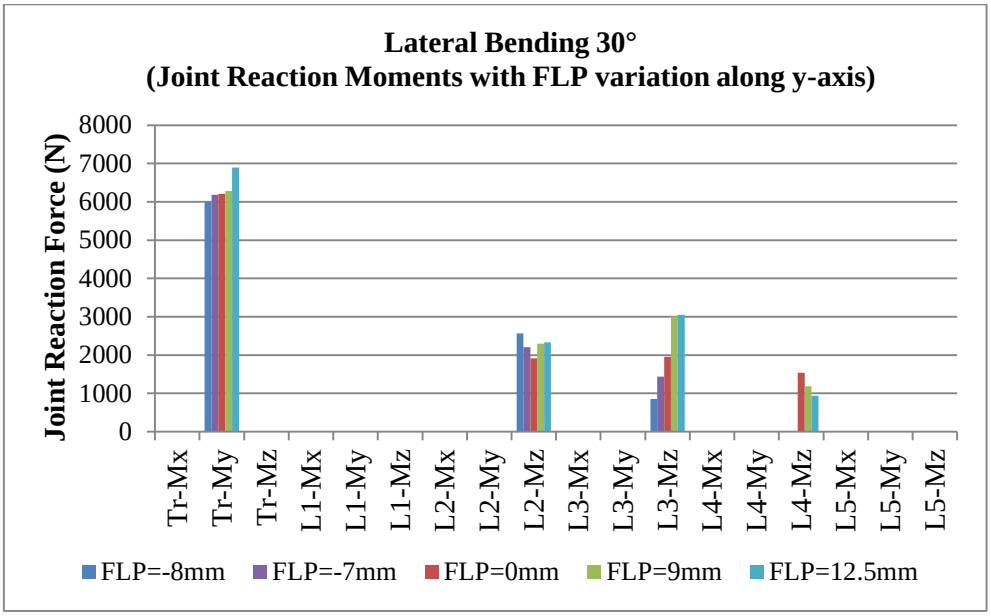

Figure 5-24 Comparison of joint reaction moments with FLP variation along y-axis for right lateral bending 30° (x=0mm)

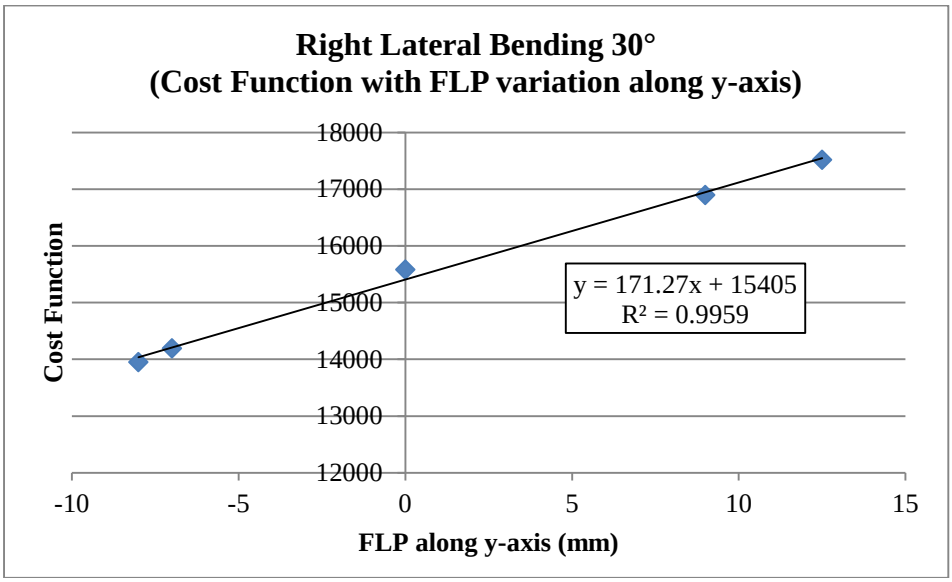

Figure 5-25 Comparison of cost functions with FLP variation along y-axis for right lateral bending 30°

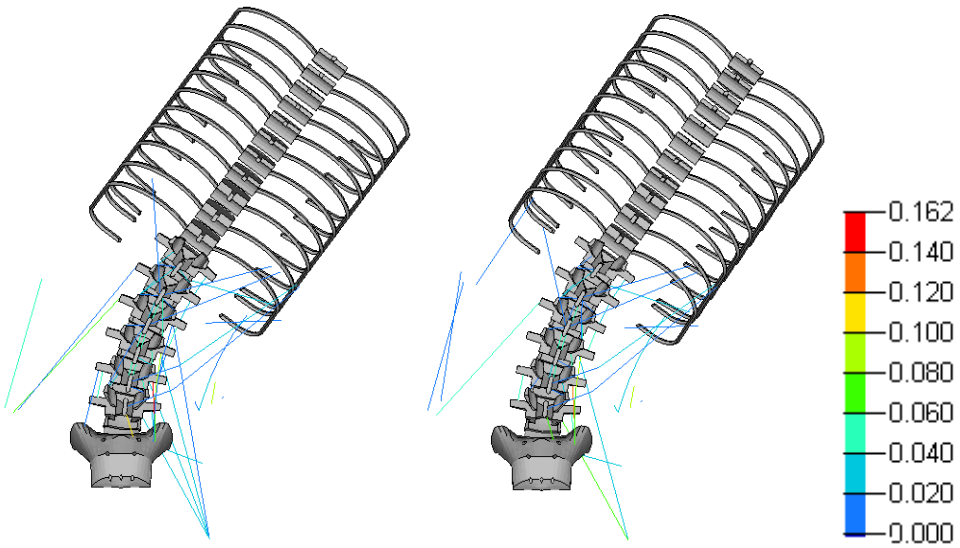

(a) FLP= -3.8mm (66 muscles) (b) FLP=2.7mm (56 muscles)

Figure 5-26 Muscles recruited when (a) FLP= -3.8mm and (b) FLP=2.7mm along x-axis for lateral bending 30° (all muscle forces are in kN)

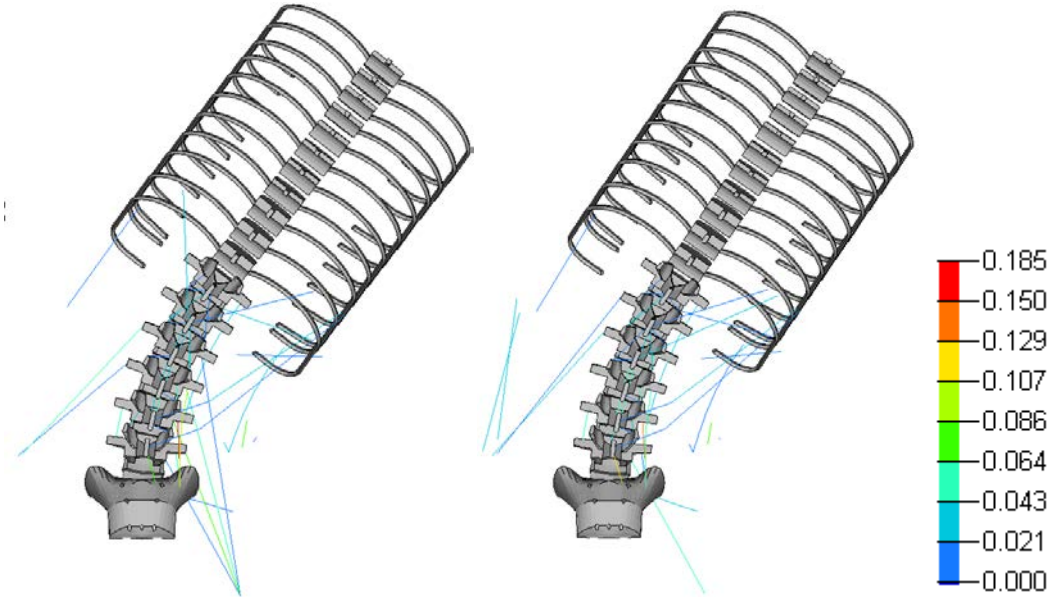

(a) FLP= -7.5mm (56 muscles) (b) FLP=9.3mm (57 muscles)

Figure 5-27 Muscles recruited when (a) FLP= -7.5mm and (b) FLP=9.3mm along y-axis for lateral bending 30° (all muscle forces are in kN)

The absolute trunk sway at different FLPs along x-axis that keeps the spine stable for right lateral bending 30° is shown in Figure 5-28 and along y-axis is shown in Figure 5-29. In both cases, there was a parabolic relationship between the trunk sway and FLP. As FLP moved away from the GC of the vertebra, the trunk sway was increased. The minimum trunk sway occurred at about FLP= -0.6mm along x-axis and at about FLP=1mm along y-axis. As the FLP moved further away along x-axis and y-axis, there were large increases in trunk sway shown in Figures 5-30 and 5-31 indicating instability of the spine.

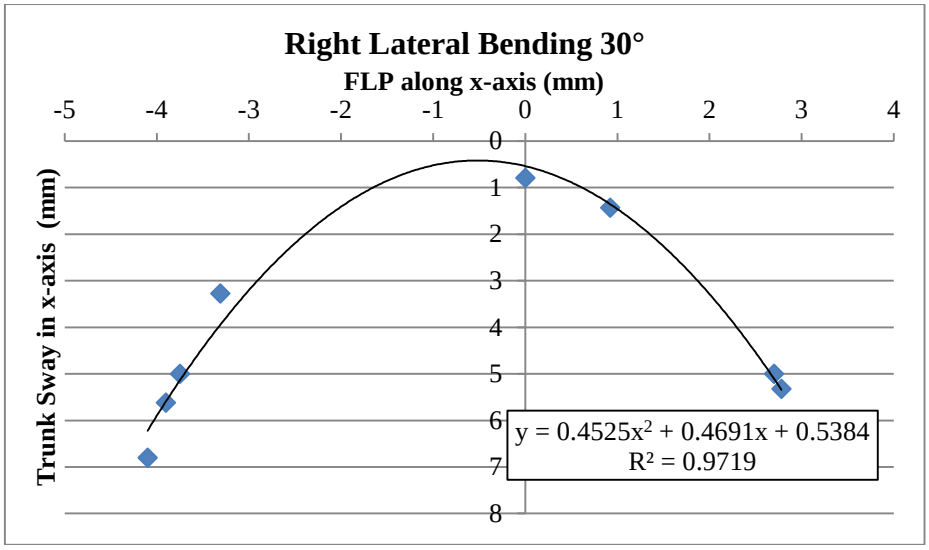

Figure 5-28 Trunk sway at different FLPs within the stable FLP range along x-axis (y=0mm) for right lateral bending 30°.

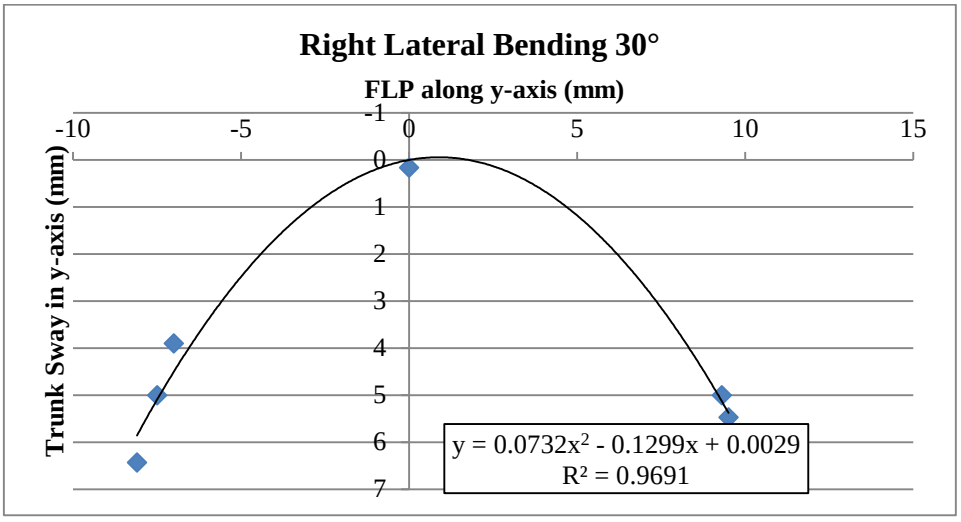

Figure 5-29 Trunk sway at different FLPs within the stable FLP range along y-axis (x=0mm) for right lateral bending 30°.

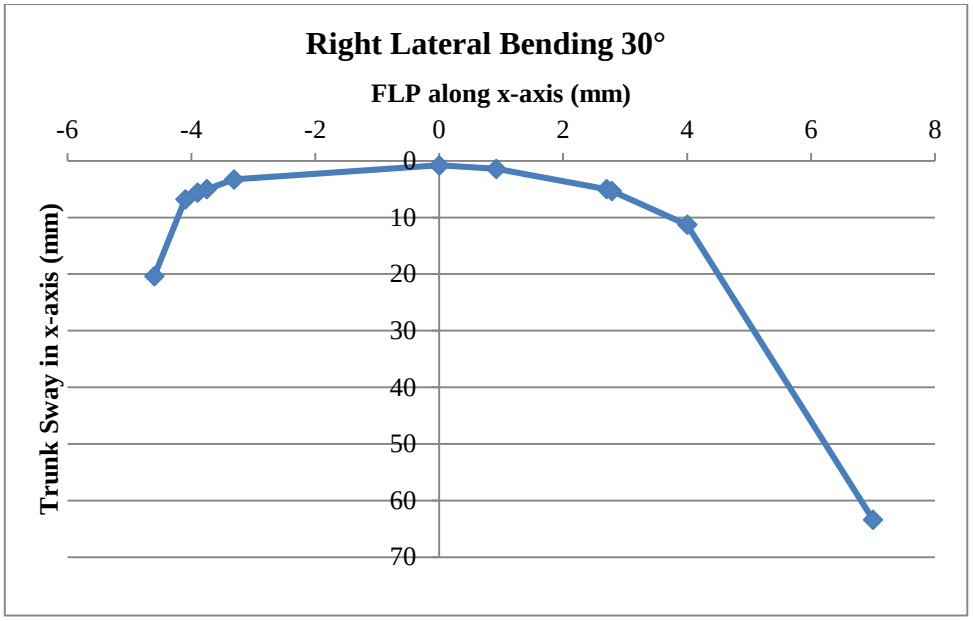

Figure 5-30 Trunk sway at different FLPs along x-axis (y=0mm) for right lateral bending 30°. The spine buckled and no solution was obtained after FLP=-5mm

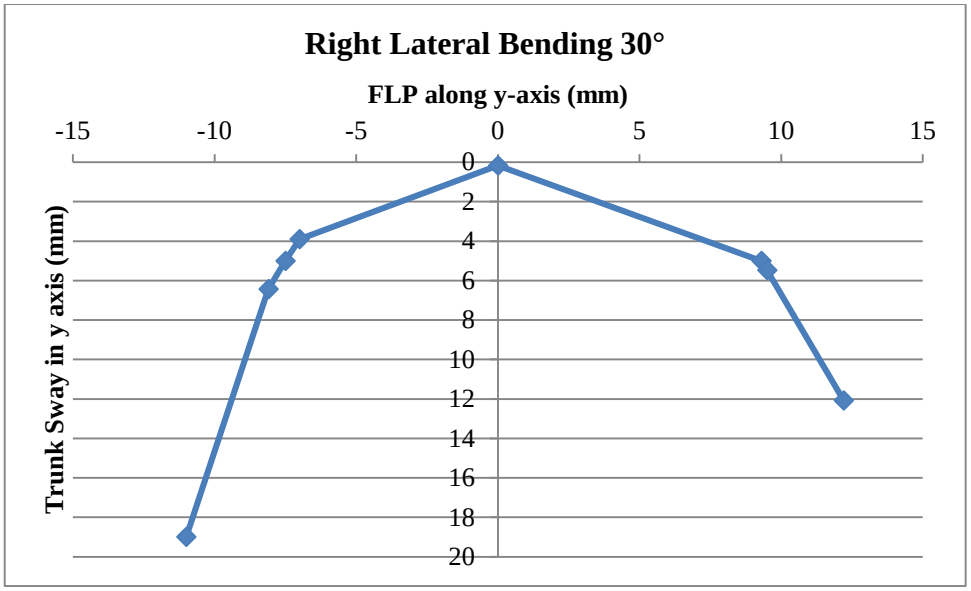

Figure 5-31 Trunk sway at different FLPs along y-axis (x=0mm) for right lateral bending 30°

5.5 Left Axial Rotation 10° (MFC=45 N/cm^2)

The FLP range for left axial rotation 10° was found to be between 2.1mm and -1.3mm along x-axis and between 6.5mm and -5.7mm along y-axis shown in Figure 5-1. The JRFs calculated from the optimization model at different FLPs are compared and shown in Figures 5-32 and 5-33. The JRFs increased as FLP moved to the anterior part of the vertebrae body in the sagittal plane and decreased as FLP moved to the posterior part of the body. This result is the same as the postures along the sagittal plane. Figure 5-34 shows that when FLP=-1.3mm, 44 muscle fascicles were recruited. As FLP moved to 2.1mm, the number of recruited muscle fascicles was increased to 49. The muscle forces of the recruited muscle at FLP=2.1mm were also higher than the muscle forces obtained at FLP= -1.3mm shown in Figure 5-34 and Table 5-1. There was a great increase in the forces of EO, IO, SIMs and longissimus. Since both the number of recruited muscles fascicles and the muscle forces were increased as FLP moved to the anterior part of the vertebrae body, the JRFs were increased.

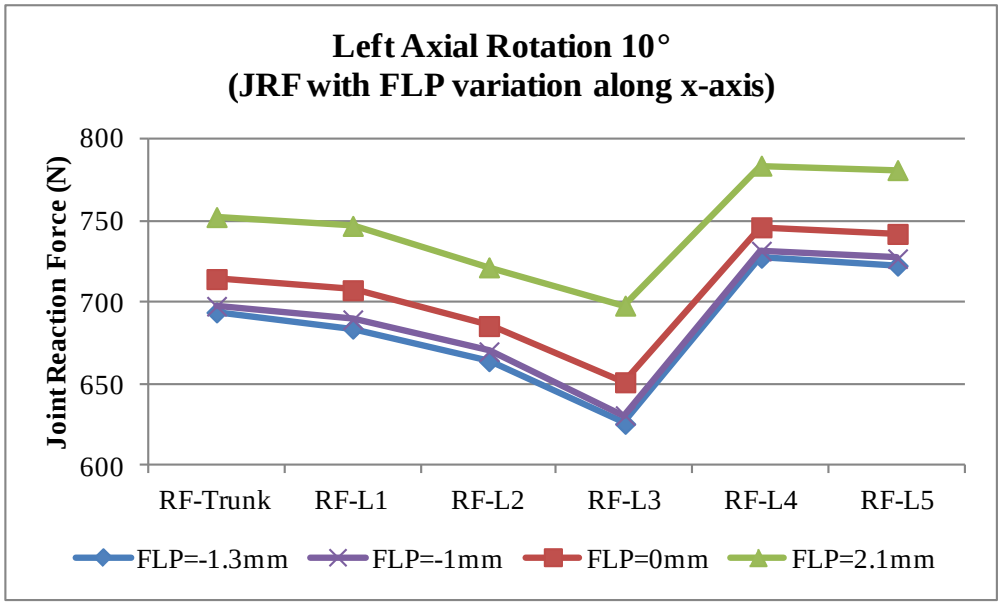

Figure 5-32 Comparison of JRFs (or CFLs) with FLP variation along x-axis for left axial rotation 10° (y=0mm)

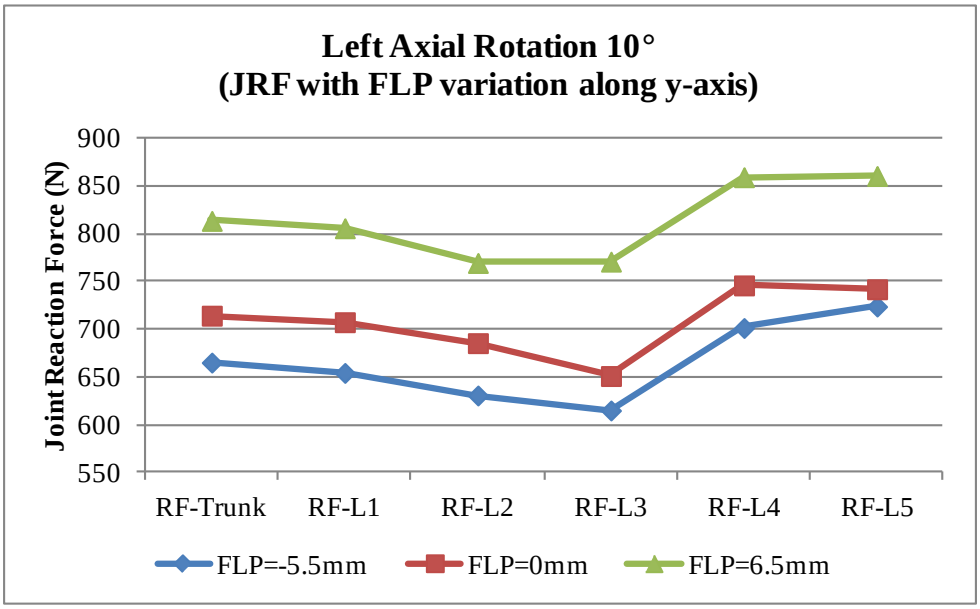

Figure 5-33 Comparison of JRFs (or CFLs) with FLP variation along y-axis for left axial rotation 10° (x=0mm)

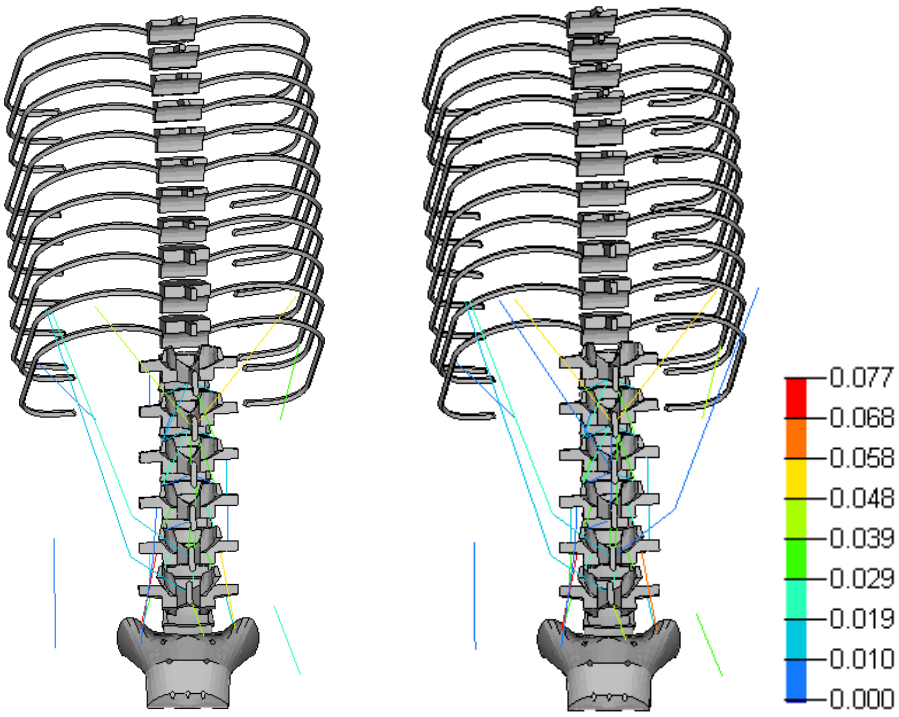

(a) FLP= -1.3mm (44 muscles) (b) FLP=2.1mm (49 muscles)

Figure 5-34 Muscles recruited when (a) FLP= -1.3mm and (b) FLP=2.1mm along x-axis (all muscle forces are in kN)

Left Axial rotation is also an unsymmetrical posture in coronal plane. Unlike all the other postures, the lowest JRFs did not occur at FLP=0mm. The JRFs were the lowest when FLP was set on the negative y-axis and highest when FLP was set on the positive y-axis. This is because the recruited number of muscle fascicles was increased as the FLP moved from negative y-axis to positive shown in Figure 5-35 and Table 5-2. There was more SPI, LD, longissimus, EO, IO, multifidus and SIMs activated. The muscles forces of the already activated muscles were also increased.

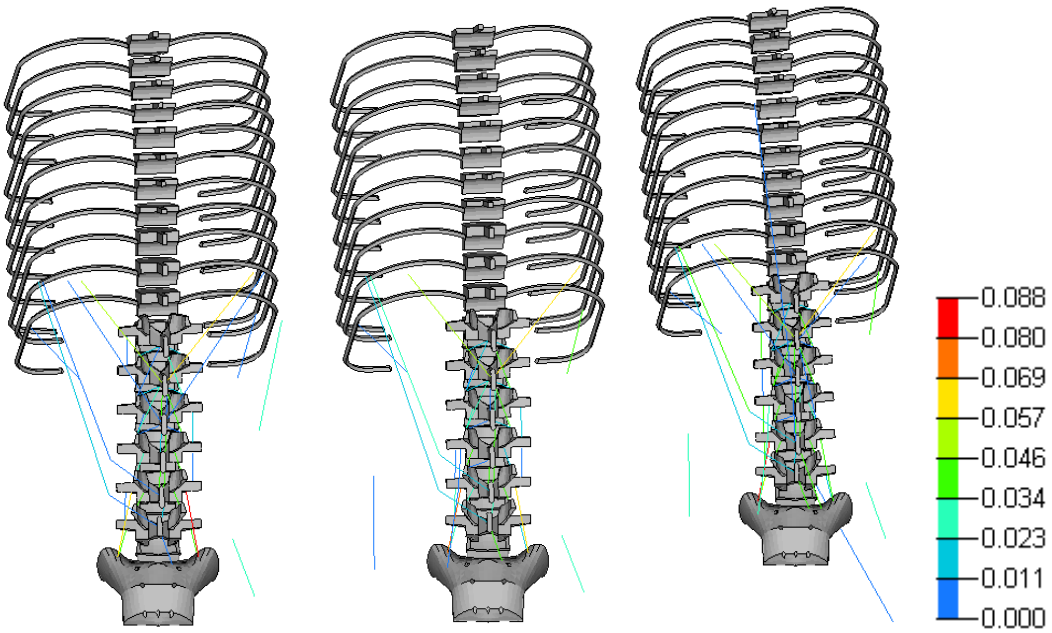

(a) FLP= -5.5mm (43 muscles) (b) FLP=0mm (45 muscles) (c) FLP=6.5mm (58 muscles)

Figure 5-35 Muscles recruited when (a) FLP= -5.5mm (b) FLP=0mm and (c) FLP=6.5mm along y-axis (all muscle forces are in kN)

The absolute trunk sway at different FLPs within the stable range along x-axis for left axial rotation 10° is shown in Figure 5-36 and along y-axis is shown in Figure 5-37. The minimum sway of the trunk occurred at about FLP=0.4mm along x-axis and at about FLP=0mm along y-axis. Again, there was the parabolic relationship

between trunk sway and FLP for both cases. Figures 5-38 and 5-39 shows that as the FLP moved further away along both x and y axes, there were large increases in trunk sway or the spine was buckled.

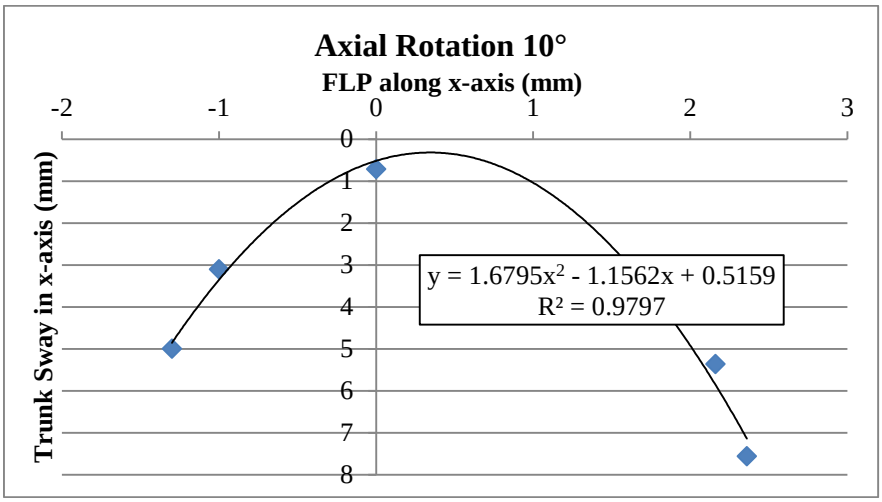

Figure 5-36 Trunk sway at different FLPs within the stable range along x-axis (y=0mm) for left axial rotation 10°

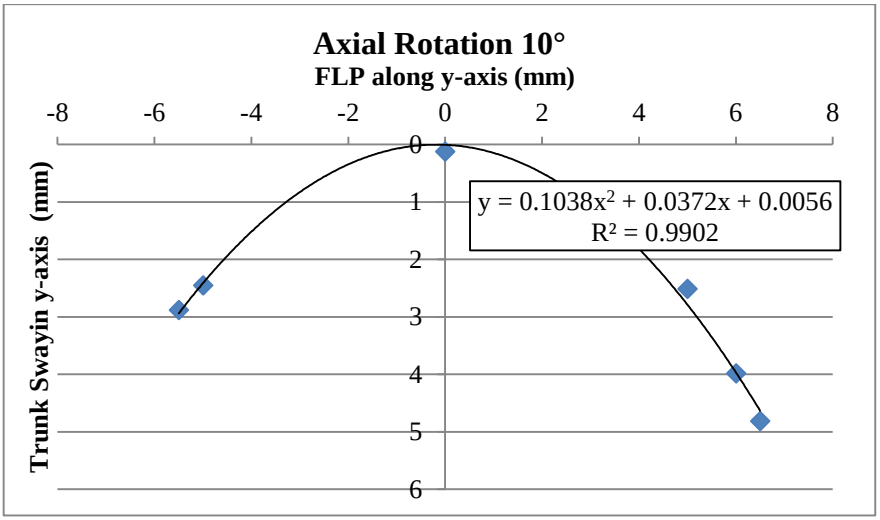

Figure 5-37 Trunk sway at different FLPs within the stable range along y-axis (x=0mm) for left axial rotation 10°

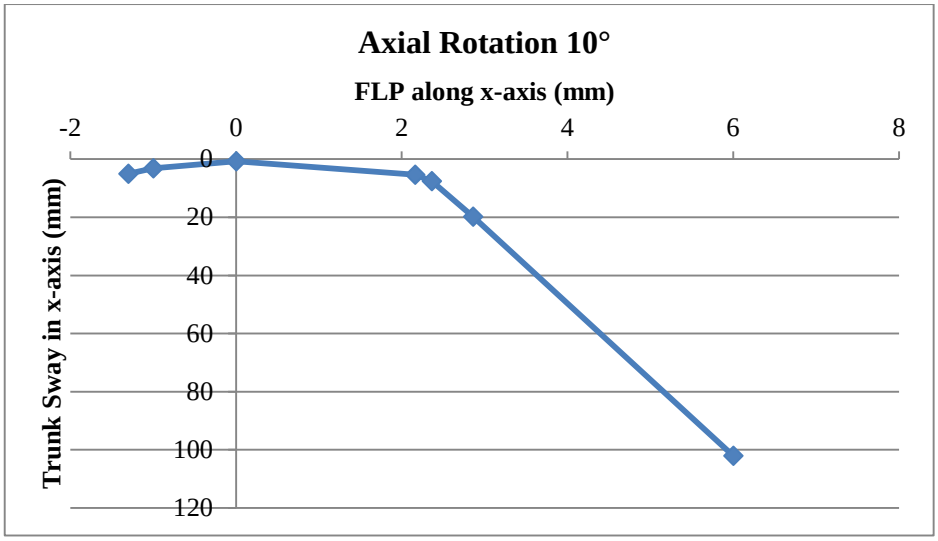

Figure 5-38 Trunk sway at different FLPs along x-axis (y=0mm) for left axial rotation 10°. The spine buckled and no solution was obtained after FLP=-1.3mm

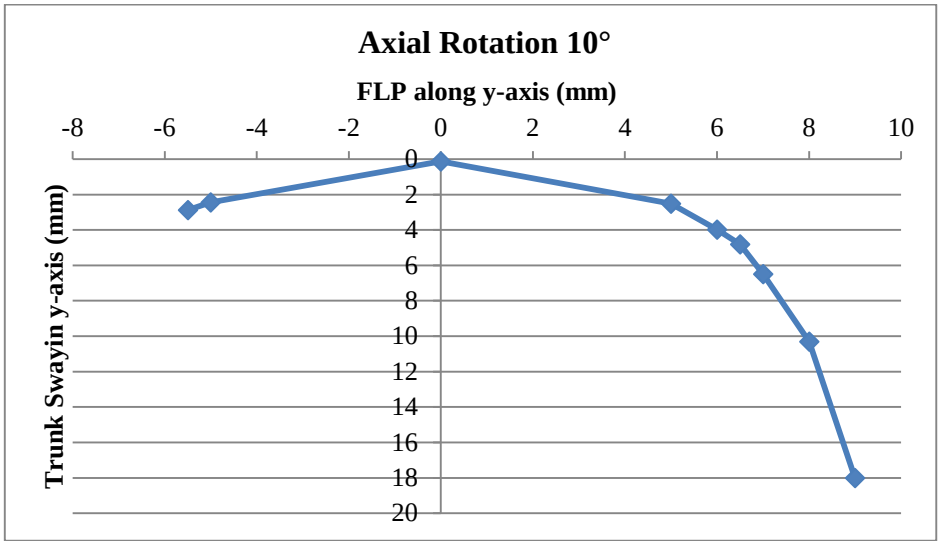

Figure 5-39 Trunk sway at different FLPs along y-axis (x=0mm) for left axial rotation 10°. The spine buckled and no solution was obtained at FLP=-6mm

Table 5-1 Muscle forces at the upper and lower limit FLPs along x-axis for each posture

	Neutral		**Flex. 40°**		**Ext. 5°**		**LB30°**		**AR10°**	
FLP along x-axis	**-1.3**	**1.8**	**-5**	**3**	**-1**	**1.5**	**-3.8**	**2.7**	**-1.3**	**2.1**
SerratusPI_L1_Rib11_L	0	0	83	83	0	0	0	0	0	0
SerratusPI_L1_Rib11_R	0	0	79	75	0	0	0	0	0	0
SerratusPI_L2_Rib12_L	0	0	0	0	0	0	0	19	0	0
LatissimusDorsi_L1_Hum_L	54	85	0	0	85	85	2	0	73	82
LatissimusDorsi_L1_Hum_R	54	85	0	0	85	85	71	52	85	85
LatissimusDorsi_L2_Hum_L	38	13	0	0	8	16	0	0	0	2
LatissimusDorsi_L2_Hum_R	38	13	0	0	9	16	15	15	0	0
LatissimusDorsi_L3_Hum_L	17	21	0	0	41	43	0	0	30	33
LatissimusDorsi_L3_Hum_R	17	21	0	0	41	43	43	43	0	1
LatissimusDorsi_L4_Hum_L	0	3	0	0	0	0	0	0	25	25
LatissimusDorsi_L4_Hum_R	0	3	0	0	0	0	25	25	0	0
Iliocostalis_Sacrum_Rib12_R	0	0	0	0	0	0	21	25	0	0
Longissimus_Sacrum_Rib11_R	0	0	58	54	0	0	0	0	0	0
Longissimus_Sacrum_Rib12_L	0	0	0	0	0	0	0	0	0	0
Longissimus_Sacrum_Rib12_R	0	0	3	2	0	0	0	0	0	0
Longissimus_L3_T3_L	0	0	48	34	0	0	0	0	0	0
Longissimus_L3_T3_R	0	0	5	28	0	0	0	0	0	0
Longissimus_L4_T5_L	0	0	0	0	0	3	0	0	0	0
Longissimus_L4_T5_R	0	0	0	0	0	3	0	0	0	0
Longissimus_Sacrum_T12_L	0	0	53	58	0	0	0	0	0	0
RecAbdominis_Pel_Rib5_L	0	0	1	28	0	0	0	0	0	0
RecAbdominis_Pel_Rib5_R	0	0	0	22	0	0	0	0	0	0
ExternalOb_Pel_Rib7_L	11	14	88	88	47	55	0	21	1	2
ExternalOb_Pel_Rib7_R	11	14	88	88	47	55	88	88	43	57
ExternalOb_Pel_Rib8_R	0	0	0	0	0	0	104	104	0	0
ExternalOb_Pel_Rib12_L	0	0	0	0	0	0	44	1	0	0
InternalOb_Pel_Rib12_L	24	35	0	0	26	33	0	0	0	0
InternalOb_Pel_Rib12_R	24	35	0	0	26	33	58	77	39	50
InternalOb_Pel_Rib11a_L	0	0	0	0	0	0	0	0	1	10
InternalOb_Pel_Rib10b_L	0	0	0	0	0	0	0	2	0	0
InternalOb_Pel_Rib10b_R	0	0	0	0	0	0	52	39	0	0
InternalOb_Pel_Rib11b_R	0	0	0	0	0	0	93	93	0	0
Intertransversarii_L1_T12_La_L	0	0	0	0	0	0	0	0	2	0
Intertransversarii_L1_T12_La_R	0	0	0	5	0	0	45	45	0	0
Intertransversarii_L1_T12_Me_L	0	0	45	45	0	0	35	3	0	0
Intertransversarii_L1_T12_Me_R	0	0	45	45	0	0	0	0	0	0
Rotatores_L1_T12_L	45	45	0	0	45	45	45	45	45	45
Rotatores_L1_T12_R	45	45	0	0	45	45	45	0	45	45
Rotatores_L2_T12_L	0	0	0	0	45	45	45	45	18	36

Table 5-1 Continued

	Neutral		Flex. 40°		Ext. 5°		LB30°		AR10°	
FLP along x-axis	**-1.3**	**1.8**	**-5**	**3**	**-1**	**1.5**	**-3.8**	**2.7**	**-1.3**	**2.1**
Rotatores_L2_T12_R	0	0	0	0	45	45	0	0	45	45
Interspinales_L2_L1_L	13	22	45	45	45	45	41	17	40	2
Interspinales_L2_L1_R	13	22	14	25	44	45	45	45	0	39
Intertransversarii_L2_L1_La_L	0	0	5	0	0	0	0	0	0	0
Intertransversarii_L2_L1_La_R	0	0	0	0	0	0	45	45	0	0
Intertransversarii_L2_L1_Me_L	0	0	28	18	0	0	45	45	2	8
Intertransversarii_L2_L1_Me_R	0	0	40	29	0	0	0	0	0	0
Rotatores_L2_L1_L	45	45	1	0	39	34	45	45	45	45
Rotatores_L2_L1_R	45	45	0	2	39	35	23	18	37	45
Rotatores_L3_L1_L	25	45	0	0	12	15	0	0	39	38
Rotatores_L3_L1_R	25	45	0	0	12	12	45	14	45	45
Longissimus_Sacrum_L2_R	0	0	0	0	0	0	6	0	0	0
Multifidus_L5_L2_F3_L	0	0	0	0	0	0	11	0	0	0
PsoasMajor_Fe_L2_L	0	0	12	27	0	0	0	0	0	0
PsoasMajor_Fe_L2_R	0	0	25	43	0	0	19	0	0	0
QuadratusLum_Pel_L2_L	0	0	5	0	0	0	86	74	0	0
Interspinales_L3_L2_L	45	39	0	0	45	45	45	45	0	7
Interspinales_L3_L2_R	45	39	0	0	45	45	45	45	43	45
Intertransversarii_L3_L2_La_L	0	0	0	0	0	15	0	0	0	0
Intertransversarii_L3_L2_La_R	0	0	0	0	0	16	45	45	22	19
Intertransversarii_L3_L2_Me_L	0	0	0	0	44	45	0	0	30	40
Intertransversarii_L3_L2_Me_R	0	0	0	0	45	45	45	45	0	0
Rotatores_L3_L2_L	24	7	0	0	45	38	15	9	23	30
Rotatores_L3_L2_R	24	7	2	0	45	40	0	0	35	45
Longissimus_Sacrum_L3_L	0	0	0	0	26	32	0	0	2	6
Longissimus_Sacrum_L3_R	0	0	0	0	26	32	89	91	0	0
PsoasMajor_Fe_L3_R	0	0	0	0	0	0	31	22	0	0
QuadratusLum_Pel_L3_L	0	0	12	18	0	0	0	0	0	0
QuadratusLum_Pel_L3_R	0	0	12	18	0	0	0	0	0	0
Interspinales_L4_L3_L	44	45	0	0	45	45	45	32	45	45
Interspinales_L4_L3_R	44	45	0	0	45	45	45	45	45	45
Intertransversarii_L4_L3_La_L	0	0	0	0	35	45	0	0	0	21
Intertransversarii_L4_L3_La_R	0	0	0	0	35	45	17	0	1	16
Intertransversarii_L4_L3_Me_L	45	45	0	0	45	45	0	0	45	45
Intertransversarii_L4_L3_Me_R	45	45	0	0	45	45	45	45	29	27
Rotatores_L4_L3_L	0	0	39	44	0	0	0	0	5	5
Rotatores_L4_L3_R	0	0	45	45	0	0	45	37	0	0
Iliocostalis_ Sacrum_L4_L	0	0	0	0	0	0	14	0	0	0
Longissimus_Sacrum_L4_L	97	102	29	32	126	134	0	0	104	115

Table 5-1 Continued

	Neutral		Flex. 40°		Ext. 5°		LB30°		AR10°	
FLP along x-axis	**-1.3**	**1.8**	**-5**	**3**	**-1**	**1.5**	**-3.8**	**2.7**	**-1.3**	**2.1**
Longissimus_ Sacrum _L4_R	97	102	36	33	126	134	204	174	87	92
Multifidus_ Sacrum _L4_F1_L	0	0	23	30	0	0	0	0	0	0
Multifidus_ Sacrum _L4_F1_R	0	0	36	30	0	0	0	0	0	0
Multifidus_ Sacrum_L4_F4_R	0	0	3	3	0	0	0	0	0	0
PsoasMajor_Fe_L4_R	0	0	0	0	0	0	39	0	0	0
Interspinales_L5_L4_L	16	17	0	0	34	38	0	0	0	0
Interspinales_L5_L4_R	16	17	0	0	33	37	0	0	25	32
Intertransversarii_L5_L4_La_L	0	0	0	0	0	0	45	45	29	36
Intertransversarii_L5_L4_Me_L	45	45	0	0	45	45	45	8	34	27
Intertransversarii_L5_L4_Me_R	45	45	0	0	45	45	45	26	45	45
Rotatores_L5_L4_R	0	0	0	0	0	0	45	43	0	0
Longissimus_ Sacrum_L5_L	80	84	0	0	105	111	0	0	56	59
Longissimus_ Sacrum_L5_R	80	84	0	0	105	111	38	102	34	37
Multifidus_ Sacrum_L5_F1_L	0	0	25	0	0	0	0	0	0	0
Multifidus_ Sacrum_L5_F1_R	0	0	54	7	0	0	0	0	0	0
Multifidus_ Sacrum_L5_F2_L	0	0	38	16	0	0	0	0	0	0
Multifidus_ Sacrum_L5_F3_L	0	0	0	44	0	0	0	0	0	0
Multifidus_ Sacrum_L5_F3_R	0	0	28	82	0	0	0	0	0	0
Multifidus_ Sacrum_L5_F4_R	0	0	0	0	0	0	192	103	74	81
PsoasMajor_Fe_L5_R	0	0	0	0	0	0	44	77	0	0
Rotatores_ Sacrum_L5_L	0	0	3	6	0	0	0	0	0	0
Ligament T12_L1_R	0	0	12	12	-12	-12	-60	-60	0	0
Ligament L1_L2_R	0	0	13	13	-10	-10	-33	-33	0	0
Ligament L2_L3_R	0	0	15	15	-10	-10	-54	-54	1	1
Ligament L3_L4_R	0	0	15	15	-9	-9	-37	-37	1	1
Ligament L4_L5_R	0	0	12	12	-7	-7	-20	-20	1	1
Ligament T12_L1_L	0	0	0	0	0	0	0	0	0	0
Ligament T12_L1_L	0	0	12	12	-12	-12	5	5	-1	-1
Ligament L1_L2_L	0	0	14	14	-10	-10	4	4	-1	-1
Ligament L2_L3_L	0	0	15	15	-10	-10	5	5	-1	-1
Ligament L3_L4_L	0	0	15	15	-9	-9	5	5	-2	-2
Ligament L4_L5_L	0	0	12	12	-7	-7	4	4	-3	-3
Ligament T12_M	0	0	0	0	0	0	0	0	0	0
Ligament T12_L1_M	0	0	25	25	0	0	0	0	0	0
Ligament L1_L2_M	0	0	100	100	0	0	0	0	0	0
Ligament L2_L3_M	0	0	201	201	0	0	0	0	0	0
Ligament L3_L4_M	0	0	213	213	0	0	0	0	0	0
Ligament L4_L5_M	0	0	150	150	0	0	0	0	1	1
Ligament L5_ Sacrum_M	0	0	14	14	0	0	0	0	0	0

Table 5-1 Continued

	Neutral		**Flex. 40°**		**Ext. 5°**		**LB30°**		**AR10°**	
FLP along x-axis	**-1.3**	**1.8**	**-5**	**3**	**-1**	**1.5**	**-3.8**	**2.7**	**-1.3**	**2.1**
RF-Trunk	629	673	738	797	777	824	556	491	694	752
RF-L1	615	665	750	794	756	803	656	601	684	747
RF-L2	596	647	768	849	744	808	682	592	664	722
RF-L3	604	643	787	871	784	846	726	629	626	698
RF-L4	694	731	794	876	859	915	894	708	727	784
RF-L5	707	746	778	864	889	947	920	789	723	781
Tr-My	0	0	0	0	0	0	5914	6243	0	0
L2-Mz	0	0	0	0	0	0	1327	2007	0	0
L3-Mz	0	0	0	0	0	0	1342	2438	0	0
L4-Mz	0	0	0	0	0	0	82	2372	0	0
Cost function	3846	4105	4615	5050	4809	5143	13098	16870	4118	4484

Table 5-2 Muscle forces at the upper and lower limit FLPs along y-axis for lateral bending 30° and axial rotation 10°

	LB30		**AR10**	
FLP along y-axis	**-8**	**9**	**-6**	**7**
SerratusPI_L1_Rib11_L	0	0	0	0
SerratusPI_L1_Rib11_R	0	0	0	12
LatissimusDorsi_L1_Hum_L	40	0	83	72
LatissimusDorsi_L1_Hum_R	57	50	85	85
LatissimusDorsi_L2_Hum_L	0	0	2	6
LatissimusDorsi_L2_Hum_R	11	60	9	0
LatissimusDorsi_L3_Hum_L	0	0	13	43
LatissimusDorsi_L3_Hum_R	43	43	0	0
LatissimusDorsi_L4_Hum_L	0	0	17	25
LatissimusDorsi_L4_Hum_R	25	25	0	0
Iliocostalis_Sa_Rib12_R	40	14	0	0
Longissimus_L4_T5_L	0	0	0	5
ExternalOb_Pel_Rib7_L	22	8	2	9
ExternalOb_Pel_Rib7_R	88	88	6	52
ExternalOb_Pel_Rib8_R	104	104	41	0
ExternalOb_Pel_Rib12_L	0	39	0	0
InternalOb_Pel_Rib12_R	64	68	38	41
InternalOb_Pel_Rib11a_L	0	0	0	34
InternalOb_Pel_Rib10b_L	0	31	0	0
InternalOb_Pel_Rib10b_R	46	46	0	0
InternalOb_Pel_Rib11b_R	93	93	0	0
Intertransversarii_L1_T12_La_L	0	0	3	45
Intertransversarii_L1_T12_La_R	45	45	0	0
Intertransversarii_L1_T12_Me_L	0	4	0	0
Rotatores_L1_T12_L	45	45	41	45
Rotatores_L1_T12_R	0	25	45	45
Rotatores_L2_T12_L	45	45	4	17
Rotatores_L2_T12_R	10	0	32	45
Multifidus_ L4_L1_F4_R	0	0	0	4
QuadratusLum_Pel_L1_L	0	23	0	0
Interspinales_L2_L1_L	45	0	45	45
Interspinales_L2_L1_R	45	38	3	1
Intertransversarii_L2_L1_La_L	0	0	0	44
Intertransversarii_L2_L1_La_R	45	45	0	0
Intertransversarii_L2_L1_Me_L	25	45	0	0
Intertransversarii_L2_L1_Me_R	0	0	0	4
Rotatores_L2_L1_L	35	16	45	45
Rotatores_L2_L1_R	6	27	45	25
Rotatores_L3_L1_L	0	20	34	41

Table 5-2 Continued

	LB30		AR10	
FLP along y-axis	**-8**	**9**	**-6**	**7**
Rotatores_L3_L1_R	45	38	45	45
QuadratusLum_Pel_L2_L	57	37	0	0
Interspinales_L3_L2_L	45	45	24	45
Interspinales_L3_L2_R	45	45	45	32
Intertransversarii_L3_L2_La_L	0	0	0	12
Intertransversarii_L3_L2_La_R	45	45	17	0
Intertransversarii_L3_L2_Me_L	0	0	4	45
Intertransversarii_L3_L2_Me_R	45	45	0	0
Rotatores_L3_L2_L	16	21	18	18
Rotatores_L3_L2_R	3	0	25	31
Longissimus_ Sa_L3_L	0	0	0	28
Longissimus_ Sa_L3_R	106	67	0	0
PsoasMajor_Fe_L3_R	107	0	0	0
QuadratusLum_Pel_L3_L	39	0	0	0
Interspinales_L4_L3_L	37	44	39	45
Interspinales_L4_L3_R	45	45	45	45
Intertransversarii_L4_L3_La_L	0	0	0	45
Intertransversarii_L4_L3_La_R	29	26	10	0
Intertransversarii_L4_L3_Me_L	0	0	33	45
Intertransversarii_L4_L3_Me_R	45	45	45	39
Rotatores_L4_L3_L	0	0	0	17
Rotatores_L4_L3_R	21	45	0	0
Iliocostalis_Sa_L4_L	27	0	0	0
Longissimus_Sa_L4_L	0	0	79	122
Longissimus_Sa_L4_R	238	179	111	49
Multifidus_Sa_L4_F4_R	0	0	0	59
PsoasMajor_Fe_L4_R	101	0	0	0
Interspinales_L5_L4_L	0	34	0	25
Interspinales_L5_L4_R	0	0	20	0
Intertransversarii_L5_L4_La_L	45	45	2	45
Intertransversarii_L5_L4_Me_L	38	0	45	45
Intertransversarii_L5_L4_Me_R	0	35	45	45
Rotatores_L5_L4_R	0	45	0	0
Longissimus_Sa_L5_L	0	0	73	99
Longissimus_Sa_L5_R	124	18	78	35
Multifidus_Sa_L5_F4_R	106	194	17	63
PsoasMajor_Fe_L5_R	0	64	0	8
Ligament T12_L1_R	-60	-60	0	0
Ligament L1_L2_R	-33	-33	0	0

Table 5-2 Continued

	LB30		AR10	
FLP along y-axis	**-8**	**9**	**-6**	**7**
Ligament L2_L3_R	-54	-54	1	1
Ligament L3_L4_R	-37	-37	1	1
Ligament L4_L5_R	-20	-20	1	1
Ligament T12_L1_L	0	0	0	0
Ligament T12_L1_L	5	5	-1	-1
Ligament L1_L2_L	4	4	-1	-1
Ligament L2_L3_L	5	5	-1	-1
Ligament L3_L4_L	5	5	-2	-2
Ligament L4_L5_L	4	4	-3	-3
Ligament T12_M	0	0	0	0
Ligament T12_L1_M	0	0	0	0
Ligament L1_L2_M	0	0	0	0
Ligament L2_L3_M	0	0	0	0
Ligament L3_L4_M	0	0	0	0
Ligament L4_L5_M	0	0	1	1
Ligament L5_Sa_M	0	0	0	0
RF-Trunk	531	562	665	814
RF-L1	634	690	655	806
RF-L2	620	664	631	770
RF-L3	772	659	615	771
RF-L4	979	738	701	859
RF-L5	1002	803	724	860
Tr-My	5993	6285	0	0
L2-Mz	2565	2301	0	0
L3-Mz	853	3007	0	0
L4-Mz	0	1187	0	0
Cost function	13950	16897	3991	4879

CHAPTER 6

PARAMETRIC STUDIES

6.1 Body Weight Variation

The effect of external load variation on the lumbar spine stability achieved by creating CFLs via spinal muscle force was investigated in this study. The external load variation was simulated by changing the upper body weights the lumbar spine supported. The simulated weights were 25kg, 35kg, 40kg, and 45kg (i.e., 50% of the total body weight). These weights were applied at the CG of the trunk in both the FE and the optimization models. By constraining FLP to zero, muscle forces and patterns that create CFLs on the spinal joints and stabilize the spine were found for most of the postures studied under these body weights. The only exception was extension 5° with the body weight of 45kg. Muscle solutions were feasible in the optimization model for this case, but the spine could not be stabilized in the FE model under the solved muscle forces and patterns.

The results from this study show that as the body weight increased, the JRFs at each lumbar level were also increased in all the postures, shown in Figure 6-1. In lateral bending 30°, the joint reaction moments were also increased with the increased body weight. Since the cost function was to minimize the total joint reaction loads (both forces and moments), cost function versus upper body weights was plotted for each posture to study their correlation, shown in Figure 6-2. It was found that the cost function or joint reaction loads increased linearly with the increased upper body weight in all the postures under follower load condition.

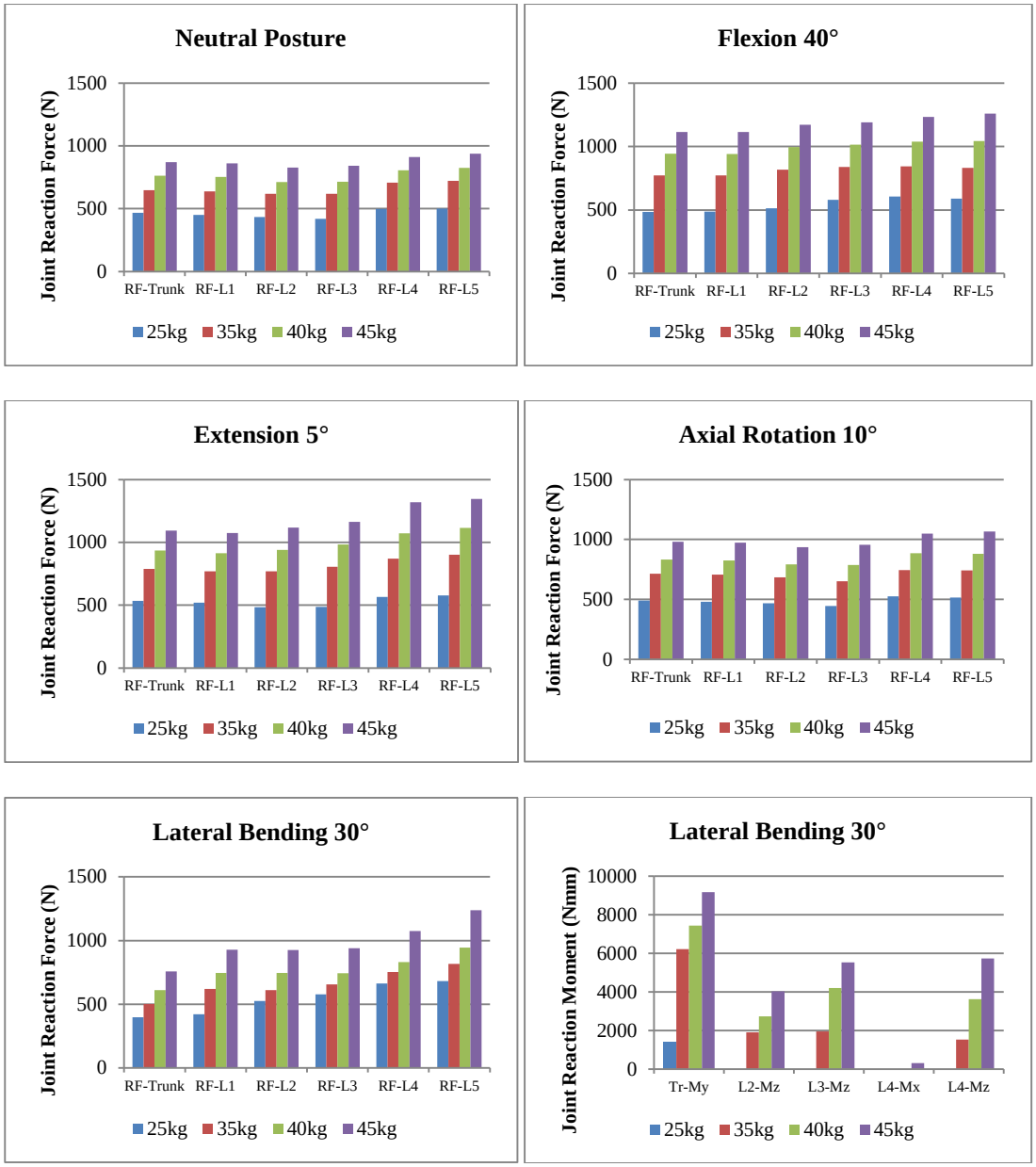

Figure 6-1 Correlation between JRFs (or CFLs) and upper trunk weight for all postures

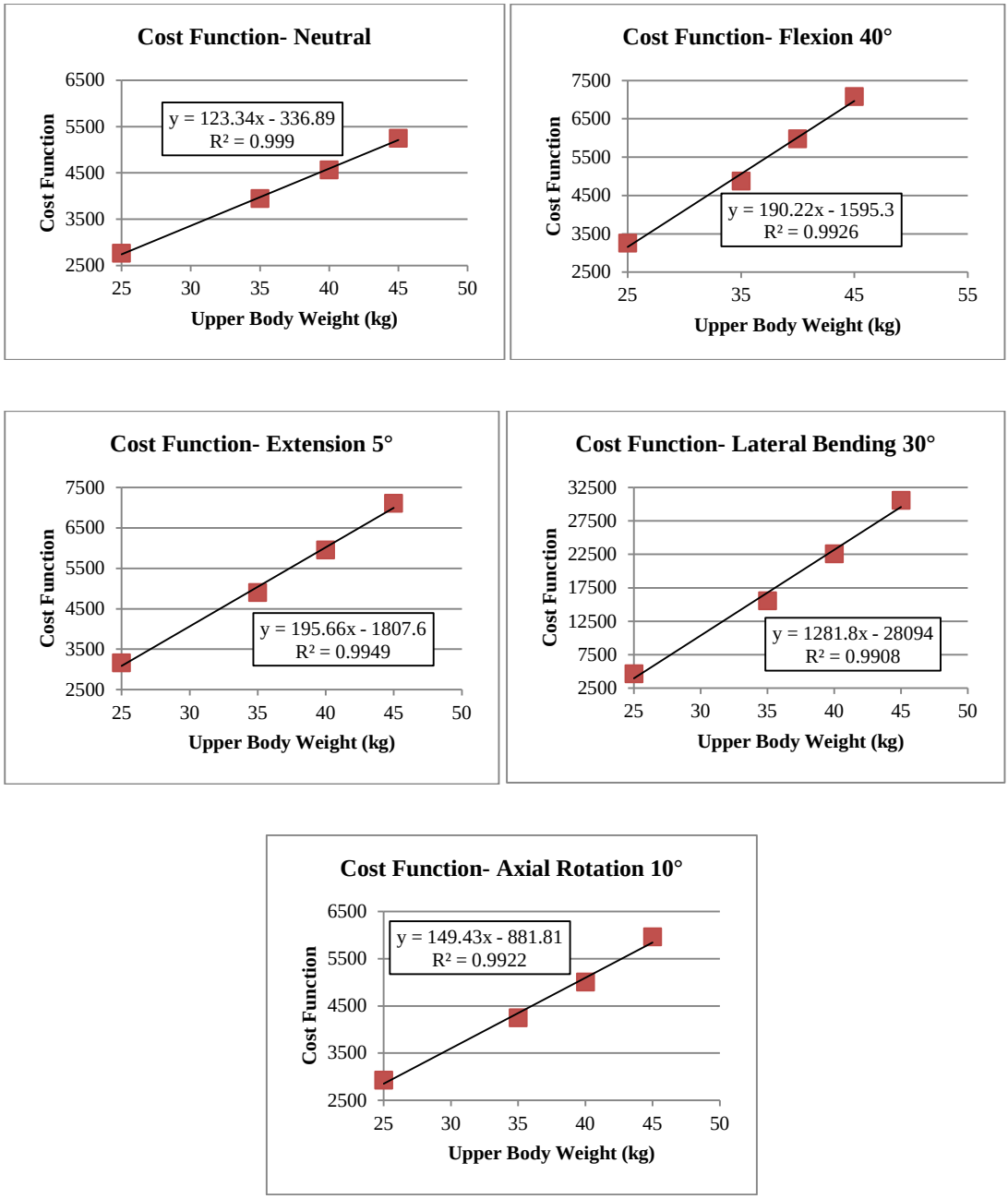

Figure 6-2 Correlation between cost function and the upper body weight

It was also interesting to study how the change in trunk weights affects the stability of the spine. Trunk sway in x-axis was considered for all the postures in sagittal plane, trunk sway in y-axis was considered for lateral bending, and trunk sway in both axes was considered for axial rotation. After applying the muscles forces

obtained from the optimization model to the FE model, it was found that the spine had small trunk sway, indicating a stable spine, for all the cases other than extension 5° with an upper body weight of 45kg. However, this study was only done at FLP=0mm. If this study would be done at a different FLP, there might exist CFLs creating muscle forces and patterns that can stabilize the spine at extension 5° with an upper body weight of 45kg. Further study is required to prove this speculation.

The recruited muscles at different body weights for all the postures are shown in Figures 6-3 to 6-7. Blue color indicates muscles with low muscle forces and red color indicates muscles with higher muscle forces. The results showed that there was an increase in muscle force as the weight increased from 25kg to 45kg for all the postures. Additionally, the total number of muscle fascicles was also increased in most postures. Table 6-1 provides the summary of the total number of muscle fascicles that were activated in all the postures under different trunk weights. As the muscle forces and the number of muscle fascicles were increased, the JRFs at all lumbar levels were also increased. This result is reasonable since as the trunk weight increases, more muscles need to be recruited to support the increased body weight and to balance the moment produced by the trunk weight. It was also observed that there were changes in muscle patterns as the trunk weight increased for all postures. For example, in neutral posture, when the trunk weight was increased from 35kg to 40kg, the number of the muscle fascicle was decreased (see Table 6-1), but the joint reaction forces at all lumbar levels were still increased due to the change in muscle patterns. This is reasonable since some of the recruited muscle fascicles might have reached their limiting capacity as the trunk weight increased. New muscle fascicles needed to be recruited or new muscle patterns needed to be formed to minimize the cost function.

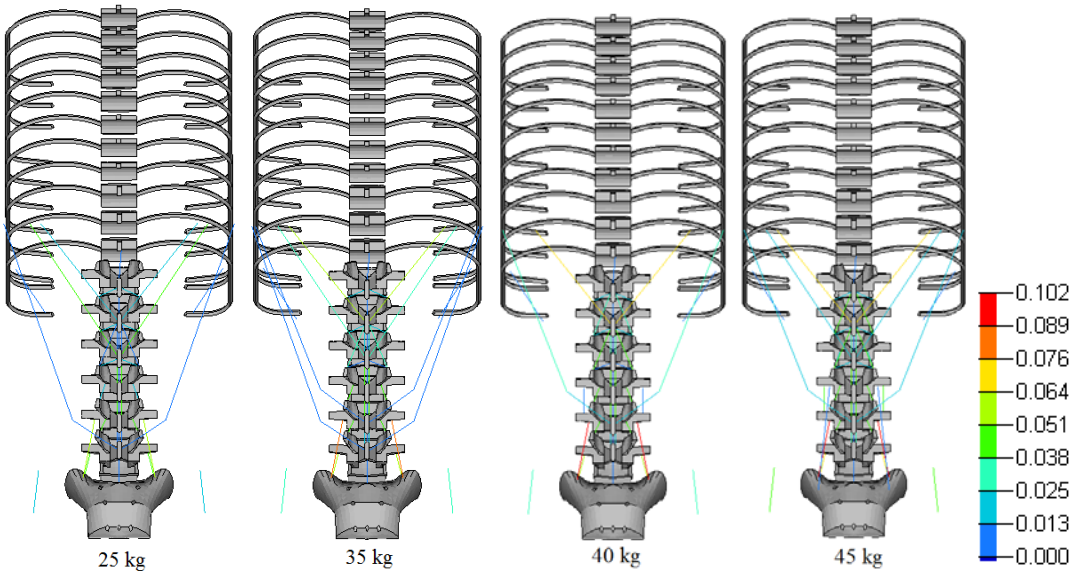

Figure 6-3 Recruited muscle fascicles for different body weights at neutral posture while constraining FLP=0mm (all muscle forces are in kN)

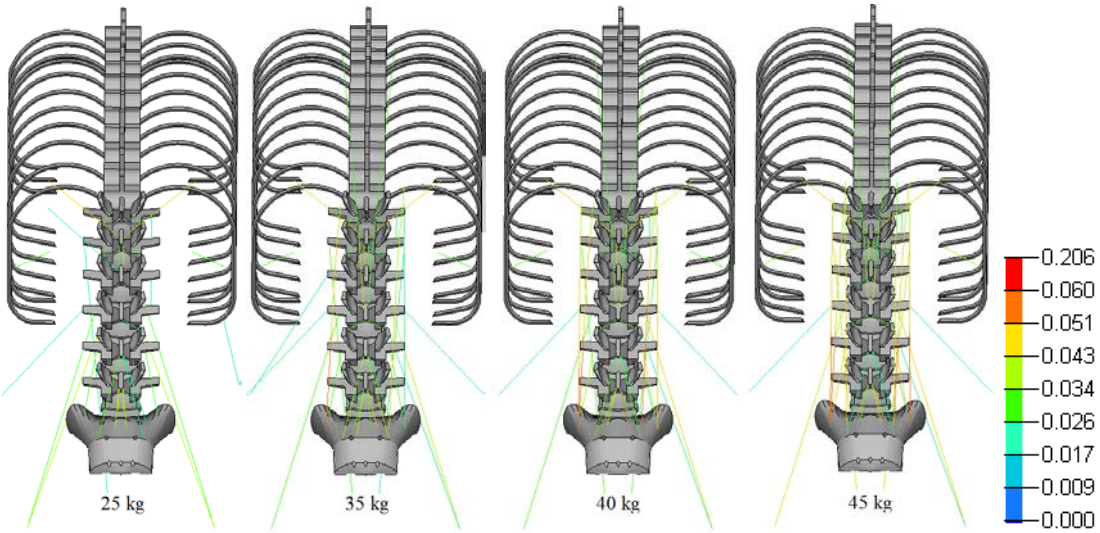

Figure 6-4 Recruited muscle fascicles for different body weights at flexion 40° while constraining FLP=0mm (all muscle forces are in kN)

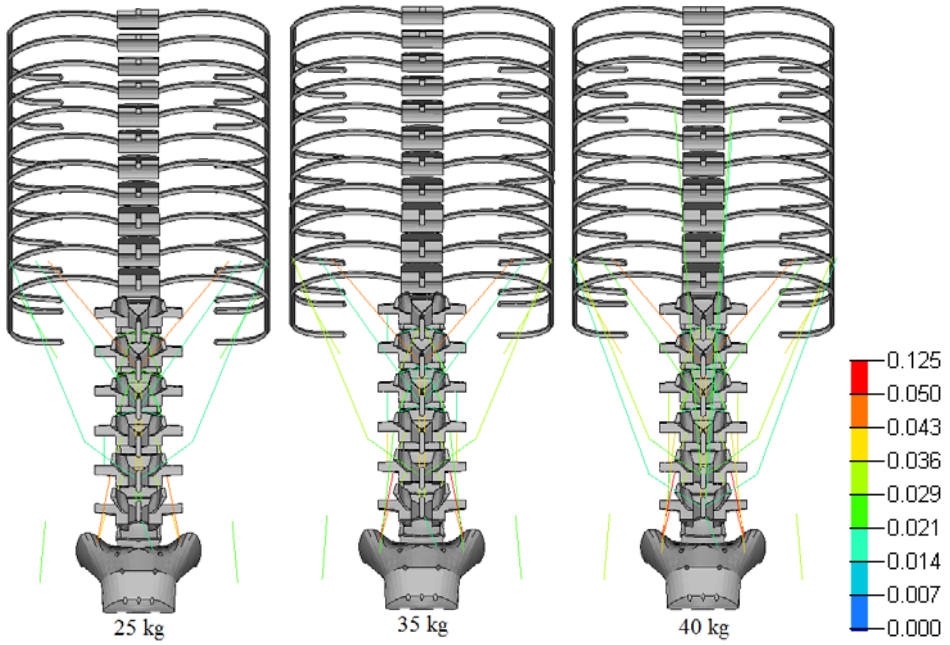

Figure 6-5 Recruited muscle fascicles for different body weights at extension 5° while constraining FLP=0mm (all muscle forces are in kN)

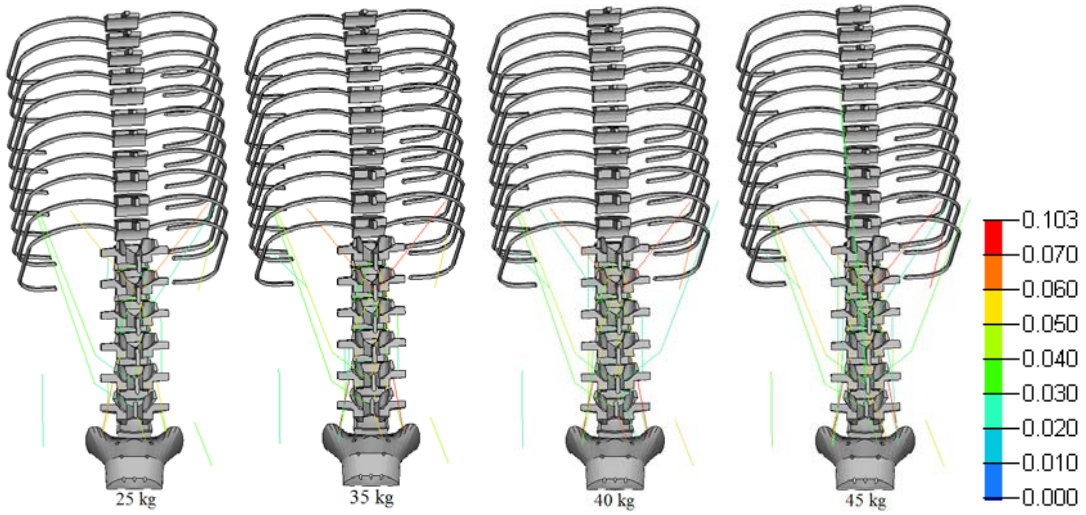

Figure 6-6 Recruited muscle fascicles for different body weights at axial rotation 10° while constraining FLP=0mm (all muscle forces are in kN)

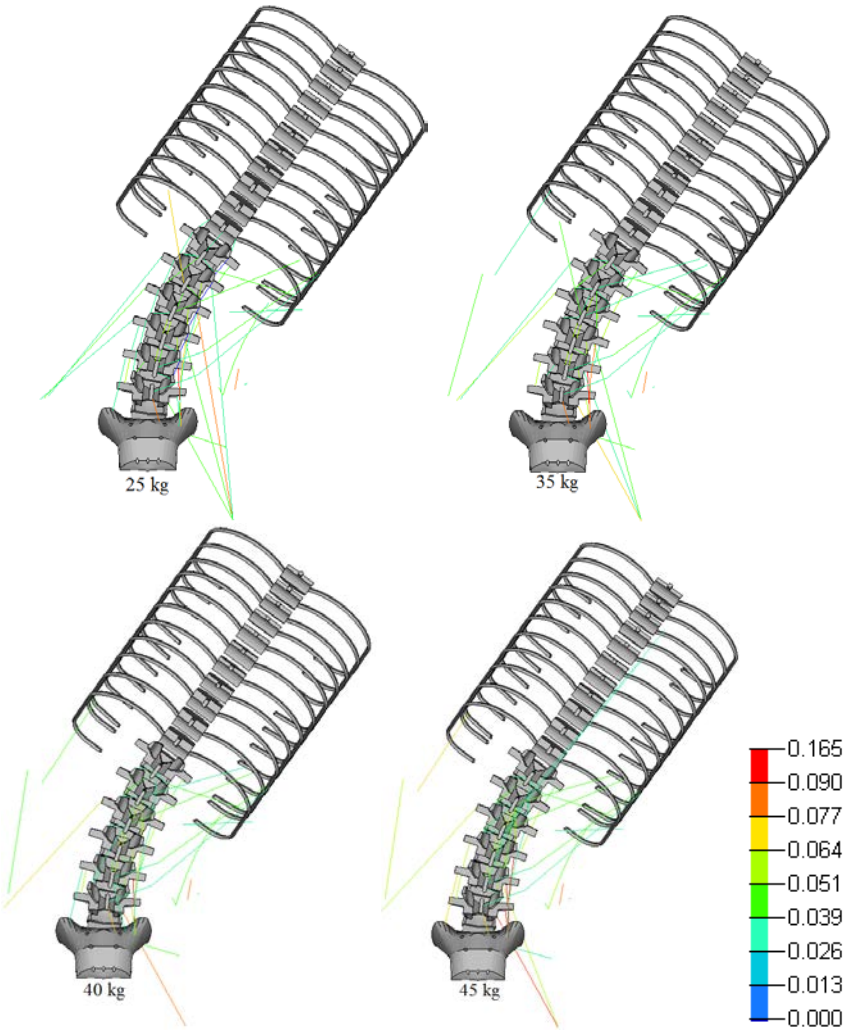

Figure 6-7 Recruited muscle fascicles for different body weights at lateral bending 30° while constraining FLP=0mm (all muscle forces are in kN)

Table 6-1 Number of recruited muscle fascicles at different upper body weights for all the postures

	Number of Muscle Fascicles				
Body Weight	Neutral	Flex. 40°	Ext. 5°	LB 30°	AR 10°
25 kg	36	30	42	54	38
35 kg	40	56	56	56	45
40 kg	38	62	72	62	52
45 kg	48	74	76	71	69

In order to prove pure CFLs are the normal physiological load on the lumbar spine, it is important to know the maximum trunk weight that CFLs can be created on

the lumbar spine for each posture. It is also important to check whether this maximum trunk weight is reasonable or not compared to the *in vivo* situations for each posture. Table 6-2 provides a summary of the trunk weight limits in all postures obtained from both optimization and FE models. These results were also obtained at FLP=0mm. It was found that in the optimization model, as the body weight increased, joint reaction moments started to be generated in all the postures other than flexion 40°. Originally, at the trunk weight of 35kg, the joint reaction moments were zero in all the postures other than lateral bending 30°. For example, in neutral posture, when the trunk weight was equal or below 990N, CFLs were created at all lumbar levels without any joint reaction moments. When the trunk weight was increased beyond 990N, joint reaction moments were generated. The maximum trunk weight with the joint reaction moments that could be solved using the optimization model was 1330N in neutral posture. By importing the optimization model results to the FE model, it was found that the spine buckled at a trunk weight above 500N. Mathematically, these joint reactions moments were generated to balance the moments caused by the muscles, trunk weight and ligaments. However, these joint reaction moments may induce spinal instability of the lumbar spine.

Table 6-2 Maximum body weight that can be applied to each posture at FLP=0mm a) in the optimization model without generating any JRM; b) in the optimization model with generating joint reaction moments; c) in the FE model. OPT=optimization model; JRM=joint reaction moments

Postures	OPT model w/o JRM	OPT model w JRM	FE model
Neutral	990N	1330N	500N
Flexion 40°	1070N	N/A	500N
Extension 5°	600N	850N	420N
LB 30°	N/A	850N	450N
AR 10°	470N	1250N	470N

The maximum trunk weight calculated from the optimization model was greater than the maximum trunk weight that stabilized the spine in the FE model for each posture. This is because unlike the FE model, the optimization model did not include any material properties of the discs, ligaments, facet, muscles, etc, thus it did not provide any information on stability of the spine. On the other hand, the FE model had its limitation too. It was not designed to be subject-specific. Depending on the material properties that were given to the ligaments and muscles, the maximum trunk weight that could stabilize the spine would be different. Also, the spinal vertebrae and the disc sizes of the FE model were smaller compared to an average person. As a result, the FE spine model has a smaller area moment of inertia to resist the bending moment generated by the muscles. Thus, even though some of the solutions obtained from the optimization model did not stabilize the spine in the current FE model, it does not mean these solutions are not able to stabilize the spine at all. Depending on how the material properties are specified in the FE model, some of these solutions from the optimization model may be able to stabilize the spine. For future studies, we would like to vary the material properties of the ligaments and increase the spin size of the FE model to study their effects on the maximum trunk weight.

The JRFs at all lumbar level for all postures at the maximum trunk weights of the optimization model and the FE model were plotted on Figures 6-8 to 6-10. According to Jager and Luttman's cadaveric study on 307 lumbar segments, they found that the average maximum compressive strength of the lumbar segments was 4.4kN with a standard deviation of 1.88kN [39]. This large variability was probably caused by the difference in lumbar strength depending on the age, bone mineral

content, and degenerative changes of the spine [39]. Based on their study and many other studies, Waters et al. stated that 3.4kN to be the compressive force that defines an increase risk of low-back injury [40]. By setting 3.4kN as the limiting criteria, Figures 6-8 and 6-9 show that the results obtained from the optimization model were reasonable since the JRFs obtained from the maximum trunk weights were comparable to 3.4kN. This indicated that CFLs at all lumbar levels can be created with any physiological body weight. On the other hand, the maximum trunk weights that stabilized the spine in the FE model were significantly lower in all postures. By plotting JRFs versus lumbar level, Figure 6-10 showed that in all the postures other than flexion, the JRFs reached about 1000N to 1200N at all lumbar levels before the spine buckled. This may indicate that the FE model has reached its saturation point and the maximum JRFs it could withstand was about 1000N to 1200N. Flexion posture was an exception since it is the most stable posture.

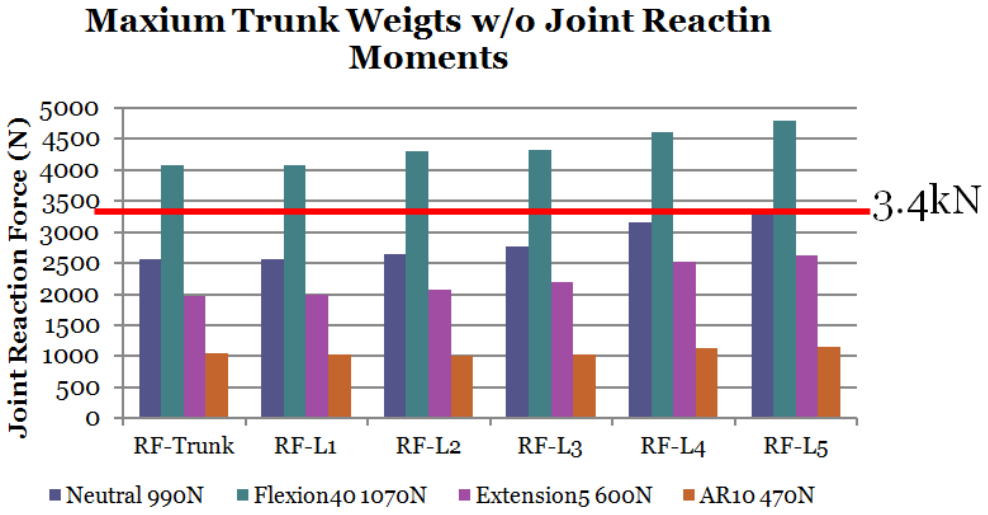

Figure 6-8 JRFs (or CFLs) at all lumbar levels for all the postures at the maximum trunk weights without the generating of the joint reaction moments

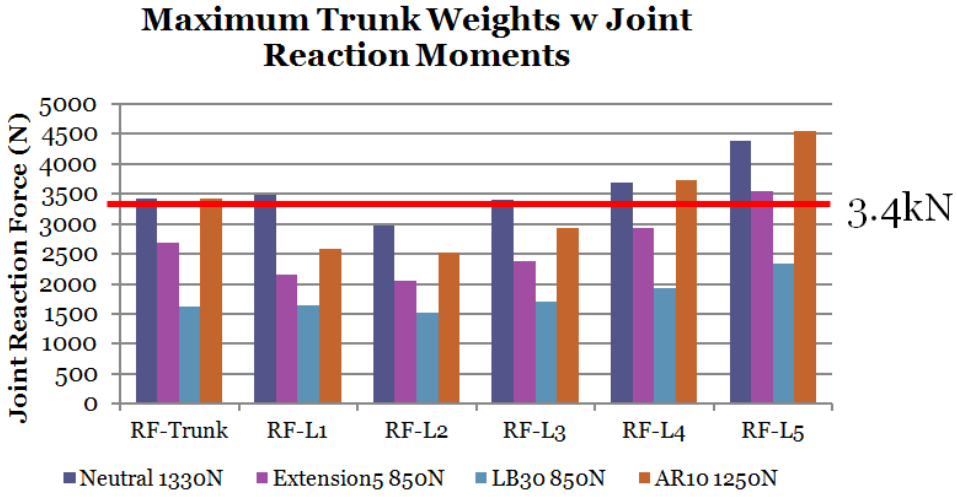

Figure 6-9 JRFs (or CFLs) at all lumbar levels for all the postures at the maximum trunk weights with the generating of the joint reaction moments

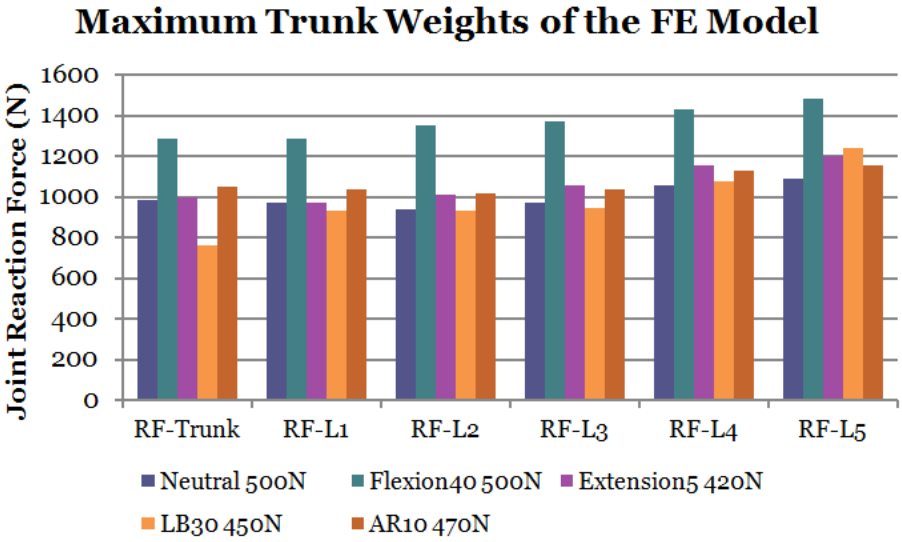

Figure 6-10 JRFs (or CFLs) at all lumbar levels for all the postures at the maximum trunk weights of the FE model

6.2 Disc Property Variation

It was also interesting to know how the change in disc property at one lumbar level, mimicking disc degeneration, affects the spinal stability under CFLs for each posture. Four cases were simulated, 25% and 50% reduction of the young's modulus of the intervertebral disc at L4/L5 level and L5/S1 level, respectively. Since the optimization model did not incorporate the material properties of the discs, changing disc properties did not have any effects on the muscle recruiting patterns, recall that muscle recruiting patterns were calculated from the optimization model only. As a result, the same muscle forces and patterns from the normal spine solved at FLP=0mm were applied to these four cases. Since this was not intend to be an intensive study on disc degeneration under CFLs, but just to check the feasibility of CFLs creating muscles forces to stabilize the spine under these four conditions, the limitation in the optimization model would not affect the study. It was found that the spine was stabilized in all four cases in neutral posture, but was buckled in all four cases in all the other postures shown in Tables 6-3 and 6-4.

Table 6-3 Comparison of trunk sway of 25% and 50% reduction of the young's modulus of the L4/L5 disc with the original model at FLP=0mm. Trunk sway of 5mm or greater are considered that spine is unstable.

L4/L5 Level						
FLP=0mm	Original		25% Reduction		50% Reduction	
(Trunk Sway)	x (mm)	y (mm)	x (mm)	y (mm)	x (mm)	y (mm)
Neutral	-0.5	-0.02	-0.945	-0.0314	-5.75	0.18
Flexion 40°	0.65	-0.061	86.53	-0.285	87.82	-0.29
Extension 5°	-1.16	-0.15	69.99	-0.189	73.03	-0.232
Lateral Bending 30°	0.788	0.163	82.36	-25.71	80.65	-23.88
Axial Rotation 10°	-0.71	-0.12	109.97	18.95	112.15	21.86

Table 6-4 Comparison of trunk sway of 25% and 50% reduction of the young's modulus of the L5/S1 disc with the original model at FLP=0mm

L5/S1 Level						
FLP=0mm	Original		25% Reduction		50% Reduction	
(Trunk Sway)	x (mm)	y (mm)	x (mm)	y (mm)	x (mm)	y (mm)
Neutral	-0.5	-0.02	-0.5	-0.046	0.353	-0.07055
Flexion 40°	0.65	-0.061	87.95	-0.29	90.72	-0.36
Extension 5°	-1.16	-0.15	70.39	-0.1244	72.04	-0.28
Lateral Bending 30°	0.788	0.163	82.6	-0.249	81.04	-23.62
Axial Rotation 10°	-0.71	-0.12	110.9	19.03	112.89	18.47

CHAPTER 7

DISCUSSION

It is generally believed that the root of low back disorders is most likely due to the mechanical insufficiency of the spinal column. However, it still remains unclear how the flexible spine can support large weight in a stable manner. Reviews from previous studies showed that shear forces increased the rate of disc degeneration and the ligamentous lumbar spine could withstand 1200N force without buckling while maintaining its flexibility under CFLs [8, 9]. These results point us to question whether CFLs at all lumbar spine levels could be the normal physiological load on spine.

To answer this question, it is important to first determine if the spinal muscles are able to generate CFLs at all lumbar levels in all postures. Patwardhan et al. first investigated the role of spinal muscles on the generation of CFLs in frontal plane posture using a homogeneous isotropic beam-column model [24]. They found that CFLs could be generated by the spinal muscles in frontal plane posture. However, their model was very simplified, by simulating the spinal system using one single beam-column instead of multi-segments and only five muscles were modeled. They also only performed the study in frontal plane posture. Kim and Kim developed a more complicated model which also included SIMs, but they were not able to find the perfect CFLs as shear forces were present in their results [25]. By developing an optimization model including 232 spinal muscle fibers, Han et al. found that it was feasible for the spinal muscles to create CFLs at all lumbar spine levels in sagittal plane postures. However, they did not perform any study in laterally bended postures

and axially rotated postures [27, 28].

It is not enough to just find out the feasibility of spinal muscles to create CFLs, since the final goal is to see whether these CFLs creating spinal muscles are able to stabilize the spine and maintain its flexibility or not. Kim et al. picked up Han's study by building a FE model to study the stability of the spine under the muscles forces solved through the optimization model [23, 29]. They found that the spine was able to be stabilized in the postures of sagittal plane. However, they also did not perform any study in the postures of other planes.

7.1 Feasibility of CFLs in all 3-D Postures

The optimization analyses of this study showed that it is feasible for spinal muscles to create perfect CFLs at numerous spinal muscle forces combinations varying as a function of the FLP location in all 3-D postures tested in this study. However, the FE analyses revealed that only optimization solutions of muscle forces creating perfect CFLs along the curve in the vicinity of the baseline curve (FLP=0mm) stabilized the lumbar spine.

From Figure 5-1, extension 5° showed the least available solutions that could stabilize the spine. This is reasonable since extension is the most unstable posture *in vivo* compared to other postures. Researchers have shown that people find extension uncomfortable and hard to maintain [41]. On the other hand, flexion 40 degrees had the most available solutions. This is also reasonable since people find that it is easier to stay balanced for a longer time in a flexed position. These results agreed with Han et. al's results that flexed postures showed more favorable results than other postures in the sagittal plane [28]. This may be possibly because that there are many more back

extensor muscles can be recruited to stabilize the spine during flexion compared to the fewer numbers of flexor muscles recruited to stabilize the spine during extension. The model predictions from this study reflected such phenomena.

The stable FLP range for right lateral bending 30° was comparable with the FLP range for flexion 40° and the area was more shifted toward the right side of the vertebral body shown in Figure 5-1. The stable FLP range for left axial rotation was relatively small and more shifted toward the left side of the vertebral body, also see Figure 5-1. The difference in the areas of the stable FLP ranges for the studied postures might be caused by the number and architecture of the spinal muscles that could be recruited for the posture. The unsymmetrical shape of the stable FLP range along coronal plane for right lateral bending 30° and left axial rotation 10° might be caused by the lateral moment generated by the body weight and the asymmetrically recruited spinal muscles. The stable FLP ranges were larger in lateral direction than anterior-posterior direction for all postures. This was most likely resulted from the shape of the intervertebral joint and the mid-sagittal symmetry of the spinal muscle arrangement.

By setting FLP to different values, it was found that there were many feasible muscle force combinations that created perfect CFLs at all lumbar levels and stabilized the spine. The results showed that for all the studied postures, the JRFs were decreased as FLP moved toward the posterior side of the disc and increased as FLP moved toward the anterior side of the disc. On the other hand, there was a parabolic relationship between the FLP and the trunk sway. The most stable spine (spine with the least amount of trunk sway) did not occur at the lowest JRFs, but at FLP around zero where its JRFs were neither the highest nor the lowest among the

JRFs solved from the stable FLP range for all the postures. Since the recruited muscle forces and patterns had a direct effect on the JRFs (higher muscle forces cause higher JRFs), in order to stabilize the spine, appropriate muscle forces and patterns were needed. Since the recruited muscle forces and patterns were controlled by the FLP value, it can be concluded that FLP plays an important factor on spinal stability.

Because of the parabolic relationship between the FLP and the spinal stability (trunk sway), the same level of spinal stability could be obtained at two different FLPs. However, the JRFs, the muscle patterns and the number of muscles recruited were different at these different FLPs. Thus, it can be concluded that it is feasible for a person to achieve the same level of spinal stability at a certain posture by using different muscle recruitment patterns and experiencing different spinal loads. This result contrasted the previous optimization approaches that they lacked the biological sensitivity to various possible muscle recruitment patterns since they gave the same set of muscle patterns for the same task all the time [19]. If there is only one muscle pattern available to stably maintain a certain posture, the recruited muscles will eventually become fatigue and the spine will eventually become unstable and our daily activities will be limited. The results from this study, by varying FLP, provided many feasible muscle patterns to stabilize the spine at a certain posture and seemed to be more reasonable. By having multiple feasible solutions, it can be postulated that it is feasible for the spine to maintain the same stability while performing dynamic motions. However, future studies are required to prove this postulation.

7.2 Model Validation of the Spinal Muscles and the JRFs

The spinal muscle forces and patterns and JRFs obtained at FLP equal to 0mm were chosen for the purpose of model validation. This is because it was found that the lumbar spine was generally the most stable at FLP close to zero in all postures. Careful comparison of the spinal muscle patterns at each posture from this study with the literature data showed reasonable agreements in many aspects (please see Tables 4-1 and 4-2 for detailed spinal muscle data). The model predictions of this study showed that non-zero forces in back extensor and flexor muscles are required for the stabilization of the lumbar spine in neutral standing, flexion 40°, and extension 5°. Since the CG of the trunk lies in front of the spine, extensor muscles are required to control and maintain neutral posture in a stable manner. The antagonistic co-contraction of abdominal muscles (RA, EO and IO) was also necessary to stabilize the spine around neutral posture [42]. Through surface electromyography (sEMG) study, Cholewicki et al. also found low level activity of antagonistic flexor-extensor muscle co-activation [42]. Since back muscle activities in neutral posture are low, which causes the lumbar spine more vulnerable to buckle, these antagonistic flexor muscles are needed to stabilize the spine. Furthermore, a stable neutral posture usually needs to be maintained for hours during daily activities; so the level of the activation of antagonistic flexor muscles has to be low to prevent muscle fatigue. Johsson showed that prolonged muscle contraction of 5% MVC correlated with muscle pain [43]. Our model predicted 4.7% MVC of abdominal muscle activation in neutral posture. Our results in neutral posture also agreed with Sullivan et al.'s sEMG results that the activation of IO and EO was higher than RA during erect standing with IO being the highest activity [44]. No contribution of RA muscle predicted in this study may result

from higher upper body stability due to the fixation of the pelvis than that in Sullivan et al.'s study where the sEMGs were measured from the subject standing upright with no pelvic fixation. Moreover, Cholewicki et al. found that the removal of RA from their model had a negligible deteriorating effect on spine stability [45]. In flexion, the prediction of 61 N in RA and 176 N in EO agrees with the previous identification of RA and EO muscles as the primary players in lumbar spine flexion [13]. The activation of both longissimus pars thoracis and longissimus pars lumborum agrees with Floyd and Silver's finding that there was an activation of ES at T10, T12, L2, and L4 level during flexion by using sEMG [46].

In lateral bending (LB), the model predictions showed that greater muscle forces on the ipsilateral side were needed to maintain the posture stably than those on the contralateral side. This corresponded with Potvin et al.'s sEMG study that the antagonist trunk muscle activity during LB was generally much lower than the agonist muscle activity [47]. Ipsilateral contraction of these muscles pulled the trunk to one side [48]. The primary muscle players in LB are the ES muscles and the oblique muscles [13]. The results of this study showed that the forces in the iliocostalis pars thoracis, longissimus pars lumborum, IO, and EO were relatively large. In addition, large forces in the ipsilateral LD, PM and multifidus muscles were also predicted in this study. This matched with Dumas et al's. findings of the contribution of unilateral contraction of the LD to lateral bending moment due to the orientation of force lines of action [49]. PM is also considered as a lateral flexor in the lumbar region due to its anatomic position [13]. Multifidus usually functions as a stabilizer rather than prime mover. It was found that multifidus can act as an "anti-flexor" since it could provide extension torque to counterbalance the flexion torque produced by the flexor muscles,

such as the oblique muscles [13, 50, 51]. Finally, both QL and SPI were recruited as antagonists to balance the torsion and flexion-extension moments generated by the agonist muscles, and hence help to stabilize the spine. They could also serve to augment stabilization from passive tissues, stiffen the joints, and regulate stress distributions during joint contact [47, 52].

There is no trunk muscle that is specifically designed for axial rotation. Axial rotation is always accompanied with significant flexion-extension and LB moments [53]. Kumar et al. found that the highest contributing muscles in AR were the contralateral EO, ipsilateral ES, and ipsilateral LD [54]. This agrees with our results shown in Table 4-1. McGill also reported that the LD and EO were strongly active as agonists during AR to generate the axial torque [55]. Even though the ES (longissimus) was very active to maintain the axially rotated posture, it did not generate axial torque. It was probably recruited as an antagonist to counterbalance the flexion torques produced by the oblique muscles and body weight in order to stabilize the spine. Multifidus muscles were also active in AR, agreeing with Morris et al.'s finding [48] of the action of multifidus muscles as "anti-flexors" to stabilize the spine by balancing the flexion torque together with the longissimus.

The JRFs predicted in this study at FLP equal to 0mm also showed strong agreement with those in the literature. The JRFs predicted at neutral standing posture ranged from 618 N (L2-L3) to 721 N (L5-S1). These values were comparable to those measured in *in vitro* and *in vivo* studies, which were between 500 N and 800 N [12, 56-58]. For FLEX40, the predicted disc load at the L3 disc (L3-L4) was 840N, while Nachemson's *in vivo* study showed that the disc load at the L3 disc was 1000N on an average body weight of 70kg [12]. The smaller JRFs in our model would be most

likely due to the firm fixation of the pelvis and sacrum simulated in this study, because the maintenance of flexion 40° with no pelvic fixation should be more mechanically challenging. Also, the pressure of the disc is not equally distributed in all directions during *in vivo* experiment of measuring spinal load. Depending on the location and the sensitivity of the pressure transducers, there might be some differences in readings. Actually, for postures like flexion, none of the previous *in vivo* studies had the exactly same result despite of the same boundary conditions and similar body weight [12, 58, 59]. JRFs were increased during extension compared to that predicted from the neutral posture. This is consistent with Katsuhiko et al.'s finding that the spinal load increased with both forward bending and backward bending [58]. The JRFs from LB and AR postures were lower than flexion and extension postures. This result is consistent with Van Dieen's finding that producing an asymmetric moment appears to cause slightly lower forces on the lumbosacral joint as compared to a symmetric moment [38]. It also agrees with Nachemson's *in vivo* result that twisting and sideway bending caused relatively minor increases in spinal load compared to forward bending [60]. Since the JRFs are mainly the result of the back muscles forces, these decreased JRFs in the asymmetric postures may be caused by the higher mechanical advantage of the lateral flexors (longer moment arms) as compared to the back extensors [38]. Compared to neutral posture, the JRFs for AR was increased, which was also found in other studies done by other groups [61, 62]. It was proposed that the increase in JRFs was caused by the increased tensile stress on the annular fibers during AR which would compress the discs [63].

7.3 Importance of SIMs

Another interesting finding of this study is the significant roles of SIMs in the stabilization of the lumbar spine. Bergmark [11] defined all the SIMs as the “local stabilizing system” which controls the curvature of the spine and increases sagittal and lateral stiffness to maintain the mechanical stability of the lumbar spine. He found that at a given activation level of the local stabilizing system, there was an upper limit of the activation of large muscles before the spine buckles. Cholewicki and McGill [19] also found that instability of the spine can be prevented by increasing the stiffness of the small muscles or increasing passive joint stiffness. There are several reasons the SIMs are preferred in lumbar spinal stability. First, these SIMs only span one or two FSUs, while large muscles span several FSUs. When the lumbar spine suddenly loses its stability and the motor control system faces the danger of lumbar spine buckling, large muscles are not suitable for regaining spine stability since activation of large muscles will increase the inferior intervertebral JRFs which magnify the effects of buckling. A more reasonable response would be the activation of the small muscles that cross a particular unstable joint to counteract the large displacements [19]. Second, these SIMs contain more Type I muscle fibers are better suited for fatigue resistance required for efficient maintenance of a lumbar posture over a longer time period. Third, a mechanical advantage of lumbar spine stabilization using SIM forces would be higher flexibility of the lumbar spine than stabilization only using long muscle forces.

The feasibility of optimum solutions from the model without SIMs indicates that perfect CFLs at all lumbar spine levels can be created with no contribution of SIM forces. However, the JRFs increased significantly due to an increased number of

recruited spinal muscles. The higher increase in JRFs in extension and axial rotation postures than neutral and flexed postures indicates that these postures are harder to maintain. High JRFs on lumbar spine are generally not desirable since they may cause low back problems. The results of FE analyses also clearly showed higher trunk displacement with no contributions of SIM forces, especially in extension and axial rotation postures where spinal instability occurred. These results agreed with the JRFs results and further indicated that maintaining lumbar spine in extended and axially rotated postures particularly without SIMs would be challenging.

These results indicate that the contribution of SIM forces is required to stabilize the spine more effectively with less JRFs. Clinical implication of the predictions of SIM forces would be that the damages or elimination of these SIMs during surgeries may cause a higher risk of future spinal problems such as segmental instability, early disc degeneration at adjacent levels, deformity, and/or early failure of fixation devices. Training of the long back muscles alone during rehabilitation after the surgery is not sufficient to help the patient with their back problem in the future. Instead, training of the SIMs during rehabilitation can be more important for better stabilization of the spine in a long run. Higher forces in SIMs predicted in the upper levels compared to the L4-5 and L5-S1 indicate that such risk of postoperative problems may be significantly higher with the surgical dissection of SIMs in upper lumbar and/or thoracolumbar regions.

7.4 Feasibility of CFLs in Parametric Studies

The results from the parametric study of trunk weight variation also showed that it was feasible for the spinal muscle forces to create CFLs and stabilize the spine at different body weights for all the postures. The only exception was extension 5° at the trunk weight of 45kg. However, this study was only done at FLP equal to 0mm, there may exist feasible solutions for extension 5° with the trunk weight 45kg at other FLP values. Future study is required to prove this postulation.

As the trunk weight increased, the JRFs increased. This was mostly because more muscles were recruited and muscle forces were increased in order to balance the forces and moments produced by the additional trunk weights. As the trunk weight continually increased in the optimization model, joint reaction moments started to appear (where they were zero before except in lateral bending 30°) in all the postures except flexion 40° in order to balance the moments generated by the trunk weight. The maximum trunk weight that the spine can support stably in the FE model for each posture was much lower than the maximum trunk weight obtained from the optimization model. However, this study was only performed at FLP=0mm. By varying FLP, the maximum trunk weight in the FE model might be increased. Also, by adjusting different parameters of the FE model, such as disc stiffness, the maximum trunk weight in the FE model might be increased. The spine size of the FE model used in this study was in fact smaller than the spine size of an average person. By increasing the size of the vertebrae and intervertebral disc, the moment of inertia would be increased and more trunk weight would be supported stably. Thus, even though the muscle forces and patterns obtained from the optimization model at a high trunk weight did not stabilize the spine in the current FE model, this does not mean

these solutions should be rejected.

The JRFs obtained at the maximum trunk weight from the optimization model showed agreement with the physiological compressive strength that would cause an increased risk of low-back injury. From Kim's study on maximum muscle force capacity, he found that as the maximum force of the muscles were increased, the JRFs at all lumbar levels decreased [23]. This is because as the maximum forces of the SIMs were increased, less big muscles were recruited to support the body and as a result, JRFs were decreased [23]. Based on his results, it can be proposed that if the maximum force of the muscles were increased in both models, the maximum trunk weights would also be increased in both models.

Overall, the results from body weight study further supported that CFLs could be the normal physiological load. The muscle patterns were also changed as the trunk weight increased for all postures. This might be because some of the recruited muscle fascicles had reached their limiting force capacity as the trunk weight increased. New muscle fascicles needed to be recruited or new muscle patterns needed to be formed to minimize the cost function.

The results from the disc property variation also showed that there were muscle forces and patterns available to create CFLs and stabilize the spine in neutral posture. However, the spine buckled in the FE model for all the other postures. This potentially means patients with degenerated disc are not able to stabilize the spine under perfect CFLs for all the postures other than neutral posture. Since patients with degenerated disc do not experience catastrophic buckling of the spine, these results potentially reveal that if CFLs are the normal physiological load, people with degenerated disc may experience abnormal load on their spine, such as shear forces.

This abnormal load on the spine may increase the rate of further disc degeneration and possibly LBP. On the other hand, patients with degenerated disc may adjust their postures to reduce the amount of shear forces and potentially pain. Based on the results from this study, the daily activities of these people may also be limited since any posture other than neutral posture would induce shear forces on the discs. Further studies need to be done to confirm these speculations. Also, this study was only done at FLP=0mm, it needs to be repeated at other FLPs to confirm that the CFLs creating spine muscles forces cannot stabilize the spine in all the postures other than neutral standing posture under disc degeneration.

7.5 Limitations and Future Studies

One limitation for this study is the lack of validation of CFLs *in vivo*. Though from the optimization and the FE models, the direction the JRFs can be determined, direct measurement of the direction of the JRFs *in vivo* is not feasible with the current technology. Not only just the direct measurement of the directions of the JRFs is limited, the direct measurement of the magnitude of the JRFs *in vivo* is also not practical. There have been concerns of ethical issues of introducing the needle transducers into the intervertebral discs and to control the many variables involved [12, 13]. The JRFs from this study were validated with the literature data, since direct validation through experiments was not done due to practical difficulties, and the results showed good agreement.

Another limitation for this study is the validation of the muscle forces. The muscle forces obtained from this study was also validated with the literature data since EMG study is expensive. However, the boundary conditions and the loading conditions from the literature are not all exactly the same as the ones in the models of this study. Thus, direct comparison of muscle force values with literature data could not be done. For future study, *in-vivo* measurement of spinal muscle contraction patterns, such as surface EMG study, is required for all the postures modeled in this study. However, the EMG technology itself also has many limitations which discussed in Chapter 2.

The models used in this study also had limitations. We did not model the muscles as two components, the active and passive components, but a single component. The total muscle force (active plus passive muscle force), which creates CFLs at all lumbar levels, was calculated in the optimization model and imported to

the FE model. The FE model simulated the muscle fascicle by using a single tension spring element. In order to gain a better understanding of the muscle activities, the active and passive components should be simulated separately in both optimization and FE models in the future. Moreover, the anatomy of the spine in the FE model was simplified. In order to reduce the computational cost, the anatomical details of the facet joints, intervertebral discs, ligaments and bones were neglected. However, this should not affect our current studies since the FE model was validated by comparing the ROM of the spine model with the literature data. For future study, the FE model should be refined to better represent the anatomy of the spine.

Finally, only static analyses were done in this study for all the postures. For future study, dynamic analyses also need to be performed in order to investigate the feasibility of spinal muscles creating CFLs during motions. More parametric studies are also required for future studies. Only body weight analyses and disc material property analyses at FLP equal to 0mm were done in this study, it would be interesting to see how the changes in FLPs would affect the results. Since our models are not subject specific and different people have different muscle stiffness, muscle cross-sectional area, disc stiffness, etc, it is important to perform the parametric studies on all of these variables to check if it is still feasible for spinal muscles to create CFLs and stabilize the spine. Non-follower load study also needs to be done in the future in order to understand how non-follower load can affect the JRFs at all lumbar spine levels and the stability of the lumbar spine.

CHAPTER 8

CONCLUSIONS

The results of this study are physiologically reasonable through comparison with literature data. They clearly demonstrate the feasibility of spinal muscles to created perfect CFLs at all lumbar spine levels and stabilize the lumbar spine in 3-D postures. Unlike the conventional optimization models where the muscle recruiting pattern converge to the same solution for the same task, the optimization model from this study showed there are many muscle recruiting patterns available to create CFLs in all the studied postures by varying the FLP. Additionally, the FE model from this study showed that only muscle forces and patterns solved at FLPs along the curve in the vicinity of the baseline curve (FLP=0mm) stabilized the lumbar spine. This non-uniqueness of the muscle recruiting patterns for the same posture explains the reason why people can performing the same takes for a long time during daily activities.

The parametric study on trunk weight analyses also showed that it is feasible for the spinal muscles to create CFLs and stabilize the spine at different trunks weights for all postures. The parametric study on disc property variation showed that it was only feasible for the CFLs creating spinal muscles to stabilize the spine in neutral standing posture. However, this does not mean that CFLs cannot be the normal physiological load, but people with degenerated disc may experience abnormal load, such as shear forces, on their spine.

Another important finding of this study was the biomechanical roles of SIMs. Based on the model predictions in this study, the JRFs were significantly increased without the contributions of SIM in all postures. The predictions of SIM forces are

required to create JRFs with less magnitude suggest the need of SIM inclusion in future spine biomechanics studies. This result also suggests that clinically, damages to the SIMs, such as dissection during surgery, may have a high risk of future spinal problems, such as spinal instability, early disc degeneration, deformity and/or early failure of spinal fixation devices. In conclusion, all the results from this study support at least in part an idea that the perfect CFLs at all lumbar levels could be the normal physiological load under which the lumbar spinal column could support large load without buckling while allowing flexibility as suggested by Patwardhan et al. [8].

REFERENCES

1. Ehrlich, S.D. *Low back pain*. 2012; Available from: https://umm.edu/health/medical/altmed/condition/low-back-pain.

2. Ehrlich, G.E., *Low back pain.* Bulletin of the World Health Organization, 2003. **81**: p. 671-676.

3. Office of, C. and L. Public. *Low Back Pain Fact Sheet*. 2012.

4. Crisco, J.J. and M.M. Panjabi, *Euler Stability of the Human Ligamentous Lumbar Spine .1. Theory.* Clinical Biomechanics, 1992. **7**(1): p. 19-26.

5. White, A.A. and M.M. Panjabi, *Clinical biomechanics of the spine*. 1978, Philadelphia: Lippincott. xxii, 534 p.

6. Crisco, J.J., et al., *Euler Stability of the Human Ligamentous Lumbar Spine .2. Experiment.* Clinical Biomechanics, 1992. **7**(1): p. 27-32.

7. Granata, K.P. and S.E. Wilson, *Trunk posture and spinal stability.* Clinical Biomechanics, 2001. **16**(8): p. 650-659.

8. Patwardhan, A.G., et al., *A follower load increases the load-carrying capacity of the lumbar spine in compression.* Spine, 1999. **24**(10): p. 1003.

9. Kim, J., et al., *Effect of shear force on intervertebral disc (IVD) degeneration: an in vivo rat study.* Ann Biomed Eng, 2012. **40**(9): p. 1996-2004.

10. Lotz, J.C. and J.R. Chin, *Intervertebral Disc Cell Death Is Dependent on the Magnitude and Duration of Spinal Loading.* Spine, 2000. **25**(12): p. 1477-1483.

11. Bergmark, A., *Stability of the lumbar spine. A study in mechanical engineering.* Acta orthopaedica Scandinavica.Supplementum, 1989. **230**: p. 1.

12. Nachemson, A.L., *Disk Pressure Measurements.* Spine, 1981. **6**(1): p. 93.

13. Neumann, D.A., *Kinesiology of the Musculoskeletal System Foundations for Rehabilitation*. Second Edition ed. 2010, United States: MOSBY ELSEVIER. 725.

14. Panjabi, M.M., *Clinical spinal instability and low back pain.* Journal of electromyography and kinesiology, 2003. **13**(4): p. 371-379.

15. Bogduk, N., J.E. Macintosh, and M.J. Pearcy, *A Universal Model of the Lumbar Back Muscles in the Upright Position.* Spine, 1992. **17**(8): p. 897.

16. Netter, F.H., *Atlas of human anatomy*. Third Edition ed. 2003: Elsevier Health Sciences.

17. Skandalakis, J.E., G.L. Colborn, and T.A. Weidman, *Skandalakis' surgical anatomy*. 2004: McGraw-Hill Companies.

18. Joseph Hamill, K.K., Timothy Derrick, *Biomechanical Basis of Human Movement*. Fourth, North American Edition ed. 2014: Wolters Kluwer.

19. Cholewicki, J. and S.M. McGill, *Mechanical stability of the in vivo lumbar spine: Implications for injury and chronic low back pain.* Clinical Biomechanics, 1996. **11**(1): p. 1.

20. Gramoll, K., *Multimedia Engineering Mechanics of Materials*. eCourses.

21. Timoshenko S, J.G., *Theory of elastic stability*. 1961, New York: Mcgrow-Hill.

22. Bazant ZP, C.L., *Stability of Structures*. 1991: Oxford University Press;.

23. Kim, B.S., *A follower load as a muscle control mechanism to stabilize the lumbar spine.* 2011.

24. Patwardhan, A.G., K.P. Meade, and B. Lee, *A frontal plane model of the lumbar spine subjected to a follower load: Implications for the role of muscles.* Journal of Biomechanical Engineering-Transactions of the Asme, 2001. **123**(3): p. 212.

25. Kim, K. and Y.H. Kim, *Role of trunk muscles in generating follower load in the lumbar spine of neutral standing posture.* Journal of biomechanical engineering, 2008. **130**(4): p. 041005.

26. Kim, K., Y.H. Kim, and S. Lee, *Investigation of optimal follower load path generated by trunk muscle coordination.* Journal of biomechanics, 2011. **44**(8): p. 1614-1617.

27. Han, K.-S., et al., *Spinal muscles can create compressive follower loads in the lumbar spine in a neutral standing posture.* Medical engineering & physics, 2011. **33**(4): p. 472.

28. Han, K.-S., *Feasibility of Creating Follower Compressive Loads and Roles of Spinal Muscles in Stabilizing the Lumbar Spine.* 2008.

29. Kim, B.S., et al., *Feasibility of compressive follower load on spine in a simplified dynamic state: A simulation study.* Bio-Medical Materials and Engineering, 2014. **24**: p. 2319-2329.

30. Voutsinas, S.A. and G.D. Macewen, *Sagittal Profiles of the Spine.* Clinical Orthopaedics and Related Research, 1986(210): p. 235-242.

31. Jackson, R.P., et al., *Lumbopelvic lordosis and pelvic balance on repeated standing lateral radiographs of adult volunteers and untreated patients with constant low back pain.* Spine, 2000. **25**(5): p. 575-586.

32. Gill, J., et al., *Trunk sway measures of postural stability during clinical balance tests: Effects of age.* Journals of Gerontology Series A-Biological Sciences and Medical Sciences, 2001. **56**(7): p. M438.

33. Parnianpour, M., et al., *The effect of variations in trunk models in predicting muscle strength and spinal loading.* 1997. **1**: p. 55-69.

34. Kaufman, K., et al., *Physiological prediction of muscle forces—I. Theoretical formulation.* Neuroscience, 1991. **40**(3): p. 781-792.

35. McGill, S.M., N. Patt, and R.W. Norman, *Measurement of the Trunk Musculature of Active Males using Ct Scan Radiography - Implications for Force and Moment Generating Capacity about the L4/l5 Joint.* Journal of Biomechanics, 1988. **21**(4): p. 329.

36. Ikai, M. and T. Fukunaga, *Calculation of muscle strength per unit cross-sectional area of human muscle by means of ultrasonic measurement.* Internationale Zeitschrift fuer Angewandte Physiologie Einschliesslich Arbeitsphysiologie, 1968. **26**(1): p. 26-32.

37. Cholewicki, J., S.M. McGill, and R.W. Norman, *Comparison of muscle forces and joint load from an optimization and EMG assisted lumbar spine model: towards development of a hybrid approach.* Journal of biomechanics, 1995. **28**(3): p. 321-331.

38. Van Dieen, J.H. and I. Kingma, *Total trunk muscle force and spinal compression are lower in asymmetric moments as compared to pure extension moments.* Journal of Biomechanics, 1999. **32**(7): p. 681.

39. Jager, M. and A. Luttmann, *Biomechanical analysis and assessment of lumbar stress during load lifting using a dynamic 19-segment human model.* Ergonomics, 1989. **32**(1): p. 93-112.

40. Waters, T.R., et al., *Revised NIOSH equation for the design and evaluation of manual lifting tasks.* Ergonomics, 1993. **36**(7): p. 749-776.

41. Reynolds, P.M.G., *Measurement of Spinal Mobility - Comparison of 3 Methods.* Scandinavian Journal of Rheumatology, 1975. **4**: p. 2016-2016.

42. Cholewicki, J., M.M. Panjabi, and A. Khachatryan, *Stabilizing Function of Trunk Flexor-Extensor Muscles Around a Neutral Spine Posture.* Spine, 1997. **22**(19): p. 2207-2212.

43. Jonsson, B., *Vocational electromyography.* Amsterdam: Cobband WA, 1978.

44. O'Sullivan, P.B., et al., *The effect of different standing and sitting postures on trunk muscle activity in a pain-free population.* Spine, 2002. **27**(11): p. 1238.

45. Cholewicki, J. and J.J. VanVliet, *Relative contribution of trunk muscles to the stability of the lumbar spine during isometric exertions.* Clinical Biomechanics, 2002. **17**(2): p. 99.

46. Floyd, W. and P. SILVER, *Function of Erector Spinae on Flexion of the Trunk.* American Journal of Physical Medicine & Rehabilitation, 1951. **30**(3): p. 180.

47. Potvin, J.R. and P.R. O'Brien, *Trunk muscle co-contraction increases during fatiguing, isometric, lateral bend exertions - Possible implications for spine stability.* Spine, 1998. **23**(7): p. 774.

48. Morris, J.M., G. Benner, and D.B. Lucas, *An electromyographic study of the intrinsic muscles of the back in man.* Journal of anatomy, 1962. **96**(Pt 4): p. 509.

49. Dumas, G.A., et al., *Orientation and Moment Arms of some Trunk Muscles.* Spine, 1991. **16**(3): p. 293.

50. Kay, A.G., *An extensive literature review of the lumbar multifidus: biomechanics.* Journal of Manual & Manipulative Therapy, 2001. **9**(1): p. 17-39.

51. Macintosh, J.E. and N. Bogduk, *The biomechanics of the lumbar multifidus.* Clinical Biomechanics, 1986. **1**(4): p. 205-213.

52. Thelen, D.G., A.B. Schultz, and J.A. Ashtonmiller, *Cocontraction of Lumbar Muscles during the Development of Time-Varying Triaxial Moments.* Journal of Orthopaedic Research, 1995. **13**(3): p. 390.

53. Marras, W. and K. Granata, *A biomechanical assessment and model of axial twisting in the thoracolumbar spine.* Spine, 1995. **20**(13): p. 1440-1451.

54. Kumar, S., Y. Narayan, and M. Zedka, *An electromyographic study of unresisted trunk rotation with normal velocity among healthy subjects.* Spine, 1996. **21**(13): p. 1500-1512.

55. McGill, S.M., *Electromyographic activity of the abdominal and low-back musculature during the generation of isometric and dynamic axial trunk torque - implications for lumbar mechanics* Journal of Orthopaedic Research, 1991. **9**(1): p. 91-103.

56. Dennison, C.R., et al., *Ex vivo measurement of lumbar intervertebral disc pressure using fibre-Bragg gratings.* Journal of biomechanics, 2008. **41**(1): p. 221-225.

57. McNally, D. and M. Adams, *Internal intervertebral disc mechanics as revealed by stress profilometry.* Spine, 1992. **17**(1): p. 66-73.

58. Sato, K., S. Kikuchi, and T. Yonezawa, *In vivo intradiscal pressure measurement in healthy individuals and in patients with ongoing back problems.* Spine, 1999. **24**(23): p. 2468.

59. Wilke, H.J., et al., *New in vivo measurements of pressures in the intervertebral disc in daily life.* Spine, 1999. **24**(8): p. 755-762.

60. Nachemson, A. and G. Elfstrom, *Intravital dynamic pressure measurements in lumbar discs.* Scand J Rehabil Med, 1970. **2**(suppl 1): p. 1-40.

61. Steffen, T., et al., *Lumbar intradiscal pressure measured in the anterior and posterolateral annular regions during asymmetrical loading.* Clinical Biomechanics, 1998. **13**(7): p. 495-505.

62. Schultz, A.B., *Loads on the Human Lumbar Spine.* Mechanical Engineering, 1986. **108**(1): p. 36-41.

63. Shirazi-Adl, A., A.M. Ahmed, and S.C. Shrivastava, *Mechanical response of a lumbar motion segment in axial torque alone and combined with compression.* Spine (Phila Pa 1976), 1986. **11**(9): p. 914-27.